UNIVERSITY OF CAMBRIDGE

BP INSTITUTE FOR MULTIPHASE FLOW


# The control of natural ventilation with opposing wind and buoyancy

Ben Lishman, Darwin College

This dissertation is submitted for the degree of Doctor of Philosophy

May 30, 2007

Supervisor: Prof. Andrew Woods, BP Institute for Multiphase Flow

## Declaration

This dissertation is the result of my own work and includes nothing which is the outcome of work done in collaboration except where specifically indicated in the text.

This thesis contains less than 275 pages as required by the Department of Earth Sciences.

Ben Lishman

Cambridge, May 30, 2007

**Acknowledgements**

I would like to thank Andy Woods, who has been an inspirational supervisor throughout my PhD. His insight into science has been a superb education for me over the last three years.

I would also like to thank Andrew Pluck, for building and modifying my experimental apparatus; Lotty Gladstone, for help and advice in the laboratory throughout my PhD; Chris Richardson, for patient help with computing problems; and Shaun Fitzgerald, Colm Caulfield, and Stephen Livermore, for guidance and advice on natural ventilation questions.

I'd like to thank my family, for their great support, and their proofreading.

Finally, my thanks to the BP Institute and the Cambridge-MIT institute for funding this research.

**Abstract**

This thesis is an investigation of the control of naturally ventilated buildings subject to opposing wind and buoyancy. Previous research shows that the interaction of wind and buoyancy can lead to complicated behaviour, and that this in turn can make it difficult to design controllers for naturally ventilated buildings. The aim of this research is therefore to aid in the design of such controllers.

In chapter 3 we investigate the transient evolutions between multiple flow regimes. The wind driven regime exists only for certain heat loads and wind forcing, so outside these conditions the building will evolve to the buoyancy driven regime. The buoyancy driven regime exists for all conditions. However, under varying wind, the system may evolve from the buoyancy driven regime to the wind driven regime. We find the minimum increase in wind, and the minimum rate of change of wind, which can cause such an evolution.

In chapter 4 we show that the transient evolution between flow regimes is further complicated by thermal mass. In heavyweight buildings, the temperature evolves along two separate timescales: a fast timescale, as the air in the building tends to equilibrium, and a slow timescale, as the thermal mass tends to equilibrium. In buildings with multiple flow regimes, this can lead to a series of slow evolutions punctuated by rapid, unpredictable temperature swings as the flow regime evolves.

Chapter 5 is an investigation of how building geometry may affect the different flow regimes which can occur under opposing wind and buoyancy. Our new research shows that when a third opening is introduced, the system has a unique steady state for any given heat load. Further, the existence of multiple steady states can be predicted for buildings with three openings, based on the size and height of the openings alone.

In each case, the predictions are supported by new analogue laboratory experiments. Each chapter concludes with a demonstration of how the new understanding might be applied to a real building.

# Contents

# 1. Introduction

*This thesis is an investigation of the fluid dynamics of naturally ventilated buildings, and in particular the nonlinear interactions between wind and buoyancy forces. The aim of the work is to improve the control of naturally ventilated buildings. This introduction begins with a brief overview and history of natural ventilation. There follows a discussion, with particular reference to the work in this thesis, of how an understanding of the fluid dynamics of ventilation can lead to improved control systems, and hence more efficient, comfortable buildings. The introduction ends with an overview of the rest of the thesis, and a reference table of nomenclature.*

## 1.1. Background and motivation

The Oxford English Dictionary defines ventilation as:

"The admission of a proper supply of fresh air, esp. to a room, building, ... or other place ... ; the means or method by which this is accomplished."

This "supply of fresh air" is used to maintain comfortable levels of carbon dioxide in a building, and to remove local pollutants (e.g. odours and moisture). Since ventilation usually replaces warm interior air with cold exterior air, it also affects the temperature in a space, and can help to provide a comfortable thermal environment for occupants. We can therefore list three possible aims of ventilation (Steemers, Chenvidyakarn, and Woods 2002):

- maintaining air quality
- space cooling, and
- occupant cooling

Figure 1.1.: *The interior courtyard of the Medersa Bou Inania, in Fez, Morocco.*

At times the requirements may conflict: for example in the need to "offer fresh air without discomfort from cold draughts" (Steemers, Chenvidyakarn, and Woods 2002).

Natural ventilation, as its name suggests, uses naturally occurring pressure differences (due to wind and buoyancy) to drive ventilation flows. The technology has a rich history. Figure 1.1 shows an illustrative historical example of a naturally ventilated building: the Medersa Bou Inania, in Fez, Morocco. The design is a common one in medieval Mediterranean architecture: rooms are built around a shaded internal courtyard. The rooms have low openings to the courtyard, and high openings to the exterior, such that local sources of heating (e.g. people) in the buildings drive a buoyant flow, bringing in cool air from the shaded courtyard, and expelling warm air to the street. Such buildings are also often built of heavy stone, which cools throughout the night and then absorbs heat during the day, helping to preserve a comfortable temperature (see the discussion of thermal mass in the literature review, chapter 2).

In the twentieth century, new technology was devised to improve our indoor

comfort. In 1902, Willis Haviland Carrier invented the first modern electrical air conditioning system. After this buildings were increasingly designed as sealed units to be ventilated using a combination of forced ventilation (e.g. with mechanical fans) and air conditioning systems. This allows internal temperature to be fixed precisely.

In the twenty-first century, however, global energy consumption is rising, and it is becoming increasingly challenging to meet energy demands. There is therefore a need for improved energy efficiency, and one area where substantial improvements are possible is in building ventilation. Recent figures show that buildings account for 47% of energy consumption in the UK (Department of Trade and Industry 2004) and 39% of energy consumption in the USA (US Department of Energy 2006). Natural ventilation, as an alternative to air conditioning, can provide an opportunity for significant reductions in energy consumption. Recent studies suggest that naturally ventilated offices can offer a 50% reduction in energy use, from 400kWh/m$^2$ annually in an air conditioned office to 200kWh/m$^2$ annually in a naturally ventilated office (Action Energy 2003). Natural ventilation is also popular as it is quieter than mechanical ventilation, and may avoid some health worries associated with poorly operated mechanical ventilation. However, in order for natural ventilation to be a credible alternative, it must provide an environment of comparable thermal comfort to that associated with a purely mechanical ventilation system. This is a substantial challenge, since the controls available for natural ventilation systems are limited, and therefore we require a much deeper understanding of the flow patterns within a building.

The aim of this thesis is to provide new insights into such flow patterns in buildings. This will allow building designers and controllers to improve thermal comfort, and will therefore increase the feasibility of natural ventilation.

## 1.2. The control of natural ventilation

Natural ventilation control has relatively simple requirements, as listed at the start of this introduction: to keep the building temperature within a comfortable range, and to maintain sufficiently low carbon dioxide levels. Natural ventilation therefore faces problems which are different from many typical control systems: accuracy and speed of response are not as important as, for example, in aviation control. However, the control of a naturally ventilated building is complicated by the fact that the controller has access to only a few, simple actuators. Most obviously, these might be

- window openings, and
- heating.

A very general control system for a building with these actuators would be as follows: if the building is too hot, do *some combination* of opening the windows and reducing the heating. If the building is too cold, increase the heating and reduce the window aperture. If we assume approximately linear relationships between heating and temperature, and between window area and temperature, this control system should allow us to set the temperature in the building. Exactly *what* combination of changing the windows and changing the heating will be determined by economics (e.g. how much does the heating cost?) and by practicalities (e.g. minimum ventilation rates, as required in building regulations). By considering this general control system, we can outline three important research topics which may help to improve the control of naturally ventilated buildings.

One important step in ventilation control system design is to quantify as much as possible about the system. This will inform economic and practical decisions, as illustrated above. We therefore need to understand the flow regimes associated with different natural ventilation schemes, to understand the key parameters which affect these flow regimes, and to understand how the actuators available can affect these parameters.

A second part of control system design is to identify potential failures in this simple controller. This would include buildings for which the relationships between heating, window area and temperature are far from linear, and where catastrophic changes (e.g. flow regime changes) may occur which "confuse" our controller or lead to uncomfortable local climates (e.g. for those sitting near windows).

A third possible task is to understand the effects of external disturbances (for example gusts of wind) so that these do not cause regular discomfort for building occupants.

This thesis focusses on a building design in which two flow regimes are possible and multiple steady states occur for a given heating load and window area. First, we try to understand how transitions between regimes may occur, by studying the transient evolutions in both lightweight and heavyweight buildings. This will allow improved building and control system design, and also help to understand the effects of disturbances (and hence how to minimize them). We then investigate how changing the building design may eliminate multiple states.

This new understanding will help to maintain thermal comfort in naturally ventilated buildings, and hence help to make natural ventilation a feasible substitute for more energy-intensive systems.

## 1.3. Outline of thesis

The next chapter is a review of the current literature on natural ventilation. The chapter begins with a review of the current context of natural ventilation, to provide the reader with some background on current energy policy globally and in the UK, the role of improved building technology within this context, and the legislation currently in place to enforce improved building technology in the UK. After this background, we go on to discuss the fluid dynamics of natural ventilation, focussing particularly on research which provides a basis for the new research presented later in this thesis. The literature review focusses, in particular, on buoyancy driven ventilation caused by a distributed heat source;

the effects of wind; the value of water bath modelling in ventilation research; and situations in which multiple steady states can occur for a given set of conditions.

After this summary of context, we move on to present new research in three distinct sections, as chapters 3, 4 and 5. Throughout the thesis the research is focussed on the competition between wind and buoyancy in natural ventilation, which is known to lead to multiple steady states for certain building configurations. It is known from the literature that a stable wind driven regime and a stable buoyancy driven regime occur, and that these are joined by an unstable wind driven regime.

In chapter 3, we consider the nature of transient evolutions between flow regimes, caused by fluctuations in wind. We show that transitions from the wind driven regime to the buoyancy driven regime occur at a fixed wind. The reverse transition, however, depends on both the magnitude and rate of the increase in wind. We develop a model to predict when a change in flow regime will occur. This allows a designer or controller to avoid uncomfortable temperature swings within their building.

In chapter 4, the problems of interacting wind and buoyancy are extended to incorporate the effects of thermal mass. The research shows that the building temperature evolves along two timescales: a slow timescale, as the thermal mass tends toward equilibrium; and a fast timescale, as the building scale ventilation flow changes regime. We also find that the predictions of chapter 3 need to be modified when considering heavyweight buildings, and in particular that thermal mass may limit the range of winds over which a buoyancy driven regime can occur. Again, we provide a methodology which allows building controllers to avoid occupant discomfort.

In chapter 5, we investigate whether the model changes qualitatively if the building has more than two openings, since this is the case in most real buildings. We find that while in a building with a single high upwind opening and a single low downwind opening, there are multiple flow regimes and steady states

for a given set of input conditions, the introduction of a third opening can allow the flow regime to be uniquely determined for all input conditions. Further, we find that the existence of multiple steady states can be determined based on building geometry alone.

The theory of each of chapters 3, 4 and 5 is supported by new laboratory experiments, presented in these chapters. Each chapter concludes with a discussion of how the new understanding presented could be applied to real building design and control.

The thesis concludes with a summary of the findings of each of these elements of new research. The conclusions from each of the three main chapters are then drawn together to show the new understanding which is brought to the general field of nonlinear fluid dynamical systems. We then show how the findings of the three main research strands can be combined to allow improved building design and control, and hence improved occupant comfort. The thesis ends with suggestions of further topics for useful and relevant research, which would extend the range of conditions to which our findings are applicable.

## 1.4. Nomenclature

All symbols used in this report are explained below. Values for density, thermal expansion coefficient and specific heat capacity are for water, as is the formula for effective gravity.

| Symbol | Quantity | Typical experimental value | Units |
|---|---|---|---|
| $\Delta p$ | Pressure Difference | 1 | Pa |
| $\rho$ | Density | 1000 | $\mathrm{kgm^{-3}}$ |
| $\beta$ | Thermal Expansion Coefficient | 0.36 | $\mathrm{kgm^{-3}K^{-1}}$ |
| $C_p$ | Specific Heat Capacity | 4184 | $\mathrm{Jkg^{-1}K^{-1}}$ |
| $\nu$ | Kinematic viscosity | $10^{-6}$ | $\mathrm{m^2s^{-1}}$ |
| $\kappa$ | Thermal diffusivity | $10^{-7}$ | $\mathrm{m^2s^{-1}}$ |
| $g$ | Gravity | 9.81 | $\mathrm{ms^{-2}}$ |
| $g'$ | Effective Gravity | | $\mathrm{ms^{-2}}$ |
| $h$ | Height | 0.1 | m |
| $A$ | Area | $10^{-3}$ | $\mathrm{m^2}$ |
| $V$ | Volume | $10^{-3}$ | $\mathrm{m^3}$ |
| $S$ | Thermal mass surface area | | $\mathrm{m^2}$ |
| $q$ | Volume Flux | $10^{-5}$ | $\mathrm{m^3s^{-1}}$ |
| $H$ | Heat Flux | 100 | $\mathrm{Js^{-1}}$ |
| $\Delta T$ | Temperature Difference | 2 | K |
| $c^*$ | Loss Coefficient | 0.7 | |
| $\lambda$ | Entrainment coefficient | 0.16 | |
| $h$ | Heat transfer coefficient | | $\mathrm{Wm^{-2}K^{-1}}$ |

| Symbol | Dimensionless parameter |
|---|---|
| $\theta$ | Dimensionless temperature, scaled on initial/fixed wind (chapter 3,5) |
| $\Theta$ | Dimensionless temperature, scaled on fixed heat flux (chapter 4) |
| $Q$ | Dimensionless heat flux, scaled on initial/fixed wind (chapter 3,5) |
| $\hat{W}$ | Dimensionless wind, scaled on initial wind (chapter 3) |
| $W$ | Dimensionless wind, scaled on fixed heat flux (chapter 4) |
| $t^*$ | Dimensionless time, scaled on initial wind (chapter 3) |
| $\hat{t}$ | Dimensionless time, scaled on fixed heat flux (chapter 4) |
| $\eta$ | Dimensionless rate of increase of wind speed (chapter 3,4) |
| $\mu$ | Dimensionless heat exchange parameter (chapter 4) |
| $M$ | Dimensionless thermal mass parameter (chapter 4) |
| $\alpha$ | Area ratio (chapter 5) |
| $\omega$ | Opening height ratio (chapter 5) |
| $\Gamma$ | Dimensionless neutral level height (chapter 5) |
| $p$ | Dimensionless pressure (chapter 5) |

Subscripts are used frequently and explained in the text. Commonly used subscripts include:

b - buoyancy

c - critical

i - interior-exterior

I - interface

l - lower

n - neutral level

p - plume

q - heating

tm - thermal mass

u - upper

v - ventilation

w - wind

x - general

# 2. Literature

*This thesis aims to inform the design and control of naturally ventilated buildings by an understanding of the fluid dynamics involved. We therefore discuss relevant literature in two distinct sections. In the first section we focus on naturally ventilated buildings, and in particular the current social, environmental, political and economic climate relating to energy use in the UK. In the second section we discuss the fluid dynamics relating to natural ventilation, and present a review of the literature on the mathematics and fluid dynamics which is most relevant to the principles of natural ventilation used later.*

## 2.1. Context: social, environmental, political and economic

This section summarises the key literature which explains the motivations for natural ventilation. First, we outline the need for improved energy efficiency; and second, we discuss the implications for building design and natural ventilation.

### 2.1.1. Energy policy

The 2003 UK government White Paper on energy summarises the need for energy efficiency. In his introduction, Tony Blair, the Prime Minister, states that "energy can no longer be thought of as a short-term domestic issue", and discusses the dangers of climate change and the difficulty of maintaining energy supply. He also notes that "science and technology are vital" to meeting these challenges (Energy White Paper 2003).

The potential dangers of climate change are now widely known; newspa-

pers frequently report on climate science, and the recent film "An Inconvenient Truth", based around a lecture about climate change given by Al Gore, was a box office hit. Climate change affects, and will continue to affect, the global economy. In 2006, the British Treasury commissioned the former Senior Vice-President of the World Bank, Sir Nicholas Stern, to investigate the likely economic effect of climate change. His report predicts that the economic cost of climate change, if left unchecked will be $5-20\%$ of global GDP, and states that:

> "Much of the risk can be reduced ... at a far lower cost than those calculated for the impacts" (Stern 2006)

In other words, it will prove cheaper in the long term if we act now.

Much of the uncertainty in predictions about climate change arises because the processes involve complicated feedback loops: for example, as ice melts, less of the sun's energy is reflected, and so the planet may become warmer. With this in mind, it is interesting to note some visible effects of climate change: the White Paper notes that:

- global mean sea level rose by an average of 1-2mm a year during the 20th century, and
- global snow cover has decreased by 10% since the 1960s.

There is a perception that these occurrences are connected to increased atmospheric $CO_2$, which in turn is connected to the increased use of fossil fuels over the last century. To help prevent further possible nonlinear changes in the earth's environment, the British government has committed to reducing carbon dioxide emissions. The UK is a signatory to the Kyoto Protocol to the United Nations Framework Convention on Climate Change, which agrees that:

> "industrialised countries will reduce their collective emissions of greenhouse gases by 5.2% compared to the year 1990." (Kyoto Protocol 1998)

The 2003 White Paper goes further, accepting a (more vague) recommendation that:

> "The UK should put itself on a path towards a reduction in carbon dioxide emissions of some 60% from current (1990) levels by about 2050." (Energy White Paper 2003)

To meet these targets, the UK will have to reduce its dependency on fossil fuels. The White Paper notes that such a reduction will require both an increase in renewable energy supply, and a reduction in energy consumption. The White Paper also notes that 26% of UK energy use in 2000 was for space heating, while recent government estimates of energy use show that overall, buildings account for 47% of total energy consumption in the United Kingdom (Department of Trade and Industry 2004), which suggests that improvements in building design and ventilation offer significant opportunities for energy efficiency. Increased energy efficiency in buildings is a key tenet of current government policy. The White Paper commits to promoting buildings which

> "combine energy efficient technologies and renewable energy to reduce radically their demand for energy." (Energy White Paper 2003)

This section has summarised the need for a reduction in use of fossil fuels (both in the UK and globally), and suggested that improved efficiency in buildings may be part of the solution. In the next section, we investigate current British building requirements and practices, to show how and why improved efficiency in buildings may occur.

### 2.1.2. Building requirements

Building regulations in the UK are set by the Department for Communities and Local Government. Natural ventilation designers might need to consider two sections of the building regulations: part F, which covers ventilation; and part

L, which covers conservation of fuel and power. From part F, note section 0.16, which states that:

> "It is important that ventilation is controllable so that it can maintain reasonable indoor air quality and avoid waste of energy." (Part F 2006)

This thesis aims to help establish such controllability for natural ventilation schemes. Section 1 of part F focusses on dwellings, and section 2 focusses on other buildings. In this thesis we mainly consider office buildings and equivalents, so it is helpful to note section 2.12, which is a legal requirement for a ventilation rate of $10 \mathrm{ls}^{-1}$ per person in office buildings.

Part L of the building codes has recently been updated to include more stringent energy standards. Of particular interest are the new sections 17A and 17B:

> "The Secretary of State shall approve a methodology of calculation of the energy performance of buildings" (Part L 2006)

and:

> "The Secretary of State shall approve minimum energy performance requirements for new buildings, in the form of target $CO_2$ emission rates." (Part L 2006)

As the required energy performance targets become stricter, natural ventilation systems become increasingly attractive. It therefore seems likely that an understanding of the fluid mechanics of natural ventilation will become increasingly important in the first half of the twenty-first century.

An important consideration when evaluating the economic and environmental value of naturally ventilated systems is the balance of capital expenditure and operating costs. Naturally ventilated buildings avoid the expense of installing mechanical ventilation systems. Sartori and Hestnes (2006) discuss the life-cycle energy use of buildings, and find that a passive house (a building in which

the design is oriented to make maximum exploitation of passive technologies, including natural ventilation) has a third of the life-cycle energy demand of an equivalent conventional building.

### 2.1.3. Social context

As stated earlier, one of the objectives of ventilation is to maintain human comfort. It therefore seems important to discuss the literature relating to human responses to ventilation. For example, we note that people are able to adapt to predictable changes in temperature, for example by putting on extra layers of clothing in a cold environment. In the past, building regulations stipulated that the building should be maintained at $21^oC$: now, in the face of increased pressure for energy conservation, greater flexibility is often allowed. However, rapid, unpredictable changes in temperature are likely to be uncomfortable, and should be avoided. This gives some background to the discussion of varying flow regimes in chapter 3.

We also note that people's thermal comfort is determined by three factors (Fanger 1970):

- the temperature of their local environment;
- the incident thermal radiation; and
- the air speed

This seems intuitive: we are aware we feel warmer when the sun shines directly upon us, while we feel colder in a breeze. However, it can be difficult to incorporate the last two effects into natural ventilation models. Finally, we note that people may feel more comfortable when they are in control of their own environment (e.g. if they can open their windows).

### 2.1.4. Design guides

Various institutions produce documents which aim to turn the requirements of the Building Regulations into technical advice to designers. The Energy

Saving Trust has produced a document entitled "Energy efficient ventilation in dwellings - a guide for specifiers", which outlines good practice and best practice for new building design (Energy Saving Trust 2006). The Chartered Institution of Building Services Engineers (CIBSE) produces a series of guides for building design. CIBSE describes its guide A as "the premier reference source for designers of low energy sustainable buildings" (CIBSE 2006). Chapter 4 of CIBSE guide A covers ventilation, and lists useful standards related to required air change rates and $CO_2$ levels, as well as simple empirical and analytical techniques for estimating ventilation levels and wind pressures.

While basic rules for ventilation can be found in these design handbooks, the literature of fluid mechanics contains more detailed studies of flow patterns and corresponding ventilation rates under a variety of different geometries and flow conditions. In the next section we discuss this literature.

## 2.2. Research base: the fluid dynamics of natural ventilation

As seen in the previous section, natural ventilation offers significant opportunities for improved energy efficiency in buildings. However, in order to be a viable alternative to mechanical ventilation, natural ventilation should provide similar comfort levels. By understanding the fluid dynamics of ventilation we can control buildings effectively, and hence reduce energy use and cost without sacrificing occupant comfort.

In this section we discuss the fluid dynamics of natural ventilation, with reference to the literature. Work on natural ventilation often relies on simplified building geometries and assumptions about flow patterns, to establish physical models and hence general rules about the nature of building ventilation. This is the methodology used in this thesis, and so this literature review will focus on such simplified models. It is also possible to use computational fluid dynamics (CFD) to model more complex geometries and provide more detailed flow patterns. Such studies are likely to give information which is specific to

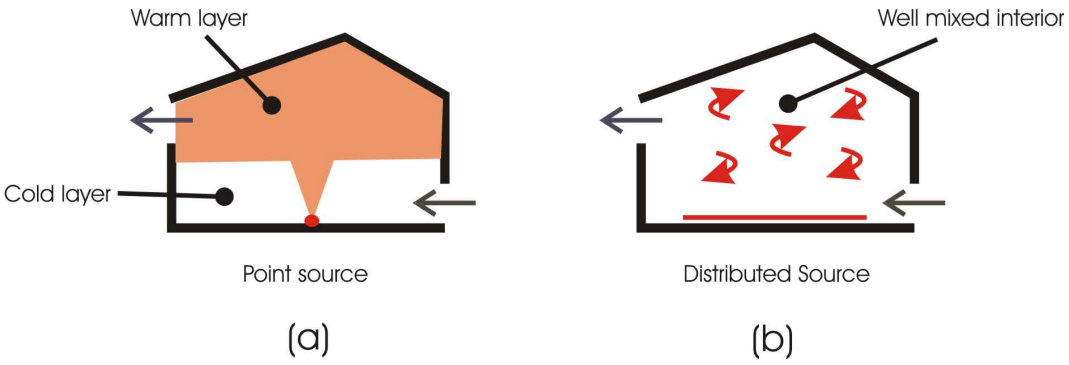


Figure 2.1.: *Cartoon showing buoyancy driven ventilation in a building with two openings. In figure (a) the heat load is generated at a single point. In figure (b) the heat load is distributed across the area of the floor.*

the geometry of the building in question, which is both an advantage (for those interested in that building) and a disadvantage (if trying to come up with more general understanding). In particular, with reference to the work in this thesis, we note that CFD will predict a single building state, and therefore may not be the best tool with which to analyse multiple states in buildings. A useful discussion of the advantages and limitations of CFD methods is given in Linden (1999), chapter 6.

### 2.2.1. Stratification and mixing in ventilation flows

We begin the discussion of more general physical models by considering two forms of buoyancy driven ventilation: mixing ventilation, which leads to a uniform temperature distribution in the building, and ventilation driven by point sources, which leads to a temperature stratification in the building (for example, a relatively warm layer above a relatively cold layer). The new research presented in this thesis largely assumes a well-mixed interior. This section provides background about the likelihood of such a scenario.

Figure 2.1 shows a cartoon showing the basic flow of ventilation for a building with a single heat source and two openings at different levels. In figure 2.1(a) the heat source is a single point. A warm plume rises off this point, entraining cold air and rising into an upper, warm layer of fluid. A stable stratification is thus created (Linden, Lane-Serff, and Smeed 1990; Linden 1999). Point heat

sources like that shown in figure 2.1(a) might be used to represent individual people or computers. Such a model is at one end a spectrum. The other end of this spectrum is shown in figure 2.1(b), in which the heat source is distributed across the entire floor. In this case the interior air will become well mixed (Gladstone and Woods 2001). As one example of a motivation for such studies, Gladstone and Woods (2001) note that:

> "In many modern office buildings solar radiation may pass through large glass panels, heating the floor and producing a distributed heat source."

They also note that a distributed heat source model is analogous to the under-floor heating systems designed by the Romans.

In most modern offices buildings (and many other buildings) we might assume that the actual heat source is best modelled as somewhere in between the two: a group of people working at computers will lead to multiple point sources of heat. As the number of such point sources increases, at some state these sources will tend to act as a single distributed source. Linden (1999) discusses the effects of multiple point sources in section 3.4.3, and shows how multiple layers may form. Equally, air movement within the room (e.g. as people move around) is likely to mix up the interior fluid, and penetrative convection of plumes at any interface between stratified layers is likely to lead to gradual rather than sharp stratification. It is therefore difficult to predict exactly the degree of stratification within a space. In this thesis we generally assume a well mixed interior, except where explicitly stated. A physical situation in which this assumption would be accurate is, for example, in a space with a ceiling fan to mix up the fluid. Often the models based on this assumption can then be generalised to more complex levels of stratification.

### 2.2.2. Derivation of model for buoyancy driven ventilation

In this subsection we derive models which describe the ventilation rates and temperatures of the buildings in figure 2.1 as a function of heat load. This

provides a theoretical basis with which building temperature evolution can be predicted. This theory can then be extended to more complicated cases: for example, later we introduce the effects of wind as well as heat sources.

The ventilation shown in figure 2.1 occurs because the air in the room is warmer, and therefore more buoyant, than the exterior air. This buoyancy leads to a greater pressure at the upper opening than at the lower opening, with the magnitude of the pressure difference given by

$$\Delta p_b = \rho g' h \tag{2.1}$$

where $\rho$ is the fluid density, $h$ is the height between the openings, and $g'$ is an effective gravity. If we define the internal fluid density as $\rho + \Delta\rho$ and the external fluid as $\rho$, the effective gravity is given by

$$g' = -g\frac{\Delta\rho}{\rho} \tag{2.2}$$

Etheridge and Sandberg (1996) have a full discussion of the derivation of $g'$ for air and for water. In deriving $g'$ for air and water, we use the Boussinesq approximation, under which we assume that the fluid is incompressible, except when determining the buoyancy force due to gravity. We can therefore, for example, ignore density differences due to temperature when stating an overall mass balance for a building, since the effects of these density differences are considered small. We also assume that the density of the fluid is a linear function of temperature.

For an ideal gas, the equation of state tells us that

$$p = \rho R T \tag{2.3}$$

where $p$ is pressure, $R$ is the gas constant, and temperature $T$ is measured in Kelvins. Assuming some reference state (subscript $_0$) and constant pressure this leads to the relation

$$\frac{\Delta\rho}{\rho_0} = -\frac{\Delta T}{T_0} \tag{2.4}$$

This allows us to write that, for air,

$$g' = \frac{\Delta T}{T_0} g \tag{2.5}$$

Similarly, for water we can write that

$$\frac{\Delta \rho}{\rho_0} = -\frac{\beta \Delta T}{\rho} \tag{2.6}$$

where $\beta$ is a thermal expansion coefficient, scaled by density, with units of $\mathrm{kgm}^{-3}\mathrm{K}^{-1}$, and

$$g' = \frac{\beta \Delta T g}{\rho} \tag{2.7}$$

This $g'$, chosen appropriately for either air or water, then gives the buoyancy pressure, which, combined with a mass balance, gives the pressure difference across each opening in the building (see chapter 3 for a full example). The volume flux through each opening is then given by (Linden, Lane-Serff, and Smeed 1990; Gladstone and Woods 2001):

$$q_x = c^* A_x \sqrt{\frac{\Delta p_x}{\rho}} \tag{2.8}$$

where $q_x$ is the volume flux through an opening, $A_x$ is the area of that opening, $\Delta p_x$ is the pressure difference between one side of the opening and the other, and $c^*$ is a loss coefficient.

### Model for distributed heat load

Heat transfer in buildings involves both convection and radiation, and there is a significant amount of both forms of heat transfer in a real building. This thesis focusses on the convective component of the heat budget. However, the effect of radiative transfer is accounted for implicitly in chapter 4, where we discuss the impact of thermal mass. The thermal mass absorbs or emits heat radiatively but also exchanges heat with the air in the convective boundary layer. For the purposes of our modelling, heat loads are assumed to be convective.

A distributed heat load will lead to a well mixed interior, so we can use a combination of a mass balance and an energy balance to develop a relation between temperature and heat flux in a building similar to that shown in figure 2.1(b). To calculate the volume flow rates in and out of the building, we combine equation 2.8 with a mass balance. In this case we use the convention that the pressure driving inflow at the lower opening on figure 2.1a is a reference exterior-interior pressure difference $\Delta p_i$. The pressure difference driving the flow across the upper opening is then $\Delta p_b - \Delta p_i$. Equating volume flux in to volume flux out, using equation 2.8, and assuming equal opening areas, we find pressure difference across the lower opening,

$$\Delta p_i = \frac{\Delta p_b}{2} \tag{2.9}$$

and we combine equations 2.8 and 2.9 to find the volume flux through the space

$$q = c^* A \sqrt{\frac{\Delta p_b}{2\rho}} \tag{2.10}$$

To find how this volume flux affects the interior temperature, we consider an energy balance (see, for example, Gladstone and Woods (2001)), equating the rate of change of thermal energy in the building to the energy added from the heat source minus the thermal energy which is vented as warm air leaves the building:

$$\rho C_p V \frac{d\Delta T}{dt} = H - \rho C_p q \Delta T \tag{2.11}$$

where $C_p$ is the specific heat capacity of the fluid and $H$ is the convective heat load supplied to the building. Finally, combining equations 2.10 and 2.11 allows us to find temperature as a function of heat load:

$$\rho C_p V \frac{d\Delta T}{dt} = H - \frac{\rho C_p c^* A}{\sqrt{2\rho}} \Delta T \sqrt{\Delta p_b} \tag{2.12}$$

with $\Delta p_b$ given by equation 2.1. Since the buoyancy pressure is a linear function of temperature, at equilibrium ($\frac{d\Delta T}{dt} = 0$) we find that the temperature is proportional to $H^{\frac{2}{3}}$.

#### Model for point source of heating

In the case of a point source of heating, a warm plume and a stratified interior environment arise, as shown in figure 2.1a. Here, the height of the interface between the stratified layers is unknown, and so a new equation determining the interface height $h_I$ is required. To find this, we note the volume flux entering the upper layer via the plume, (Morton, Taylor, and Turner 1956)

$$q_p = \lambda \left( \frac{Hg\beta}{\rho C_p} \right)^{\frac{1}{3}} {h_I}^{\frac{5}{3}} \tag{2.13}$$

where $\lambda$ is a constant dependent on the entrainment constant. We then equate this flux entering the upper layer to the flux vented from the upper layer:

$$q_v = c^* A \sqrt{\frac{\Delta p_b}{2\rho}}, \tag{2.14}$$

since the interface height must remain constant at equilibrium. $\Delta p_b$ in equation 2.14 depends on the average temperature in the room. We then can combine equations 2.13, 2.14, and 2.11 to give the interface height and the average temperature in the building as a function of the heat load (Linden, Lane-Serff, and Smeed 1990).

### 2.2.3. Wind and ventilation

This thesis is about the internal environment in buildings. This environment may be affected by wind, which can result in a pressure difference across a building. The pressure difference depends on the orientation of the building, the height of the openings, and the surrounding structures. Here we give an overview of the wind forcing which acts on buildings, considering in particular typical average pressure differences caused by wind, and how these pressure differences might evolve over time. This helps to give a more complete picture of natural ventilation, since pressure differences due to wind are often used to drive ventilation flows.

A full discussion of the relationships between wind and buildings is given in Aynsley, Melbourne, and Vickery (1977). In this thesis, we are interested in the

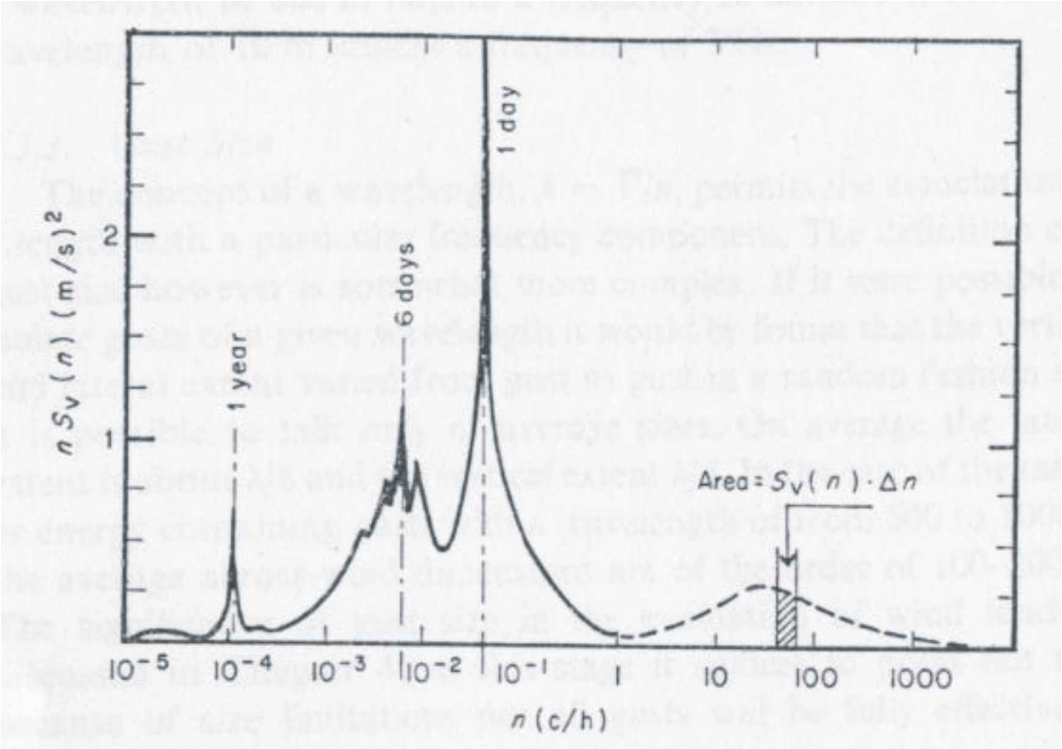


Figure 2.2.: *Spectrum showing frequencies of wind speed variations from the long term average. Four peaks are visible, corresponding, from left to right, to wind variations over one year, roughly six days, one day, and roughly two minutes. (Aynsley, Melbourne and Vickery, 1977)*

likely pressure difference which occurs between the upwind and downwind faces of a building due to wind. Rousseau (1995) suggests that the likely range of wind pressures acting on a building are from 0.1 Pa to 10 Pa. To determine the temporal variation of this pressure, we use information about wind speed as a proxy for information about the pressure differences due to wind. For example, Aynsley, Melbourne, and Vickery (1977) present a spectrum from 55 years of wind speed data, measured in Sydney, Australia, reproduced here as figure 2.2. The spectrum illustrates variations in speed about the long term average. Four peaks may be observed. One peak, at about $10^{-4}$ cycles per hour, or 1 cycle per year, is due to seasonal variations in wind speed. The next, at about one cycle per six days, is created by large scale weather systems, which pass through Sydney on average once every six days. The next is a peak at 1 cycle per day, generated by the daily cycle of heating and cooling. Finally, there is a broad peak at about 1 cycle per two minutes, related to the nature of atmospheric turbulence (Aynsley, Melbourne, and Vickery 1977). We assume that variations in pressures due to wind will occur at the same frequencies as these variations in wind speed.

We also note that in urban environments, wind speed is lowest at ground level (due to friction between the wind and the ground and other buildings) and rises with height above ground to some maximum value (Aynsley, Melbourne, and Vickery 1977). This maximum wind typically occurs in a city at a height of 400-500m. We can therefore assume that the wind pressure acting on high opening might be greater than that acting on low openings.

Some useful information about the relationships between average wind speed and observed pressure differences due to wind might be obtained using wind tunnel experiments (see discussion in Linden (1999)). However, urban environments tend to have numerous buildings acting as "obstacles" to the wind, and so the actual effects of wind at any given point are heavily dependent on local geometry. In general an isolated building has a greater pressure acting on its upwind openings than on its downwind openings. In practice the situation

may be more complicated, and the building shape, roof shape, and surrounding buildings will change the pressure difference and lead to more complex patterns. In this thesis we assume wind pressures which are likely in a typical daytime urban environment (i.e. of the order 1 Pa (Rousseau 1995)) without going into great detail about the local geometry and wind which cause such pressure differences. We also make the simplifying assumption that winds are steady, or smooth changing, whereas real winds have a large stochastic component. Our simplifying assumptions are to some extent validated by our experimental modelling, in which a flow past the building acts as an analogue to wind.

### 2.2.4. Multiple steady states in natural ventilation

In this subsection we introduce the problem of multiple steady states due to opposing wind and buoyancy, which is the focus of this thesis. We illustrate why opposing wind and buoyancy may lead to complicated building behaviour, and note the previous studies available in the literature.

Before we consider opposing wind and buoyancy, however, it is useful to consider the complementary problem of when wind and buoyancy act in the same direction, as discussed by Hunt and Linden (2001). In this case, the relationship between heating, wind and temperature is monotonic, and so the problem is similar to that of a flow driven by buoyancy alone. We also note here that if cooling is applied to our system, then the negative buoyancy acts in the same direction as the wind, and so the problem becomes analagous to that discussed by Hunt and Linden (2001).

The building model shown in figure 2.1 becomes more complicated when the effects of wind are included. To see this, let us consider a building with a wind acting inwards at the high opening, such that the wind opposes the buoyancy pressure (see e.g. figure 3.1). Clearly, at very large heat loads, the buoyancy pressure will be very strong, and we expect the flow direction to be upwards through the building ("buoyancy driven"). Similarly, under very strong winds, we might expect the air in the building to flow downwards ("wind driven"). However, this intuition does not give the full story. We might imagine a set

of circumstances in which the building begins with a relatively high heat load, and hence air flows upwards through the building. If the wind now increases, the pressure difference across the upper opening decreases, and hence the ventilation rate decreases. The building therefore heats (since less heat is being vented). This increase in heat increases the buoyancy pressure acting on the upper opening. Alternatively, imagine again a building with a very high heat load, in which the flow is upwards through the building. As the heat load is reduced, the ventilation rate will decrease. If the ventilation rate reaches zero, then any heat load present will cause the building to warm up again. There is therefore no positive heat load at which the building will change smoothly to ventilate in the opposite direction (since such a change would have to pass through a point of zero ventilation). The behaviour of the building is therefore difficult to predict intuitively. This problem has been considered before, notably in Li and Delsante (2001), Li, Delsante, Chen, Sandberg, Andersen, Bjerre, and Heiselberg (2001), Gladstone and Woods (2001), Heiselberg, Li, Andersen, Bjerre, and Chen (2004) and Hunt and Linden (2004). All of these studies find that, at low heat loads, three equilibrium regimes exist: a cool, stable wind driven regime; an unstable wind driven regime, and a warm, stable, buoyancy driven regime. The building temperature, plotted as a function of heat load (see, for example, figure 3.1), exhibits hysteresis, so that the current state is dependent not only on the current conditions, but also on the previous building states. Such multiple steady states cause several problems to building designers and controllers. Most notably:

- it may be difficult to predict whether the building is in a hot, buoyancy driven regime or a cold, wind driven regime,
- it may be difficult to maintain temperatures corresponding to the unstable wind driven regime, and
- the building may oscillate between warmer and cooler equilibria as e.g. wind forcing and heating change, leading to occupant discomfort.

In this thesis, we aim to investigate the multiple steady states caused by competition between wind and buoyancy. In chapter 3, we investigate the transient behaviour of the system as the forcing (due to wind and buoyancy) changes. In particular, we assess the impact of changing the wind forcing, and investigate how this affects the flow regime in the building, and how the temperature changes throughout the nonlinear evolutions. This understanding of the response of the flow to changes in forcing provides invaluable insights for developing strategies to control the system.

Finally, we note that multiple steady states can also occur in the absence of wind (Chenvidyakarn and Woods 2005). It is possible that some of the methodology of this thesis might be applicable to these other problems, and this seems a useful direction for further investigation.

### 2.2.5. Thermal mass

So far we have examined the literature on naturally ventilated buildings, and discussed how the interaction of wind and buoyancy leads to multiple flow regimes for identical operating conditions. Here we note that many buildings have significant thermal mass, which acts as a reservoir for heat and leads to a phase lag between external changes and corresponding variations in air temperature, and hence must be included in the temperature dynamics. This section gives a brief background: chapter 4 then provides a methodology for incorporating the effects of thermal mass into the multiple states problem described above.

Thermal mass in a building acts as a temperature buffer, attenuating the effects of temperature variations due to the diurnal cycle, and also causing the interior temperature variation to lag the exterior (Holford and Woods 2007). This can be extremely useful in designing comfortable, low energy buildings: for example, the high temperatures which might occur in the mid-afternoon in a lightweight building can be attenuated, and the peak temperature delayed until a period of low usage. However, in a cold climate, buildings with a high thermal mass may be much more expensive to heat effectively during the day

(stone cathedrals, for example) and so the introduction of extra thermal mass involves economic and practical tradeoffs.

In chapter 4 we consider how the introduction of thermal mass may affect the conclusions of chapter 3. In particular, we investigate how the introduction of thermal mass, and the associated phase lags, lead to a separation of timescales in the transient evolutions discussed in chapter 3. We also assess whether the heat absorbed by the thermal mass stops overheating and eliminates some of the warm regimes.

It is therefore useful to be able to incorporate the effects of thermal mass into our modelling of building temperature evolution. For most heat sources, the heating rate can be determined directly. However, the heat provided by thermal mass depends on the temperature difference between mass and interior air, and hence the interior temperature distribution in the building. For a building with a well mixed interior and distributed thermal mass we can simplify the problem to that of two coupled equations, one describing the temperature evolution of the interior fluid, and one describing the temperature evolution of the thermal mass. The rate at which the thermal mass supplies energy to the building interior is given by

$$H_{tm} = \chi S_{tm}(T_{tm} - T_i) \tag{2.15}$$

where $\chi$ is a heat transfer coefficient, $S_{tm}$ is the internal surface area of the mass, and $T_{tm}$ and $T_i$ are the respective temperatures of the thermal mass and the interior fluid. This rate of change of energy can then be incorporated into equation 2.12.

As the thermal mass supplies energy to the interior, the temperature of the thermal mass also changes. The thermal mass temperature evolution is given by

$$\rho_{tm} C_{ptm} V_{tm} \frac{dT_{tm}}{dt} = \chi S_{tm}(T_i - T_{tm}) \tag{2.16}$$

where the subscript $tm$ refers to the thermal mass. By combining equations

2.12, 2.15 and 2.16 it is possible to analyse the temperature evolution of the interior fluid and the thermal mass. In general, $\rho_{tm}C_{ptm}V_{tm} \gg \rho C_p V$ (i.e. the thermal mass of the air in the building is relatively small) and so the thermal mass temperature evolves much more slowly than the interior fluid temperature. For a full example of how such models can be used, see chapter 4 of this thesis, or see Holford and Woods (2007), who use thermal mass models like those above to investigate the effect of thermal mass on building behaviour with a sinusoidally varying exterior temperature, as in a typical day.

### 2.2.6. Water modelling of natural ventilation

This subsection gives background relating to the experimental work undertaken for this thesis. The experimental work is explained in each chapter, and further information on the experiments is given in appendix A.

Experimental models complement theoretical predictions both by providing support for theory and by suggesting new directions for investigation. It is therefore extremely useful to model ventilation flows experimentally. One possibility is to use actual buildings, with temperature sensors in place, as experimental models (see, for example, Fitzgerald, Lomakina, Livermore, Lishman, Walker, Norford, Gladstone, and Woods (2004)). However, such experiments are difficult to control, for example since buildings are usually occupied and hence may have unknown varying heat loads. Water bath modelling can allow building ventilation flows to be investigated experimentally on a laboratory scale, whilst allowing full control of experimental parameters (Linden 1999).

Experimental models are usually scaled on real rooms and buildings in the range $1:20-1:100$ (Hunt and Linden 1999), and made from transparent cast acrylic (Perspex). These models are placed inside a larger tank of water, which represents the ambient air. In many models, salt water, which is denser than fresh water, is injected, and acts as a source of negative buoyancy. The results of such experiments can then be inverted to show the effects of a source of positive buoyancy. Alternatively, the ambient may be made up of salt water, and fresh water injected (Woods, Chenvidyakarn, and Short 2003). Such methods

are useful when representing a point source of buoyancy, since salt water can be injected at a single point. It is more difficult, however, to produce a constant, controllable areal source of salinity, so more recent experiments have used heating plates to model distributed sources (Gladstone and Woods 2001; Fitzgerald and Woods 2004). In such experiments, a wire of given resistance (often $\sim 1$ ohm) is distributed evenly over a heatproof plate, and connected to a controllable power supply. By controlling the voltage across the hotwire, the heating power supplied to the building is controlled (since $P = V^2/R.$) Temperatures inside and outside the building model can be recorded using thermocouples. Variations in density can be observed using a shadowgraph technique, which can then be recorded and manipulated into more quantitative measurements using digital image processing (Dalziel 1993).

It is necessary to use water rather than air so that dimensional consistency is maintained while operating on a laboratory scale. Two dimensionless numbers are important for such dynamic similarity. For turbulent ventilation flows the Reynolds number $Re$ is the important dimensionless parameter,

$$Re = \frac{(g'l)^{\frac{1}{2}}l}{\nu} \tag{2.17}$$

where g' is the reduced gravity of the flow, $l$ is a lengthscale, and $\nu$ is the kinematic viscosity of the fluid (Gladstone and Woods 2001). Typical full scale values might be $g' \sim 0.4\text{ms}^{-2}$, $\nu \sim 10^{-5}\text{m}^2\text{s}^{-1}$, and $l \sim 5m$, which gives a Reynolds number $Re \sim 10^5$. Typical values for a water model might be $g' \sim 0.1\text{ms}^{-2}$, $\nu \sim 10^{-6}\text{m}^2\text{s}^{-1}$, and $l \sim 0.3m$, which gives a Reynolds number $Re \sim 10^4$. These Reynolds numbers are both sufficiently large that the flow will be turbulent in both cases, and hence dynamic similarity is maintained.

The second important dimensionless number is the Rayleigh number, which describes the relative importance of conduction and convection in heat transfer. The Rayleigh number is given by

$$Ra = \frac{g'l^3}{\kappa\nu} \tag{2.18}$$

where $\kappa$ is the thermal diffusivity of the fluid, and $\kappa \sim 10^{-5}\mathrm{m}^2\mathrm{s}^{-1}$ for air and $\kappa \sim 10^{-7}\mathrm{m}^2\mathrm{s}^{-1}$ for water. This leads to Rayleigh numbers of roughly $10^{11}$ for our typical full scale building, and roughly $10^{10}$ for the laboratory model. These high Rayleigh numbers indicate that in both cases the conductive heat flux is small compared to the convective flux, and hence to leading order it can be neglected and the system is well mixed (Gladstone and Woods 2001).

A full description of the experiments used in this thesis is given later in the thesis.

### 2.2.7. Further considerations

Finally, we note that there are further aspects of natural ventilation problems which might, in conjunction with the multiple states problem discussed in this thesis, lead to interesting new science: these include, for example, the effects of multiple stacks (Chenvidyakarn and Woods 2005), of cooling (Chenvidyakarn and Woods 2004), the introduction of multiple interconnected rooms (Livermore and Woods 2007b) and considerations of the effects of poor insulation (Livermore and Woods 2007a). Linden (1999), chapter 8, discusses such "complex effects". However, before considering the interactions between such complex effects, it is important to understand the interaction between wind and buoyancy fully. This understanding will be developed over the next two chapters.

# 3. Flow regime transitions caused by varying wind

*The interaction between wind and buoyancy in naturally ventilated buildings can lead to multiple steady states, as discussed in the literature review. Previous studies have shown that there may exist a stable wind dominated regime, an unstable wind dominated regime, and a stable buoyancy dominated regime. Here we examine the transient evolutions between these regimes which may occur, focussing specifically on the effects of varying the wind forcing. We show that the transition from the wind dominated regime to the buoyancy dominated regime occurs at a fixed wind, and that a directly analogous transition occurs under varying heating. However, the reverse transition, from the buoyancy dominated regime to the wind dominated regime, depends on both the magnitude and rate of change of the wind, and has no analogue under varying heating. We provide critical relations to determine the instantaneous increase in wind required for the system to evolve to the wind dominated regime, and to determine the minimum rate of change of wind forcing under which such a transition may occur. We support our model with new analogue water bath experiments, and the implications for building design are discussed.*

## 3.1. Introduction

To develop control systems for naturally ventilated buildings, it is useful to develop an understanding of the ventilation flows using simplified analytical models. In a large open-plan space with one upper and one lower level opening, it has been shown that the non-linear interaction of wind-induced pressure gradients and the buoyancy forces associated with internal heating can lead

to multiple flow regimes (Li, Delsante, Chen, Sandberg, Andersen, Bjerre, and Heiselberg 2001; Li and Delsante 2001; Hunt and Linden 2004; Gladstone and Woods 2001). The existence of such multiple non-linear steady states, corresponding to a wind-dominated flow and a buoyancy dominated flow, may be extremely challenging for the design of a control system. By understanding the physics of how the different states develop, there is a chance to control the building effectively. The previous studies cited show that for a building similar to that shown in figure 3.1, both a warm buoyancy dominated regime (the dotted line on figure 3.1, which is reproduced from the literature and can be derived from equation 3.4) and a cold wind dominated regime (the solid line on figure 3.1) exist and are stable to small perturbations in temperature. There is also an unstable wind dominated solution (the dashed line on figure 3.1), of intermediate temperature, which connects the buoyancy dominated and stable wind dominated solution branches. Spatially averaged flow models (Li, Delsante, Chen, Sandberg, Andersen, Bjerre, and Heiselberg 2001; Hunt and Linden 2004) and numerical models (Heiselberg, Li, Andersen, Bjerre, and Chen 2004) suggest that for all initial conditions in the shaded area of figure 3.1, the flow evolves to the steady wind dominated regime. Similarly, for all initial conditions in the unshaded area, the flow evolves to the stable buoyancy dominated regime.

These predictions have been tested using analogue water bath experiments in which the effect of changes in the heating load was explored for a fixed wind forcing (Li, Delsante, Chen, Sandberg, Andersen, Bjerre, and Heiselberg 2001; Hunt and Linden 2004). The experiments show there are multiple steady states as predicted by the model. The experiments also show that, for both point sources and distributed sources of heating, the building state evolves from the wind dominated regime to the buoyancy dominated regime if the heat input increases sufficiently. This transition is illustrated by arrow (a) on figure 3.2. The experimental data also shows that if the heat load is then reduced back to its original value, the system will initially remain in the buoyancy dominated

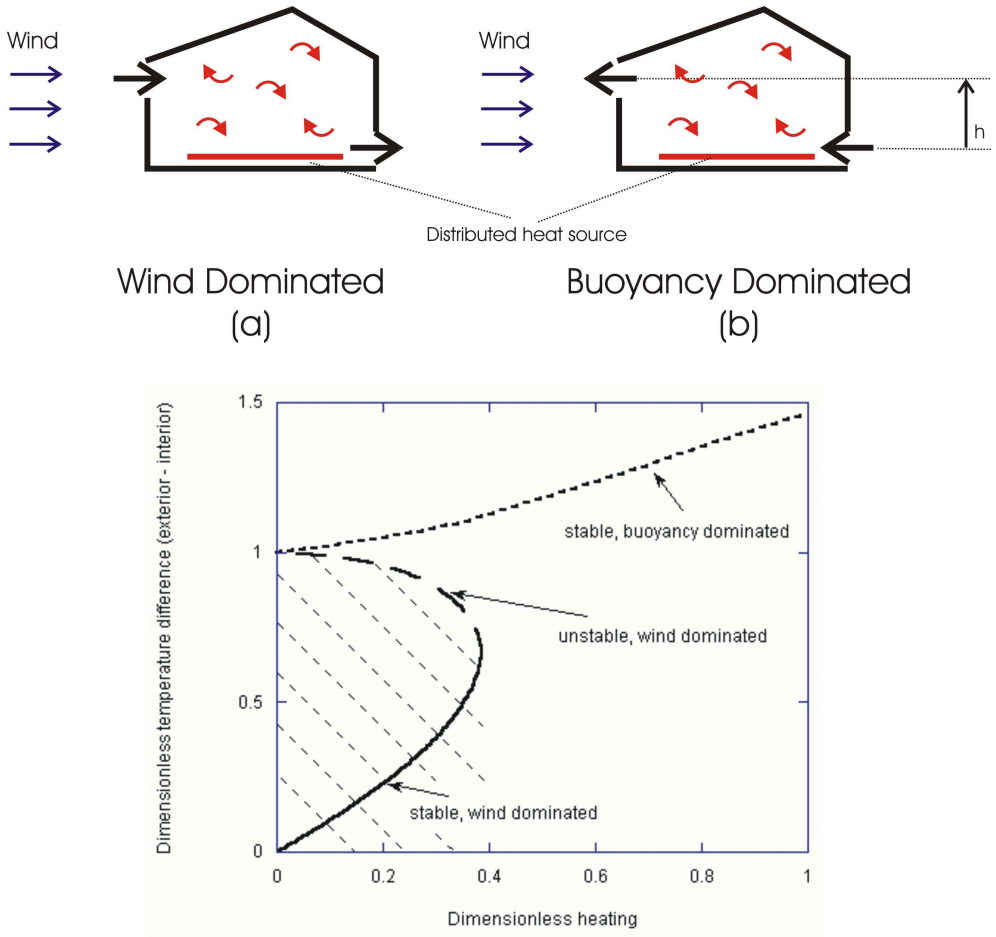


Figure 3.1.: *A schematic showing the two possible regimes in our two opening case: on the left, a wind dominated solution, with flow from left to right, and on the right, a buoyancy dominated solution, with flow from right to left, upwards through the building. The equilibria of the system, as a function of heat load, are plotted below: a warm, stable, buoyancy dominated regime (dotted line); a cold, stable, wind dominated regime (solid line); and an intermediate, unstable wind dominated regime (dashed line). Any state in the shaded area of the graph will converge to the stable wind dominated solution, while any state in the unshaded area will converge to the stable buoyancy dominated solution.*

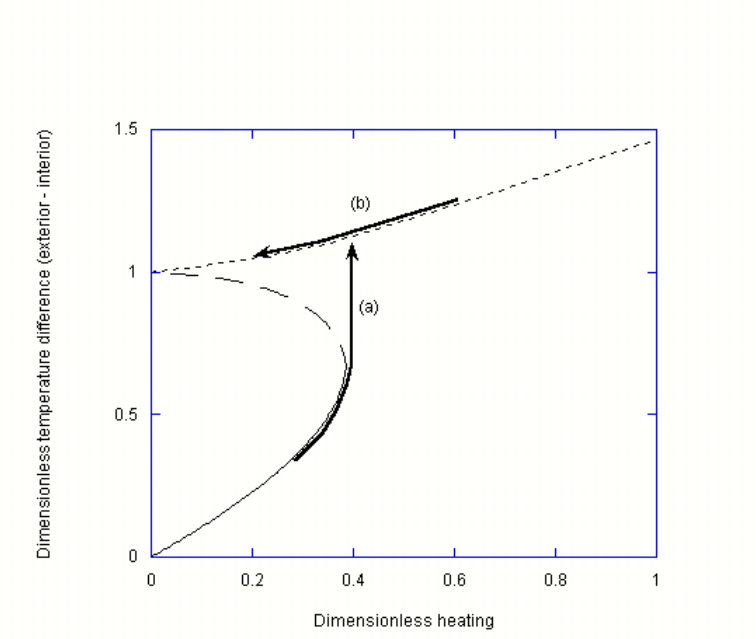


Figure 3.2.: *Variation of the temperature relative to the exterior as a function of dimensionless heating load, for a fixed wind forcing. The solid line represents the linearly stable wind dominated regime; the dashed line the linearly unstable wind dominated regime; and the dotted line represents the linearly stable buoyancy dominated regime.*

regime, exhibiting hysteresis (arrow (b) on figure 3.2). If the heat load is reduced to small values, the difference in temperature between the stable buoyancy dominated solution and the unstable wind dominated solution becomes very small (near the point $\theta = 1$ on figure 3.2). In this case it is possible for the system state to evolve back to the stable wind dominated regime, although the buoyancy dominated regime is stable for sufficiently small perturbations, and the exact mechanism by which the flow direction reverses is not well understood.

In contrast to these studies of the effect of changes in heating load with fixed wind forcing, here we explore the effect of changes in wind forcing for a fixed heating load. This is motivated by the observation that in some situations the wind forcing on a building may change with time, while the heat loads may remain steady. Although there has been some initial experimental analysis of the effect of changing wind forcing with a constant heat load (Hunt and Linden 2004) there has not been a systematic analysis of the transient evolution of

the system as wind changes from one value to another over a finite time. This forms the subject of this chapter. We find that the transition from the wind dominated regime to the buoyancy dominated regime associated with a decrease in the wind is directly analogous to that associated with an increase in the heating load (see line (a) on figure 3.2). However, we find that if the system is initially in the buoyancy dominated regime, then for a sufficiently large increase in wind the transient flow depends critically on the rate of change of wind. A rapid increase in wind forcing causes a transition to the wind dominated regime, while with a more gradual change in wind forcing the system remains in the buoyancy dominated regime. There is no analogous transition from the buoyancy dominated regime to the wind dominated regime associated with changes in the heating load.

This chapter is organised as follows. First, we develop a model describing the transitions in flow regime as a function of changes of wind forcing. We then explore two limiting cases: first with very slow changes in wind, such that the system evolves along a series of quasi-steady states; and second with instantaneous changes in wind, such that the system temperature remains constant during the variation in wind. We then produce numerical solutions showing the behaviour of the system under finite-timescale transitions in wind, and develop a relation for the critical rate of change of wind forcing which leads to a transition to the buoyancy dominated regime. We detail a series of new analogue water bath experiments which test the predictions of our model. Finally, we discuss the implications for building control and design.

## 3.2. Model

We consider a model building in which there is a distributed heat load at the floor, and a wind pressure difference $\Delta p_w$ between one side of the building and the other. The building is lightweight and well insulated, so the heating primarily affects the temperature of the air (cf. Linden, Lane-Serff, and Smeed (1990, Gladstone and Woods (2001)). We assume the building has openings

at a high level on the upwind side, and at a low level on the downwind side, both with area $A$, as shown in figure 3.1. The model can be extended to varying opening areas by combining these into a single effective area (Linden, Lane-Serff, and Smeed 1990). We assume that the underfloor distributed heating leads to high-Rayleigh-number convection and hence a well mixed interior, or that there is some mechanical mixing (Gladstone and Woods 2001). We also assume that the vertical extent of the windows is small compared to the height of the room, and hence at each opening the flow is purely in- or outflow, as controlled by the pressure difference across the mid-height of that opening (Linden 1999):

$$q_x = c^* A_x \sqrt{\frac{\Delta p_x}{\rho}}, \tag{3.1}$$

where $q_x$ is the volume flow through an opening, $A_x$ is the area of that opening, $\Delta p_x$ is the pressure difference across the opening, $c^*$ is a loss coefficient, and $\rho$ is the fluid density. For convenience, we assume that the loss coefficient $c^*$ is the same for each opening of our model.

As well as the constant pressure difference $\Delta p_w$ between the upper and lower openings, there is a hydrostatic pressure $\Delta p_b$ between the two openings caused by the density difference between the cold exterior air and warm interior air. This is given by $\Delta p_b = \rho g' h$, where $\rho$ is a reference density of the fluid, and $h$ is the distance between the mid-heights of the two openings. $g'$ is the reduced gravity defined in terms of the temperature difference between the interior and exterior, $\Delta T$, and related to gravity $g$ by $g' = \frac{\Delta T g}{T}$ for air (with $T$ measured in K), and $g' = \frac{\beta g \Delta T}{\rho}$ for water, where $\beta$ is an expansion coefficient, with units of $\mathrm{kgm^{-3}K^{-1}}$ (Turner 1973). A mass balance, under the Boussinesq approximation of effective incompressibility, gives us that the pressure differences across the openings must be equal. We then use a heat balance to equate the rate of change of thermal energy in the building to the energy added from the heat source minus the thermal energy which is vented as warm air leaves the building:

$$\rho C_p V \frac{d\Delta T}{dt} = H - \rho C_p q \Delta T \tag{3.2}$$

where $V$ is the building volume, $H$ is the heat supplied, $C_p$ is the specific heat capacity, and $q$ is the volume flux through either opening. By combining equations 3.1 and 3.2 with a mass balance in the building, we find the temperature evolution in the building is given by:

$$\rho C_p V \frac{d\Delta T}{dt} = H - \rho C_p c^* A \Delta T \sqrt{\frac{|\Delta p_w - \beta g h \Delta T|}{2\rho}} \tag{3.3}$$

(cf. Li, Delsante, Chen, Sandberg, Andersen, Bjerre, and Heiselberg (2001, Hunt and Linden (2004)). In this work we investigate changes in wind forcing on the flow and hence we scale the wind forcing, as measured by the wind-induced pressure differences across the building, relative to the initial pressure difference due to wind forcing $\Delta p_0$. We can then write in dimensionless form

$$\frac{d\theta}{dt^*} = Q - \theta \sqrt{|\hat{W} - \theta|} \tag{3.4}$$

where $\hat{W} = \frac{\Delta p_w}{\Delta p_0}$, and represents the ratio of the wind forcing to the initial wind forcing. The dimensionless temperature difference between the interior and the ambient $\theta = \frac{\Delta T}{\Delta T_w}$, where $\Delta T_w = \frac{\Delta p_0}{\beta g h}$ represents the temperature contrast which would be required to produce a pressure difference $\Delta p_0$ over the height of the building due to the buoyancy of the air. Time is scaled relative to the time for the air in the building to be replaced by wind driven flow with rate $v_w = c^* A \sqrt{\Delta p_0 / \rho}$, such that $t^* = \frac{c^* A \sqrt{\Delta p_0}}{\sqrt{2}\rho V} t$. The dimensionless heat load $Q = \frac{H}{H_w}$ where $H_w = \rho C_p \Delta T_w v_w$ i.e. $Q = \frac{\sqrt{2}\beta g h}{\sqrt{\rho} C_p c^* A \Delta p_0 ^{\frac{3}{2}}} H$.

Equilibrium temperature solutions of equation 3.4 are shown in figure 3.3 as a function of $\hat{W}$ for the case in which $Q = \frac{\sqrt{3}}{9}$ (cf. figure 3.1). The dotted line A corresponds to the stable buoyancy dominated solution; the solid line B to the stable wind dominated solution; and the dashed line C to the unstable wind dominated solution. By comparison to figure 3.1, we find that any state $(\hat{W}, \theta)$ within the shaded region tends to the stable wind dominated equilibrium (as the temperature varies according to equation 3.4), while all other solutions tend to the buoyancy dominated equilibrium.

In general a change in wind forcing leading to a change from $\hat{W} = 1$ to

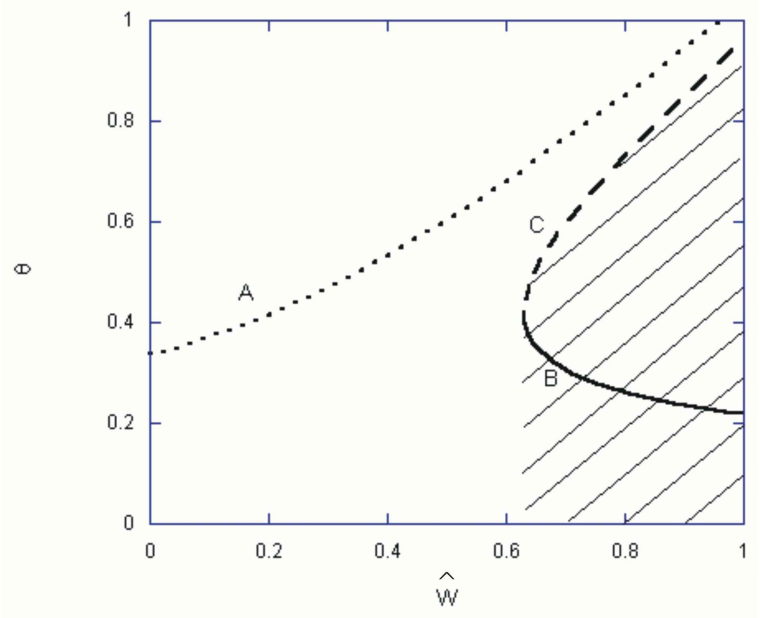


Figure 3.3.: *Variation of the temperature relative to the exterior as a function of dimensionless wind, for a fixed heating load. The dotted line A represents the linearly stable buoyancy dominated regime; the solid line B represents the linearly stable wind dominated regime; and the dashed line C the linearly unstable wind dominated regime. If the system begins in the shaded area, the temperature tends towards the stable wind dominated equilibrium; otherwise, it tends towards the stable buoyancy dominated equilibrium.*

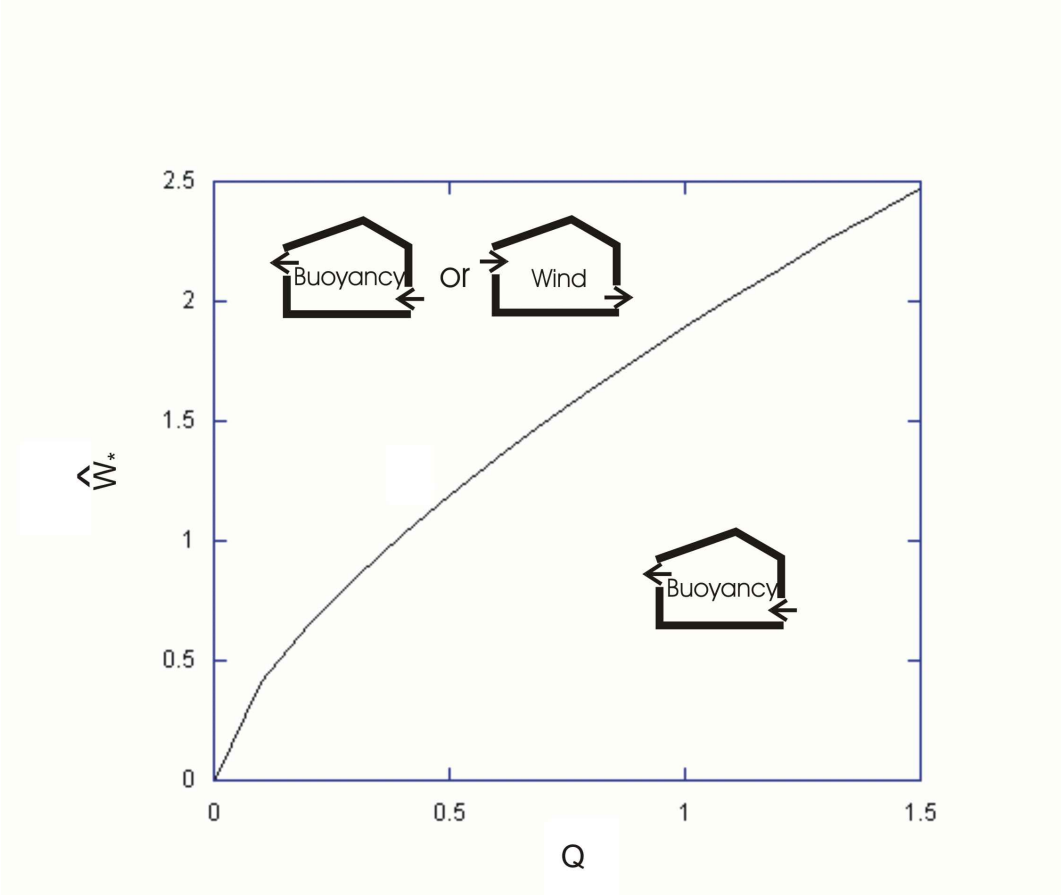


Figure 3.4.: *Plot showing the minimum wind forcing for which a wind dominated regime exists, $\hat{W}_*$, as a function of heat load $Q$. Above this wind, both a buoyancy dominated and a wind dominated regime exist, as indicated: below it, only a buoyancy dominated regime exists.*

$\hat{W} = \hat{W}_1$ occurs over some dimensionless timescale $\tau$. If $\tau \gg 1$ then the wind changes very slowly and we expect the system to evolve as a series of quasi-steady states. If $\tau \ll 1$ the system behaves as if the wind changes instantly and then the system responds according to equation 3.4. In the next section, we begin by examining these two limiting cases before investigating the more general case when $\tau \sim 1$.

## 3.3. Variations in the wind

### 3.3.1. Slow changes in wind: $\tau \gg 1$

We begin by investigating the system evolution with $\tau \gg 1$. When the changes in wind are much slower than the timescale of temperature evolution, the building temperature follows the equilibrium temperature as the wind varies.

First, we determine the initial flow regime in the building. The minimum wind forcing for which the wind dominated regime can exist is found from equation 3.4 to be (cf Hunt and Linden (2004))

$$\hat{W}_* = 3\left(\frac{Q}{2}\right)^{\frac{2}{3}} \tag{3.5}$$

and this minimum wind is plotted in figure 3.4 as a function of $Q$. This provides an important condition on the initial flow regime in the building, when $\hat{W} = 1$. If $\hat{W}_* > 1$ then only a buoyancy dominated regime exists, and so the building must begin in the buoyancy dominated regime. This corresponds to the case $Q > Q_c = \frac{2\sqrt{3}}{9}$. If $\hat{W} \leq 1$, then the building may begin in either regime. This corresponds to the case $Q \leq Q_c = \frac{2\sqrt{3}}{9}$. We consider each of these cases in turn.

$Q > Q_c$

Figure 3.5a shows the equilibria of equation 3.4, as a function of the wind forcing $\hat{W}$, for the case $Q = 2Q_c$. With this heat load, the building is initially in the buoyancy dominated regime. The buoyancy dominated equilibrium is shown as a dotted line, the stable wind dominated equilibrium as a solid line, and the unstable wind dominated equilibrium as a dashed line. Superimposed onto these equilibria as thick black arrows are possible temperature evolutions, where under a slowly changing wind the building temperature follows the equilibrium temperatures. In this case the system remains in the buoyancy dominated regime.

$Q < Q_c$

Figure 3.5b shows a plot of temperature as a function of $\hat{W}$ for $Q = Q_c/2$. Here, $Q < Q_c$, and so both regimes exist for $\hat{W} = 1$ and the system may begin

either in the buoyancy dominated regime (point $o_b$ on figure 3.5b) or in the wind dominated regime (point $o_w$ on figure 3.5b). Again, the buoyancy dominated equilibrium is shown as a dotted line, the stable wind dominated equilibrium as a solid line, and the unstable wind dominated equilibrium as a dashed line.

The possible evolutions for such a system, with $\tau \gg 1$, are shown as thick arrows. Under varying wind, the system evolves along the equilibria of the regime in which it begins. The only change in regime occurs when the system begins in the wind dominated regime, and then the wind changes such that only a buoyancy dominated regime exists (from equation 3.5 we find that the critical wind in this case is $\hat{W}_* = \frac{1}{2}^{\frac{2}{3}}$).

The behaviour of the system with such slow changes in wind ($\tau \gg 1$) is fundamentally different to that with fast changes ($\tau \ll 1$), which we discuss in the next subsection.

### 3.3.2. Fast changes in wind: $\tau \ll 1$

We now investigate the effects of fast changes in the wind from $\hat{W} = 1$ to $\hat{W} = \hat{W}_1$. Under such changes, the temperature is assumed constant during the change in wind: the temperature then evolves to equilibrium at the fixed final wind value $\hat{W}_1$.

$Q > Q_c$

As in section 3.1, if $Q > Q_c$, then the system is initially in the buoyancy dominated regime. Figure 3.6a shows again the equilibria of equation 3.4, as a function of the wind forcing $\hat{W}$, for the case $Q = 2Q_c$ (cf figures 3.3; 3.5a). The buoyancy dominated equilibrium is shown as a dotted line, the stable wind dominated equilibrium as a solid line, and the unstable wind dominated equilibrium as a dashed line. Superimposed onto these equilibria as thick black arrows are possible temperature evolutions. In this case, three qualitatively different evolutions can occur. If the wind increases by a small amount, as in the transition $o - b - b'$ then the system tends to the buoyancy dominated equilibrium. If the wind increases by a larger amount, $o - c - c'$, then the system

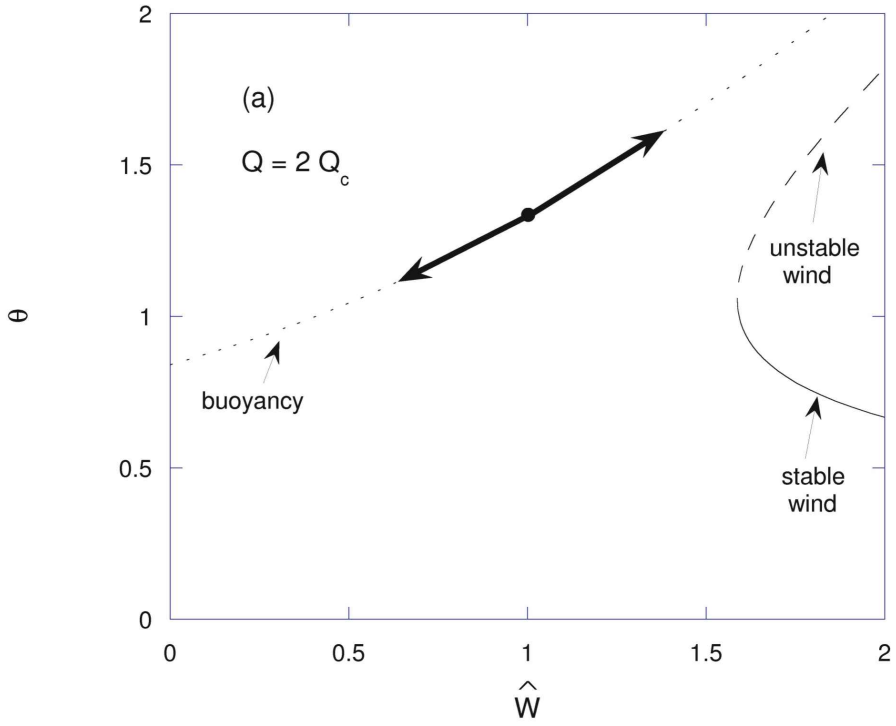


Figure 3.5a.: *System evolution under varying winds, with $\tau \gg 1$. The plot shows the equilibrium temperatures as a function of wind for the stable wind dominated regime (solid line), unstable wind dominated regime (dashed line) and buoyancy dominated regime (dotted line), for $Q = 2Q_c$. The system begins in the buoyancy dominated regime, and, under slowly changing wind, evolves along the buoyancy dominated solution.*

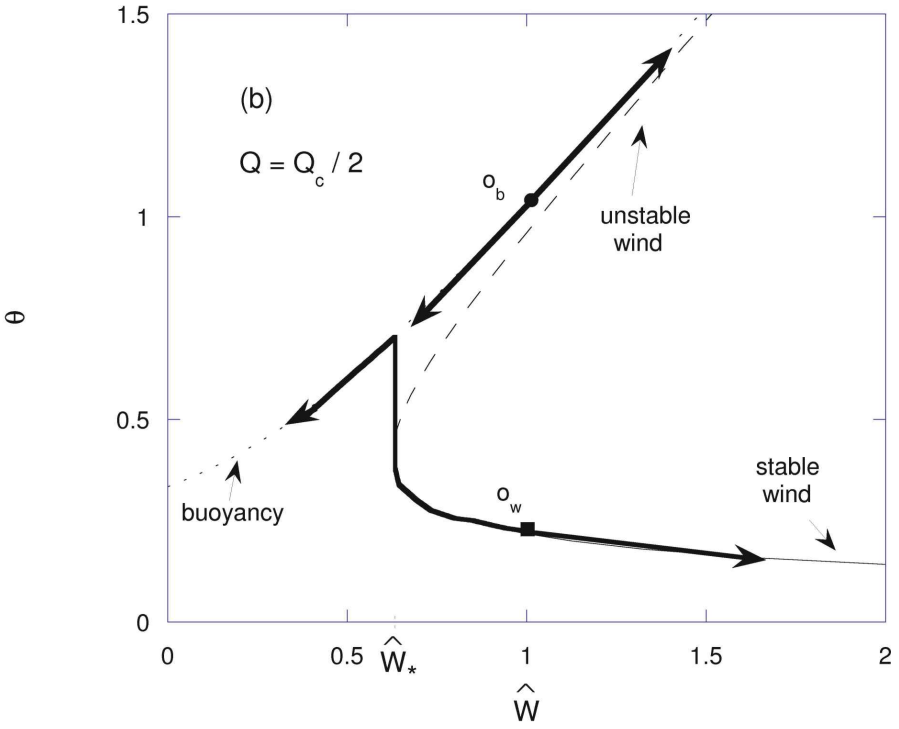


Figure 3.5b.: *System evolution under varying winds, with $\tau \gg 1$. The plot shows the equilibrium temperatures as a function of wind for the stable wind dominated regime (solid line), unstable wind dominated regime (dashed line) and buoyancy dominated regime (dotted line), for $Q = Q_c/2$. Under slowly changing wind, if the system begins in the buoyancy dominated regime (at the circular marker), the temperature evolves along the buoyancy dominated solution. If the system begins in the wind dominated regime (at the square marker), the temperature evolves along the wind dominated solution, switching to the buoyancy dominated solution when no wind dominated solution exists (i.e. if $\hat{W}_1 < \hat{W}_*$).*

tends to the wind dominated equilibrium. If the wind decreases, $o-d-d'$ then the system remains in the buoyancy dominated regime.

$Q < Q_c$

Figure 3.6b shows a plot of temperature as a function of $\hat{W}$ for $Q = Q_c/2$. Here, $Q < Q_c$, and so both regimes exist for $\hat{W} = 1$ and the system may begin either in the buoyancy dominated regime (point $o_b$ on figure 3.6b) or in the wind dominated regime (point $o_w$ on figure 3.6b). The buoyancy dominated equilibrium is shown as a dotted line, the stable wind dominated equilibrium as a solid line, and the unstable wind dominated equilibrium as a dashed line. Again, if the system begins in the buoyancy dominated regime, there are three qualitatively different possible evolutions. If the wind increases by a small amount, as in the transition $o_b - b - b'$ then the system tends to the buoyancy dominated equilibrium. If the wind increases by a larger amount, $o_b - c - c'$, then the system tends to the wind dominated equilibrium. If the wind decreases, $o_b - d - d'$ then the system remains in the buoyancy dominated regime. If the system begins in the wind dominated regime, three possible evolutions can occur. If the wind increases, $o_b - e - e'$, then the system remains in the wind dominated regime. If the wind decreases but remains above the critical wind, $\hat{W}_1 \geq \hat{W}_*$, $o_b - f - f'$ then the system remains in the wind dominated regime. If the wind decreases to below the critical wind, $\hat{W}_1 < \hat{W}_*$, as in transition $o_b - g - g'$, then the system evolves to the buoyancy dominated regime.

The analysis above suggests there is a minimum instantaneous increase in wind forcing, above which the system will evolve to the wind driven regime. This is marked as $\hat{W}_{**}$ on figure 3.6a. This critical value may be found by noting that the system will evolve to the stable wind dominated equilibrium if and only if it crosses the wind dominated equilibrium. This equilibrium is usually the unstable equilibrium: however, if the initial wind is low enough the system may cross the stable wind dominated equilibrium. In either case, the analysis is the same. In the initial state, the system is in equilibrium in the buoyancy dominated regime with $\hat{W} = 1$, and so $\theta$, the temperature, satisfies,

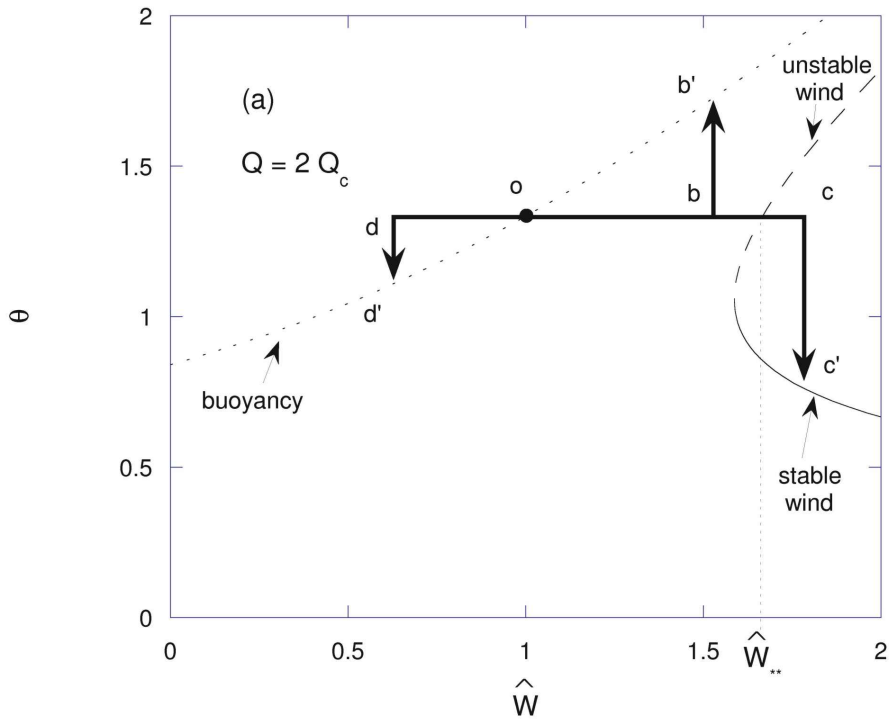


Figure 3.6a.: *System evolution under varying winds, with $\tau \ll 1$. The plot shows the equilibrium temperatures as a function of wind for the stable wind dominated regime (solid line), unstable wind dominated regime (dashed line) and buoyancy dominated regime (dotted line), for $Q = 2Q_c$. The system begins in the buoyancy dominated regime. The wind changes instantaneously, and then the system evolves, at a fixed wind, to equilibrium. If the wind increases by a sufficient amount ($\hat{W}_1 > \hat{W}_{**}$), the system evolves to the wind dominated regime.*

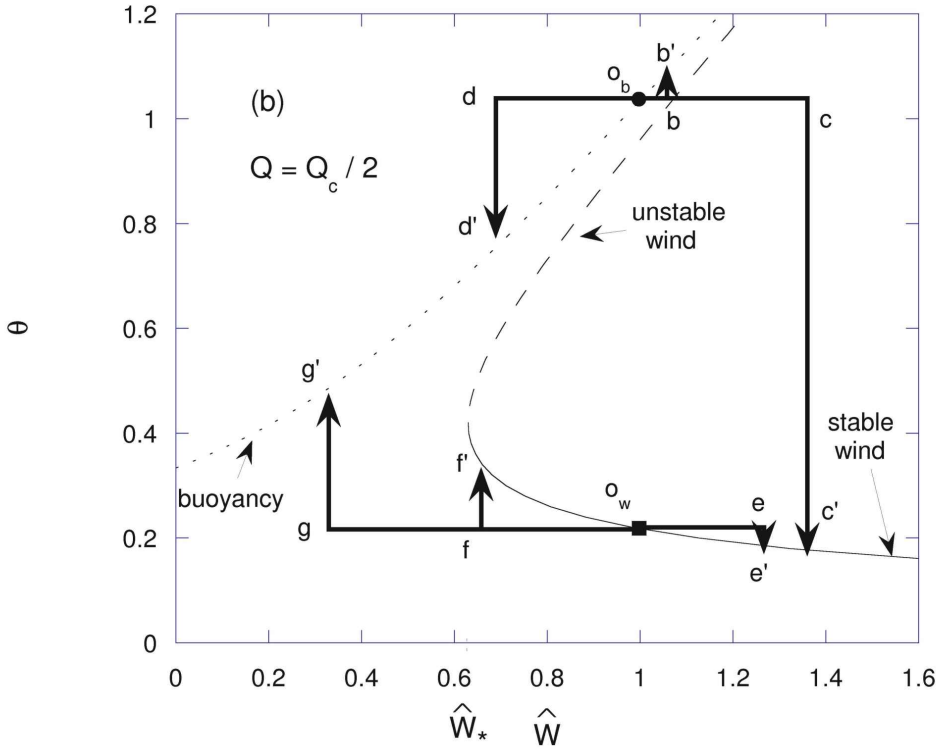


Figure 3.6b.: *System evolution under varying winds, with $\tau \ll 1$. The plot shows the equilibrium temperatures as a function of wind for the stable wind dominated regime (solid line), unstable wind dominated regime (dashed line) and buoyancy dominated regime (dotted line), for $Q = Q_c/2$. If the system begins in the buoyancy dominated regime (at the circular marker), then given a sufficient increase in wind the system will evolve to the wind dominated regime (e.g. the trajectory marked $o_b - c - c'$.) If the system begins in the wind dominated regime (at the square marker), the system will evolve to the buoyancy dominated solution when no wind dominated solution exists (e.g. the trajectory marked $o_w - g - g'$.)*

$$\theta(\theta-1)^{\frac{1}{2}} = Q \tag{3.6}$$

The minimum final wind forcing $W_{**}$ which can lead to a regime change is that at which the temperature $\theta$ is also an equilibrium solution for the wind dominated regime (usually the unstable wind dominated regime):

$$\theta(\hat{W}_{**}-\theta)^{\frac{1}{2}} = Q \tag{3.7}$$

Once the building state crosses the wind dominated solution, $\frac{d\theta}{dt}$ becomes negative, and the building will cool to the stable solution. Combining equations 3.6 and 3.7, we find a relationship between $\theta$ and $\hat{W}_{**}$,

$$\theta = \frac{\hat{W}_{**}+1}{2} \tag{3.8}$$

and it follows from 3.7 that

$$\hat{W}_{**}^3 + \hat{W}_{**}^2 - \hat{W}_{**} - 1 - 8\hat{Q}^2 = 0 \tag{3.9}$$

hence given the heat load $Q$ we can determine the minimum final wind forcing $\hat{W}_{**}$ which causes the system to evolve to the wind dominated regime. This critical final wind forcing $\hat{W}_{**}$ is plotted in figure 3.7 as a function of heat load $Q$. Here we see that the lower the heat load, the more likely a transition to the wind dominated regime.

### 3.3.3. Intermediate changes in wind: $\tau \sim 1$

So far we have illustrated the evolution of the system in the limiting cases of either very slow changes in wind forcing or instantaneous changes in wind forcing. However, these assumptions are simplifications, since winds vary with various time dependencies (see, for example, discussion of wind spectra in Aynsley, Melbourne, and Vickery (1977)). Here we investigate how transitions between regimes can occur under time dependent changes in wind forcing. We have shown that under both very slow changes and instantaneous changes, the wind-buoyancy transition is qualitatively similar, and occurs at the same wind

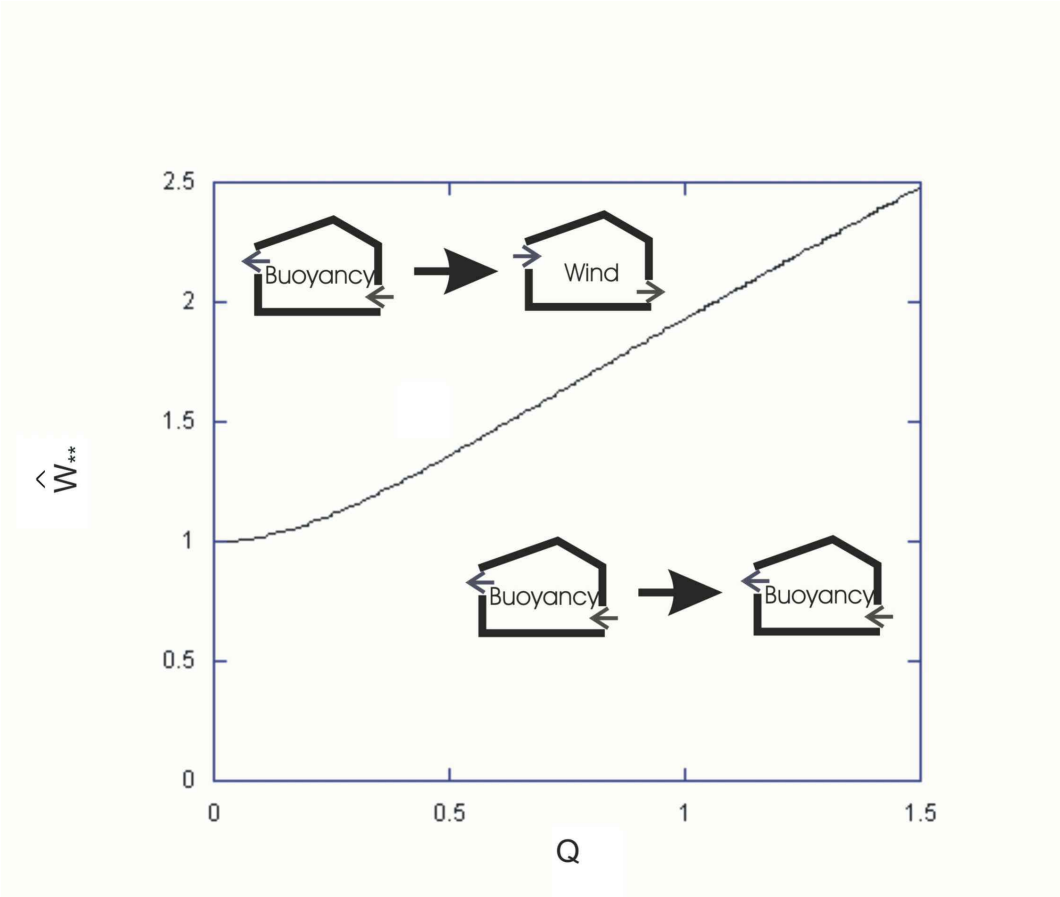


Figure 3.7.: *Plot showing the critical final wind forcing required to cause a transition from the buoyancy dominated regime to the wind dominated regime, $\hat{W}_{**}$, as a function of heat load $Q$. Given a larger final wind forcing, the system evolves to the wind dominated regime, as indicated.*

forcing. We focus here on the buoyancy-wind transition, which we have shown can occur when the wind changes on a fast timescale but not when the wind changes on a very slow timescale. We therefore expect that there exists some critical rate of change of wind, which determines whether or not the system will evolve to the wind dominated regime. To investigate the timescale-dependency further, we consider increases in wind forcing of the form

$$\hat{W}(t^*) = 1 + \eta t^* \tag{3.10}$$

where $\eta$ is the rate of increase of wind forcing. Figure 3.8 shows numerical solutions of equation 3.4 with this linearly increasing wind. The dotted lines show the equilibria of the system for $Q = 2Q_c$. The solid lines show numerically calculated temperature trajectories for $\eta = 0.3$ (marked with crosses), 0.6 (square markers), 0.9 (triangular markers), and 1.2 (circular markers). Figure 3.8 clearly shows that the final state of the system depends on the rate of increase of wind: the two faster evolutions tend towards the wind dominated solution, while the two slow evolutions remain in the buoyancy dominated regime.

We analyse this rate dependence further by investigating equation 3.4. We note that the maximum value of $\frac{d\theta}{dt^*}$ is $Q$, when $\theta = \hat{W}$. Therefore, if $\eta > Q$, the wind forcing will increase more rapidly than the temperature across all parameter space, and eventually the building state $(\theta, \hat{W})$ will cross the wind dominated curve. However, if $\eta < Q$, the increasing wind forcing will cause the system to move towards the line $\theta = \hat{W}$, and hence the temperature will increase more rapidly, tending towards $\frac{d\theta}{dt^*} = Q$. The building will therefore tend to heat up at the same rate as the increase in wind forcing, but will not cross the wind dominated curve. We therefore conclude that the transition from the buoyancy dominated regime to the wind dominated regime is time dependent, and that the critical rate of change of the wind forcing is given by

$$\eta_c = Q \tag{3.11}$$

If the dependence of wind on time has more complex functional form, the key

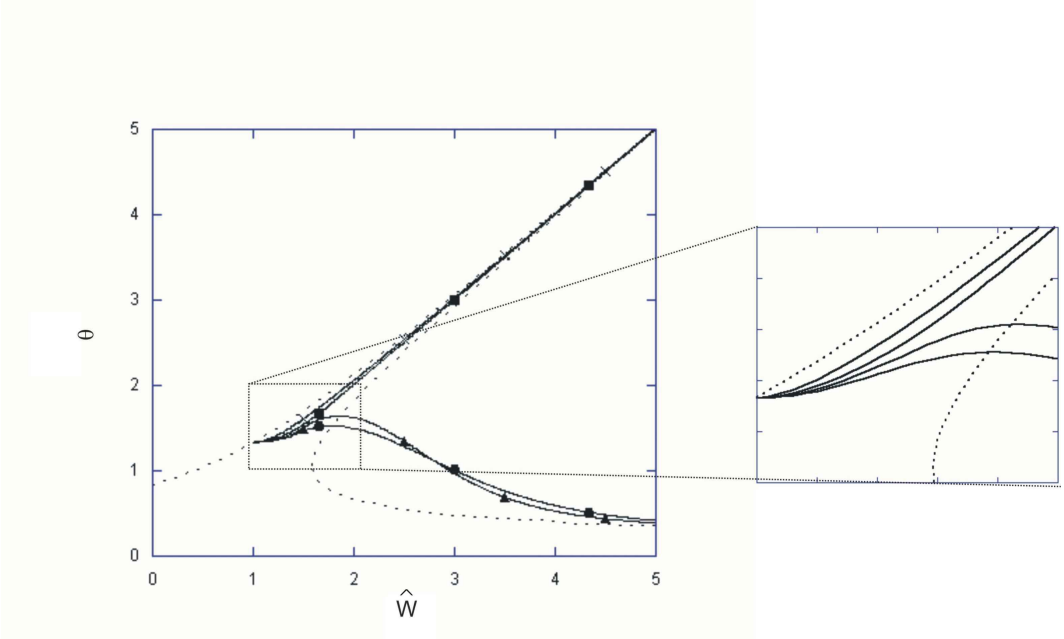


Figure 3.8.: *Numerical models of temperature evolution with linearly increasing wind. The dotted lines show the equilibria of the system for* $Q = 2Q_c$*. The solid lines show numerically calculated temperature trajectories for increasing winds with* $\eta = 0.3$ *(marked with crosses),* 0.6 *(square markers),* 0.9 *(triangular markers), and* 1.2 *(circular markers).*

requirement for the system to evolve to the wind dominated regime is that $\frac{d\hat{W}}{dt^*} > Q$ when $\theta = \hat{W}$.

## 3.4. Experiments

### 3.4.1. Structure of experiments

We have carried out new analogue laboratory experiments to test our theoretical predictions. First, we describe our experimental apparatus and test the steady state behaviour of the system. We then investigate the effect of instantaneous changes in wind. Here, the nature of transitions from the wind dominated regime to the buoyancy dominated regime is governed by the single point $\hat{W}_*$, which has already been tested experimentally in Hunt and Linden (2004). We therefore focus on the reverse transition from the buoyancy dominated regime to the wind dominated regime. Finally, we detail a preliminary experiment to show qualitatively the difference between fast and slow changes in wind.

### 3.4.2. Apparatus

The experiments are conducted using a perspex building model placed in a flume tank, in which water is pumped from one end of the tank to the other, creating a flow which serves as an analogue for wind (cf. Lishman and Woods, 2006).

The building model is a 0.1m x 0.1m x 0.1m cube. The model is placed in the flume tank in the centre of the flow, and is raised off the bottom of the flume (by roughly 0.1m). The model has a horizontal row of three circular openings at a low level on both its upwind and downwind faces, and a row at a high level (0.08m above the lower row) on both of these faces. These openings can be closed off using rubber bungs, which allows us to run experiments for various building configurations. The openings have diameter 0.01m.

The building model has a distributed hotwire covering its floor, which acts as a heating source (and hence an analogue for heating in buildings). The hotwire is controlled by a variable power supply, and can provide up to 500W heating.

The power supplied to the heating plate can be determined using multimeters to provide appropriate voltage and current measurements.

The flume tank is 3m long, 0.15m wide, and 0.35m high. Two pumps (labelled pump 1 and pump 2) deliver water from one end of the tank to the other. Pump 2 is connected to a variable ball valve, which allows two settings: fully open and half open. The flow is straightened with a series of honeycomb baffles. Dye streak tests show that the flow is reasonably constant across the cross section of the tank.

Temperatures are measured using eight thermocouples, connected to a laptop via a TC-08 cold junction (cf. Gladstone and Woods, 2001). One of these thermocouples is placed in the main flume, to give the external temperature. One thermocouple is placed in the inflow to the building, and one in the outflow, to allow inferences to be made about the structure of the flow in the building (for example, if the outflow is at the same temperature as the interior fluid, the assumption of a well mixed interior is likely to be valid). The other five are placed inside the building model at heights (above the bottom opening) of 0.01m, 0.025m, 0.04m, 0.055m, and 0.07m. These internal thermocouple readings are averaged to give the interior temperature measurement. The interior thermocouples can also be used to check that our assumption of a well-mixed interior is valid. To see the flow patterns, we use shadowgraphs and dye.

The experimental apparatus (with only pump 1 in place) is shown diagrammatically in figure 3.9, along with a photograph of the building model showing the thermocouples and heating element.

For the fluid properties of water, we use $\beta = 0.36\text{kgm}^{-3}\text{K}^{-1}$, $\rho = 1000\text{kgm}^{-3}$, and $C_p = 4184\text{Jkg}^{-1}\text{K}^{-1}$. For gravity, we use $g = 9.81\text{ms}^{-2}$. The height between openings, $h = 0.08$m and the window opening area, $A = \pi \times 0.005^2 \times 3\text{m}^2$, since there are three openings of radius 0.005m. The temperature relative to the ambient $\Delta T$ and the heat load $H$ are measured during the experiment.

Our dimensional model also requires that we know the loss coefficient $c^*$ and the effective wind pressure $\Delta p_w$ (see equation 3.3). These were inferred

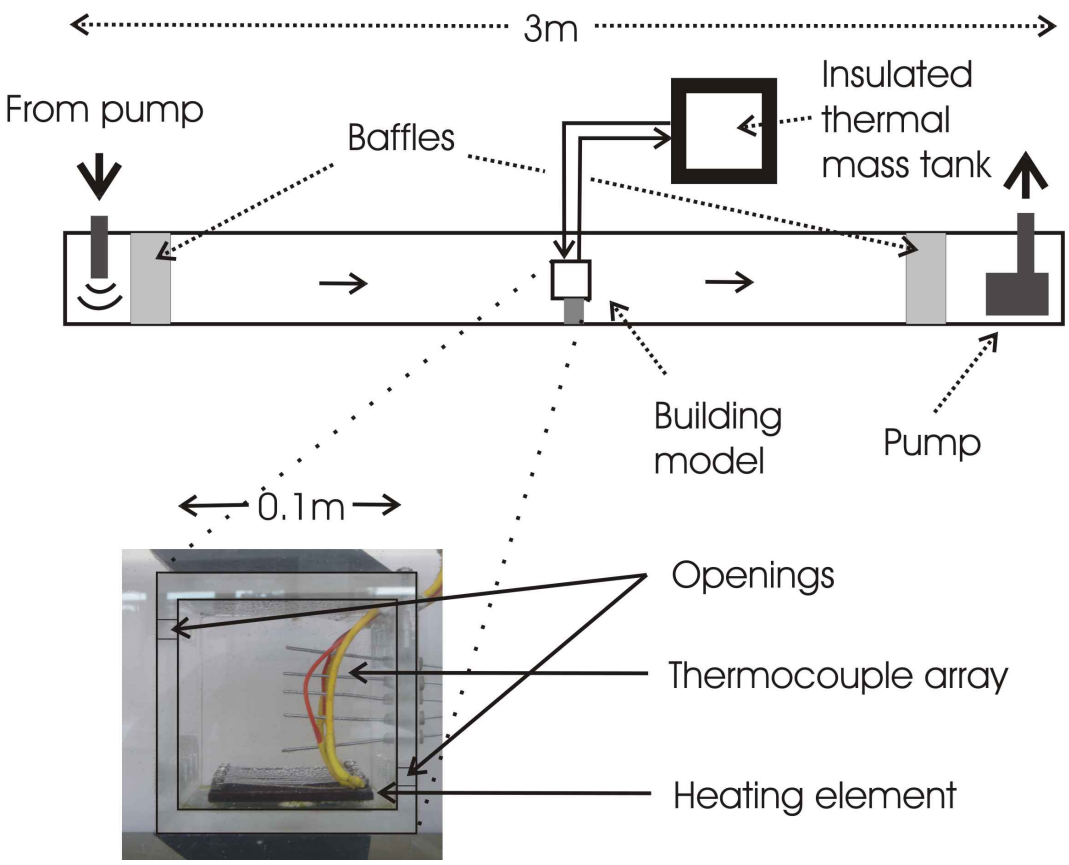


Figure 3.9.: *The experimental apparatus.*

from a series of calibration experiments (see appendix A). We find that the loss coefficient $c^* = 0.65 \pm 0.03$. The wind pressures associated with each possible pump configuration are given in table 3.1.

| Pump configuration | Calibrated pressure / pa | Error / pa |
|---|---|---|
| Pump 2, half open | 0.9 | ±0.2 |
| Pump 2, fully open | 2.4 | ±0.2 |
| Pump 1, fully open | 3.4 | ±0.3 |
| Pump 1, fully open, and pump 2, half open | 6.5 | ±0.5 |
| Both pumps fully open | 10 | ±0.5 |

Table 3.1.: Pressure difference between upper upwind and lower downwind opening, for various pump configurations

### 3.4.3. Results: steady state

We test our experimental system by modelling the equilibria of the system, first under varying heat load with a fixed wind, and secondly under varying wind, with a fixed heat load. For the first experiment we fix the wind at 2.4pa (i.e. only pump 2 on) and, increasing the heating incrementally from zero, take measurements of the steady state temperature difference. After the transition to the buoyancy dominated regime has occurred, we then incrementally decrease the heating, and again measure steady state temperature. The data collected are shown on figure 3.10a, a plot of temperature (in $^o$C) as a function of heating (in W), and are in good accord with the theory. The error bars represent the uncertainty in the thermocouple measurement ($\pm 0.1^oC$).

To show the equilibria at various wind forcings, we fix the heating at 100W, and increase the wind incrementally, measuring the steady state temperature at each data point. We then decrease the wind to achieve the wind dominated data point at a wind pressure of 3.4pa. Finally, to achieve the buoyancy dominated data point at a wind of 6.5pa, we start with the heating at 500W at this wind (hence the building is in the buoyancy dominated state), and then gradually decrease the heating to 100W. The data collected are shown on figure 3.10b, a plot of temperature (in $^o$C) as a function of wind pressure (in pa), and are in good accord with the theory. The vertical error bars represent the un-

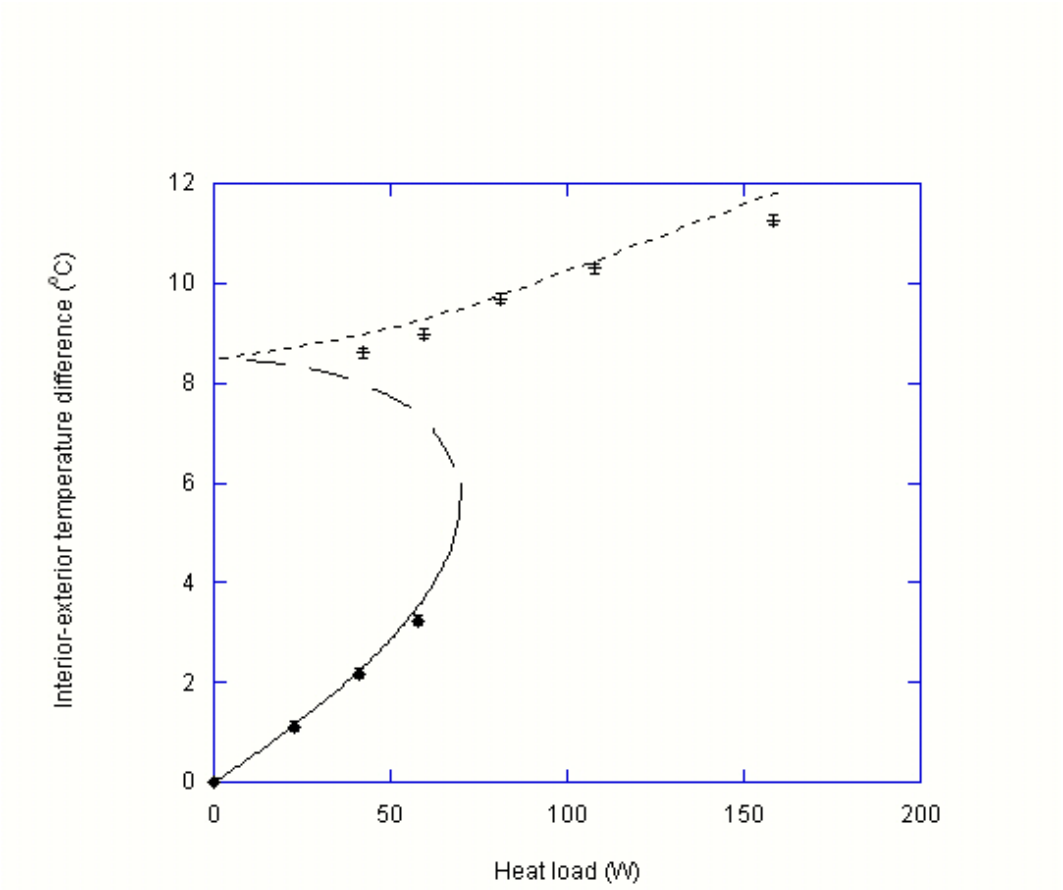


Figure 3.10a.: *A plot of temperature (in $^oC$) as a function of heating (in W), which shows experimental data points showing the equilibria of the system. The error bars represent the uncertainty in the thermocouple measurement ($\pm 0.1^oC$). There is clear experimental evidence of multiple steady states, for example at $\sim 60W$ heat load.*

certainty in the thermocouple measurement ($\pm 0.1^oC$) and the horizontal error bars represent the uncertainty in the wind measurement, as in table 3.1. In both cases, there is clear experimental evidence for the multiple steady states (for example at ∼60W heat load in figure 3.10a, and at 3.4pa wind pressure in figure 3.10b).

### 3.4.4. Results: instantaneous changes in wind

We then test the theory of figure 3.7. In order to allow convenient comparisons to figure 3.7 we present the data in dimensionless form. The dimensional winds

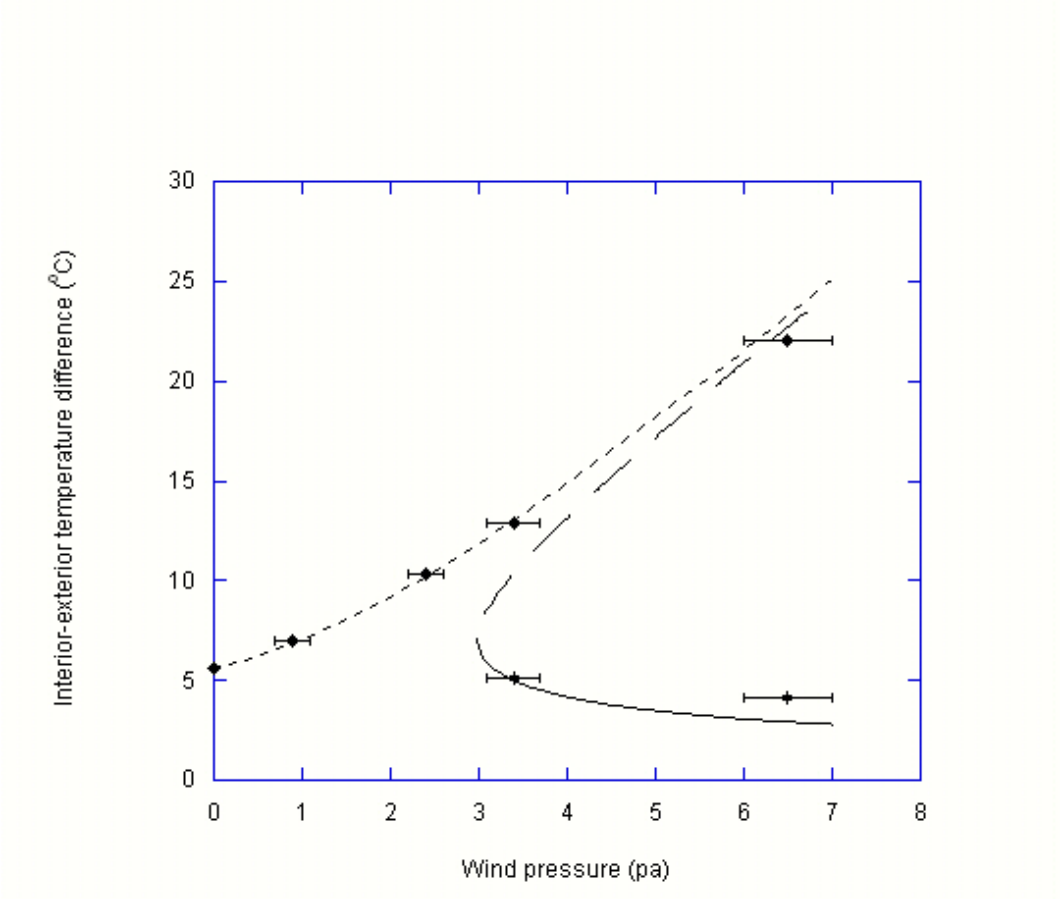


Figure 3.10b.: *A plot of temperature (in $^oC$) as a function of wind pressure (in pa), which shows experimental data points showing the equilibria of the system. The vertical error bars represent the uncertainty in the thermocouple measurement ($\pm 0.1^oC$) and the horizontal error bars represent the uncertainty in the wind measurement, as in table 3.1. There is clear experimental evidence of multiple steady states, for example at 3.4pa wind pressure.*

of table 3.1 are converted into the dimensionless variables $Q$ and $\hat{W}_{**}$ using the model described in section 2.

Figure 3.11 shows experimentally observed transitions from the buoyancy dominated regime on a plot of initial wind as a function of final wind. The crosses represent data points where a regime transition was observed, and the solid triangles represent data points where no transition was observed. The solid line shows the critical wind $\hat{W}_{**}$ as in figure 3.7. Cartoons marked on figure 3.11 illustrate the three critical behaviours: in the transition corresponding to cartoon (a), the final wind was greater than $\hat{W}_{**}$, and so the system evolved to the wind dominated regime. In the transition corresponding to cartoon (b), the wind increased, but not sufficiently to evolve to the wind dominated regime; and in the transition corresponding to cartoon (c), the wind decreased, and hence the system remained in the buoyancy dominated regime.

The experiments were undertaken as follows. All experiments were conducted at a heat load of 100W so that the available wind pressures covered a suitable range to test the theory. For each data point, the wind was set to its initial value and the heating varied to allow the required initial regime. To start the system in the buoyancy dominated regime, the heating was set to 500W and then decreased to 100W. To start in the wind dominated regime, the heating was set to 0W and then increased to 100W. The temperatures of the flow through both openings were measured, and act as a non-intrusive proxy for a measurement of flow direction (since the inflow will be at the exterior temperature, and the outflow at the interior temperature). Flow direction could also be observed using dye and shadowgraph techniques. The experimental observations match well with the theory.

### 3.4.5. Results: gradual changes in wind

Finally, we provide a preliminary test of the time dependence of the transitions illustrated in figure 3.8. Given that our pump delivers a fixed flow rate, it is difficult to produce a constantly varying wind pressure on the face of our building. However, in our experimental apparatus, the wind pressure acting

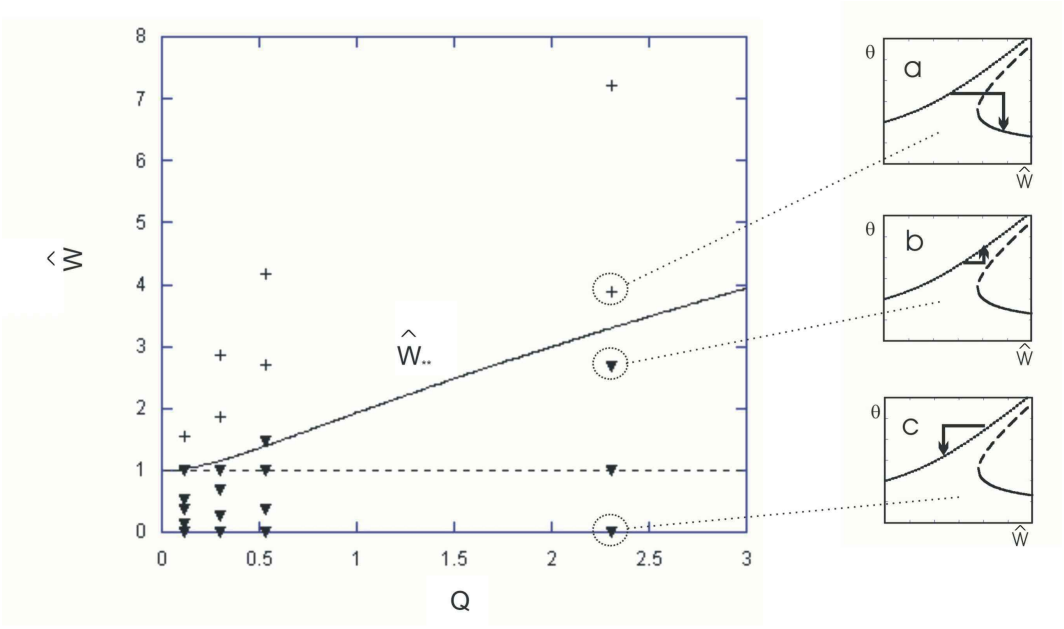


Figure 3.11.: *Experimental results showing transitions from the buoyancy dominated regime on a plot of final wind as a function of initial wind. The solid line represents the theoretical minimum final wind which will cause a transition from the buoyancy-dominated regime to the wind-dominated regime. The crosses represent experimental data points for which a regime transition was observed. The solid triangles represent data points for which no transition was observed. For clarity, error bars are not shown, but the errors associated with each data point are given in table 3.1.*

on the face of the building is a function of the height of water in the flume, since the flow rate supplied by the pump is constant. We can therefore observe the effects of increasing the wind forcing by draining the tank from one level to another. Forced ventilation experiments at each of these levels allow us to calculate the effective wind pressures at the start and end of the experiment. Figure 3.12 shows the experimentally observed effects of two such increases in wind forcing, on a plot of temperature as a function of wind forcing. In both cases, the wind pressure began at a marked level corresponding to a calibrated wind pressure of 4 Pa, and the heat load was set to 170W. The tank was then drained to a second marked level, corresponding to a wind forcing of 5.4 Pa. With this heat load and initial wind, the dimensionless heat load $Q = 0.419$ and dimensionless wind $\hat{W}_1 = 1.35$. From equation 3.11, we find the critical dimensional time over which the increase in wind must occur: $t_{crit} = 470s$. If we assume the wind increases linearly, then any faster increase in wind must lead to a change in regime, while any slower increase in wind will not. We therefore choose to drain the tank over a time $t_d \gg t_{crit}$ in one experiment and $t_d \ll t_{crit}$ in another. In the first case, marked with square markers, the tank was drained slowly through a small-bore hose, such that the increase in wind took 2000s. In the second case, marked with circular markers, the tank was drained rapidly through two hoses, such that the increase in wind took 45s. The experiments were identical except for the rate of change of increase of the wind. In the case of the slow transition, the building did not change regimes, whereas with the rapid transition the building evolved across the unstable wind dominated equilibrium and then cooled to the stable wind dominated equilibrium. This provides preliminary support to our predictions about time dependent changes in wind.

## 3.5. Further analysis: localized sources of buoyancy

The assumption of a well mixed interior is a simplification which allows us to use the model described in this paper. Real buildings are likely to have a

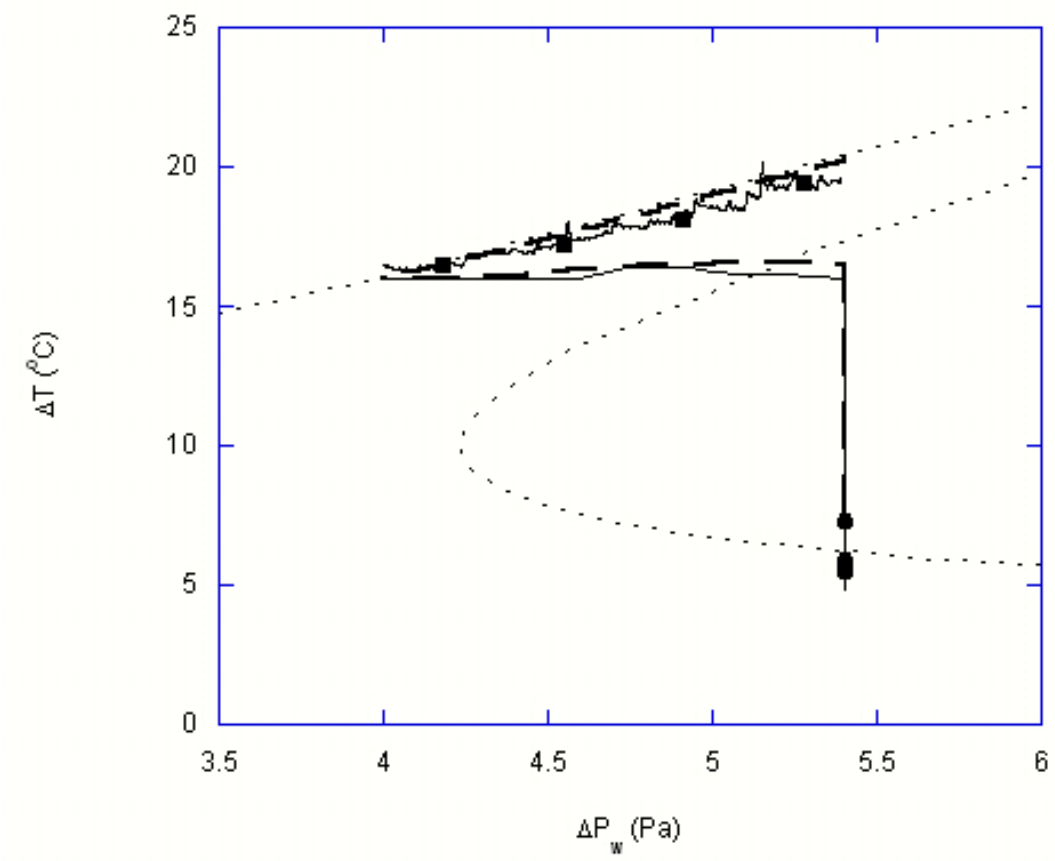


Figure 3.12.: *A plot of temperature (in $^oC$) as a function of wind pressure (in Pa), showing two transient evolutions under varying wind forcing. The dotted lines show the equilibria of the system. The solid line marked by squares shows the experimental data for a transient evolution under a slowly increasing wind (1.4Pa in 45s). The line marked by circles shows the experimental data for a transient evolution under a rapidly increasing wind (1.4Pa in 2000s). Dashed lines show numerical predictions of the transient evolution.*

variety of localised sources of heating, leading to different degrees of vertical stratification within the space. Also, during the transient adjustment of the flow from a relatively hot buoyancy driven regime to a relatively cool buoyancy driven regime, which would occur with an instantaneous decrease in wind speed or decrease in heating, the fluid in the building may become stratified. Strictly the model herein applies to the case in which the room is well mixed. However, the principles may be applied to more complicated situations.

If the assumption of a well mixed interior is relaxed, equation 3.4 can be rewritten for the buoyancy dominated regime as

$$\frac{d\bar{\theta}}{dt^*} = \hat{Q} - \theta_u \sqrt{\bar{\theta} - \hat{W}} \tag{3.12}$$

where $\bar{\theta}$ is the depth-averaged temperature in the building, and $\theta_u$ is the temperature of the fluid being ventilated, i.e. the temperature in the uppermost layer. In this case, with stable stratification,

$$\theta_u \geq \bar{\theta} \tag{3.13}$$

From equations 3.4, 3.12, and 3.13, we can conclude that

$$\bar{\theta}_{stratified} \leq \bar{\theta}_{mixed} \tag{3.14}$$

Therefore for a given heat load in steady state the instantaneous change in wind speed $W_T$ required to cause the system to evolve to the wind driven regime is also lower when the interior fluid is stratified rather than well mixed (cf. equation 3.9):

$$\Delta W_{T_{stratified}} \leq \Delta W_{T_{mixed}} \tag{3.15}$$

In addition, equation 3.11, which gives the critical rate of change of wind speed for a transition to occur, remains true for the stratified interior described in equation 3.12.

## 3.6. Applications and Conclusions

### 3.6.1. Case Study

We now explore the predictions of the model in the context of a typical building. We consider an open plan lecture area or theatre, of floor area 20m x 20m, and height 10m, and assume that the space has an upwind opening located 5m above the floor, and a downwind opening at ground level. Figure 3.13 shows how the internal equilibrium temperature, relative to the exterior temperature, varies with wind forcing. Curves are given for heat loads of 10 kW (solid line) and 15 kW (dashed line) with openings of size $5\text{m}^2$, and for a heat load of 10 kW with openings of size $8\text{m}^2$ (dotted line). As the heat load is increased, the stable equilibrium temperatures also increase. Also, as the opening area increases, the stable equilibrium temperatures decrease.

The minimum wind pressure, in Pa, above which multiple steady states can occur is shown, for the building dimensions described above as a function of heat load (in kW), for three different opening areas, in figure 3.14. Alternatively, figure 3.14 can be seen as showing the critical heat load for a given wind pressure. From equation 3.11, we find an equation for the critical rate of change of wind forcing (in Pa) required for the building to evolve to the wind dominated regime:

$$\left(\frac{d\Delta P_w}{dt}\right)_c = \frac{\beta g h H}{\rho C_p V} \tag{3.16}$$

This critical rate is plotted as a function of heat load H for our typical building in figure 3.15.

From figure 3.14 we see that, for a typical building, the critical wind pressure above which multiple steady states exists is $\sim$ 1Pa, corresponding to a wind speed of $2 - 3\text{ms}^{-1}$. The critical rate of change of wind, above which the building is likely to evolve to the wind dominated regime, is $\sim$ 1Pa/hour. Such a change in wind is quite possible, and so the building could oscillate between the buoyancy dominated regime and the wind dominated regime, leading to temperature variations of around $5^o$C, and potential occupant discomfort. The

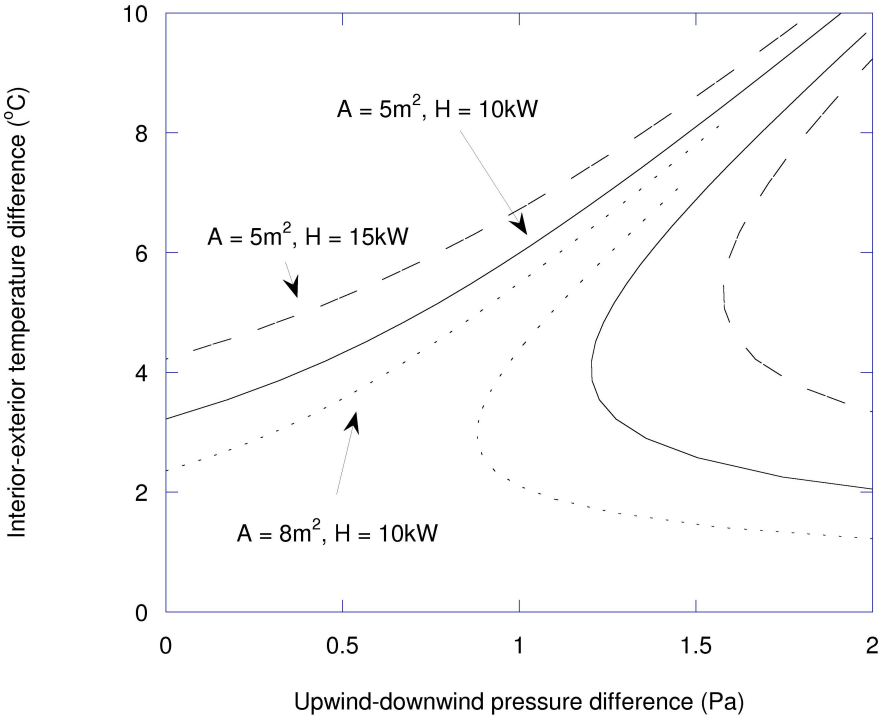


Figure 3.13.: *Dimensional plot of temperature difference (interior-exterior) in degrees Celsius as a function of wind pressure difference (upwind opening - downwind opening) in pascals. The building considered has an upwind opening at a height of 5m, and a downwind opening at floor level. Curves are given for heat loads of 10 kW (solid line) and 15 kW (dashed line) with openings of size* $5m^2$*, and for a heat load of 10 kW with openings of size* $8m^2$ *(dotted line).*

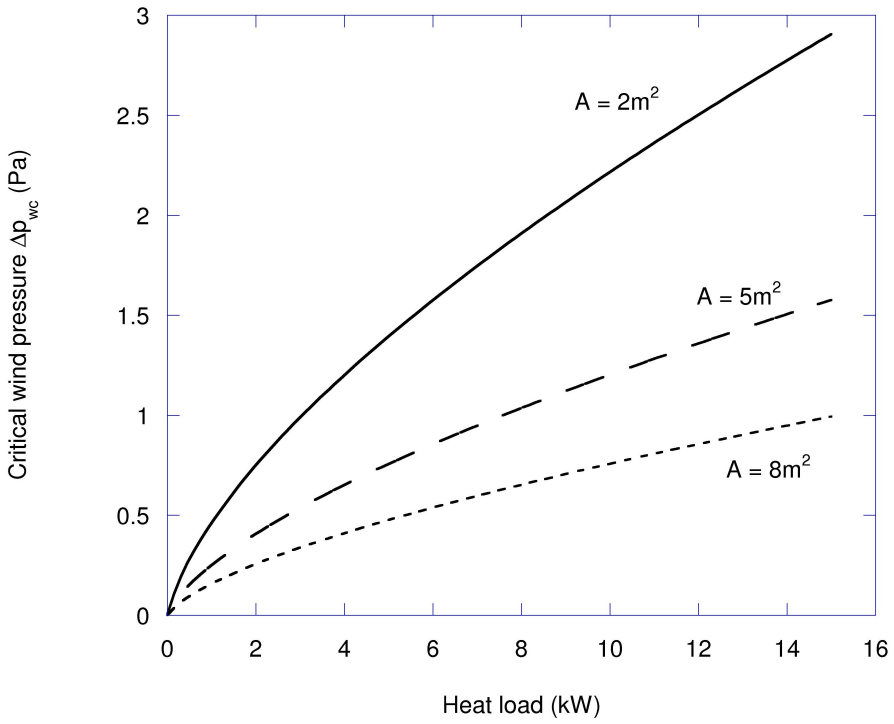


Figure 3.14.: *Dimensional plot of wind pressure (upwind opening - downwind opening), in pascals, as a function of heat load, in kW, showing the critical wind pressure above which a wind dominated regime exists. The building considered is* $20m$ *x* $20m$ *x* $10m$ *and has an upwind opening at a height of* $5m$*, and a downwind opening at floor level. The three lines represent three different opening areas: the solid line represents a window opening area of* $2m^2$*, the dashed line* $5m^2$*, and the dotted line* $8m^2$*.*

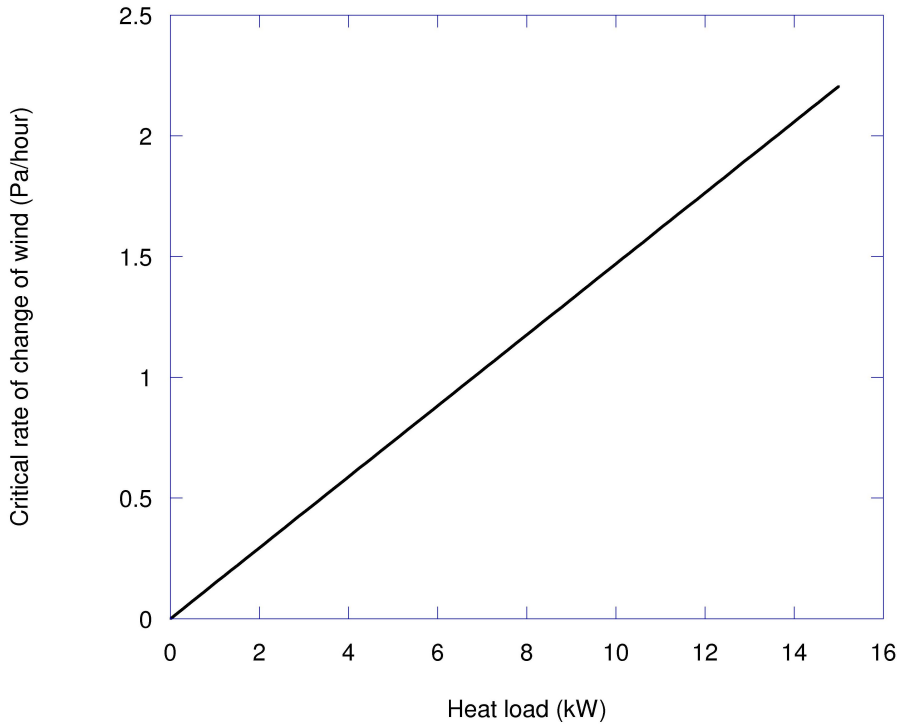


Figure 3.15.: *Dimensional plot of rate of change of wind pressure, in pascals per hour, as a function of heat load, in kW, showing the critical rate of change of wind pressure above which the building is likely to evolve to the wind dominated regime. The building considered is* $20m$ *x* $20m$ *x* $10m$ *and has an upwind opening at a height of* $5m$*, and a downwind opening at floor level.*

building could therefore be redesigned to minimize the effects of variations in the wind (see, for example, chapter 5).

### 3.6.2. Conclusions and further work

This chapter has examined, both theoretically and experimentally, the nature of transitions between regimes in a naturally ventilated building subject to wind and buoyancy forces. We have analysed the evolution of flow regimes with changes in wind forcing for fixed heat load. We have found that there is a critical relation between the wind forcing and the heat load for the wind dominated regime to exist. This is directly analogous to the findings of Li and Delsante, 2001, and Hunt and Linden, 2004. The transition from the wind dominated regime to the buoyancy dominated regime occurs when the wind dominated regime no longer exists, and is therefore analogous under changes in wind forcing or in heat load.

We have then presented new results related to the effects of changing wind forcing. When the system begins in the buoyancy dominated regime, slow changes in wind cause the system to evolve along the buoyancy dominated equilibrium and hence remain in the buoyancy dominated regime. Fast changes, however, are more complex. For an instantaneous change in wind forcing, we have shown that small changes in wind will allow the system to remain in the buoyancy dominated regime, while large changes cause the system to evolve to the buoyancy dominated regime; and we have found a critical relation determining the minimum instantaneous wind change which will cause the system to evolve to the wind dominated regime. Further, we have examined changes which occur over finite non-zero timescales, and we have found a critical rate of change of wind for the transition to the wind dominated regime to occur. Our findings are supported by new analogue water bath experiments, and the implications for building design have been discussed. Our findings are specifically for a distributed heat source and hence a well-mixed interior: however, similar results hold for a point source of heating and a stratified interior (cf. Hunt and Linden, 2004).

The asymmetry between changes in the wind forcing and changes in the heating load occurs because the temperature associated with the unstable wind dominated flow regime increases with the wind forcing for fixed heating, so for all interior temperatures there is an unstable wind dominated solution. As a result, if the room is in the buoyancy dominated regime, there is a well defined increase in wind forcing such that if $\hat{W}_1 > \hat{W}_{**}$ the system state crosses the unstable wind dominated regime, and the system cools to the stable wind dominated regime. There is no analogue of this for changes in heating, since the temperature of the unstable wind dominated regime is lower than the whole buoyancy dominated regime.

Several issues remain to be considered: in the next chapter we extend our analysis to consider how the thermal mass of a heavyweight building might affect possible regime transitions.

# 4. The interaction between wind, buoyancy and thermal mass

*So far this thesis has focussed on the interaction between wind and buoyancy in lightweight buildings. Here we extend the analysis to consider the effects of thermal mass. We begin by investigating the effects of discrete changes in ventilation strategy (e.g. increasing the ventilation areas, or increasing the heating) on temperature in heavyweight buildings with flow driven only by buoyancy. We then extend this model to investigate how the interaction between wind and buoyancy affects heavyweight buildings. We find that the building temperature evolves slowly along either the wind or buoyancy driven flow regime, with the rate of change controlled by the thermal mass parameters, but changes quickly between regimes, with the rate of change controlled by the interacting wind and buoyancy. In real buildings, such effects are likely to lead to gradual evolutions of the temperature interspersed with unpredictable rapid temperature swings and hence occupant discomfort. The predictions of the model are supported with new laboratory experiments.*

## 4.1. Introduction

The use of thermal mass is an effective tool for maintaining thermal comfort in naturally ventilated buildings, as thermal mass can store heat and hence buffer the interior temperature against large variations in the exterior temperature. One typical use of thermal mass is as part of a night-cooling strategy in warm climates: a building is thoroughly ventilated during the night, cooling the thermal mass, which thus provides a sink for heat during the day, cooling the building. Previous studies have shown theoretically and experimentally how

thermal mass may buffer building temperature assuming a sinusoidal exterior temperature cycle over one day (Yam, Li, and Zheng 2003; Holford and Woods 2007).

As well as the daily cycle of external temperature, various control strategies may lead to discrete changes in conditions: for example, when windows are opened or when heating is turned on. In this chapter, we study theoretically and experimentally the transient evolutions following such discrete changes in building state. Typically the timescale for the thermal mass to respond is much longer than the timescale for the air flow to adjust. This can lead to complexities in the transient adjustment.

One such set of complexities occurs when wind is introduced, such that ventilation is driven by interacting wind and buoyancy forces. We have already discussed how the interaction between wind and buoyancy in lightweight naturally ventilated buildings can lead to multiple flow regimes and a nonlinear relationship between heating, wind speed, and interior temperature. Here we find that the separate timescales for the thermal mass and air flow to adjust lead to interspersed slow and fast internal temperature evolutions.

This chapter is structured as follows. We begin by developing theoretical models of typical evolution with thermal mass following discrete changes in either the heating load or the areas of the vents. We assume ventilation is driven by temperature differences caused by a distributed heat load in the building and heat exchange with the thermal mass. We then introduce wind forcing into our model, such that ventilation is driven by interacting wind and buoyancy forces, as discussed in the previous chapter. We find that a thermally massive building will evolve according to two separate timescales: along equilibria the system evolves slowly, with temperature fluctuations limited by the thermal mass; while between regimes, the system temperature evolves quickly.

We then detail a series of new analogue experiments which allow us to test the theoretical models presented, and show results confirming our models. Finally, we discuss the implications for building design.

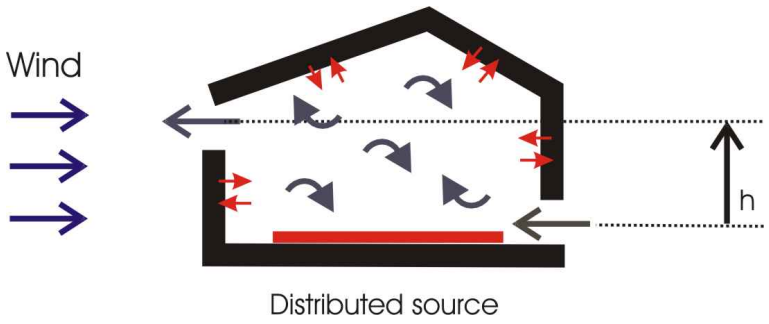


Figure 4.1.: *Schematic of the building model under consideration, with a wind acting in opposition to buoyancy, which is generated by a distributed heat source. The interior air exchanges heat with the thermally massive walls, as shown. This diagram shows the building in the buoyancy driven state, with flow upwards through the building: equivalently, a wind driven state, with flow from left to right through the building, is possible.*

## 4.2. Modelling approach

We consider a building model similar to that shown in figure 4.1, with two openings of area A, one at a high level on the left face of the building, and one at a low level on the right face of the building. In the model, there is a wind acting on the left hand face of the building, and a distributed heat source. There is also a distributed thermal mass, which exchanges heat with the interior fluid. Without this thermal mass, we know from chapter 3 (equation 3.3) that:

$$\rho C_p V \frac{d\Delta T}{dt} = H - \rho C_p c^* A \Delta T \sqrt{\frac{|\Delta p_w - \beta g h \Delta T|}{2\rho}} \tag{4.1}$$

where $\rho$ is the fluid density, $C_p$ is the specific heat capacity of the fluid, and $\beta$ is the expansion coefficient of the fluid; $V$ is the building volume, h is the height between openings, and $c^*$ is a loss coefficient associated with the openings; $g$ is acceleration due to gravity; and $H$ is the heat load, $\Delta p_w$ is the pressure difference between the openings due to wind, and $\Delta T$ is the temperature difference between the interior and exterior.

To incorporate the effects of thermal mass into such a model, we note that energy is transferred between the thermal mass and the interior fluid. We introduce a heat transfer coefficient $\chi$, defined as the heat flux transferred

per unit area, per degree difference in $\Delta T$ between the bulk interior air and the thermal mass surface. This heat transfer coefficient depends on a variety of factors, including surface orientation and air properties (Gebhart, Jaluria, Mahajan, and Sammakia 1988). Here we consider an idealised problem, and so assume some constant $\chi$ which is representative of the overall heat transfer rate, and typically around $2.5\mathrm{Wm}^{-2}\mathrm{K}^{-1}$ (cf. Holford and Woods (2007)). The heat input from the thermal mass to the interior air is therefore given by

$$P_{tm} = S\chi(\Delta T_m - \Delta T) \tag{4.2}$$

Where $S$ is the surface area of the thermal mass and $\Delta T_m$ is the temperature difference between the thermal mass and the exterior fluid. We can therefore incorporate the effects of thermal mass into the heat balance of equation 4.1:

$$\rho C_p V \frac{d\Delta T}{dt} = H - \rho C_p c^* A \Delta T \sqrt{\frac{|\Delta p_w - \beta g h \Delta T|}{2\rho}} + S\chi(\Delta T_m - \Delta T) \tag{4.3}$$

The flow direction in this case is determined by the term inside the square root: if the wind pressure $\Delta p_w$ is greater than the buoyancy pressure $\beta g h \Delta T$ then the flow will be wind driven, and if not it will be buoyancy driven. Meanwhile, the temperature of the thermal mass also evolves with time, as heat is transferred to and from the interior air:

$$\rho_m C_{pm} V_m \frac{d\Delta T_m}{dt} = S\chi(\Delta T - \Delta T_m) \tag{4.4}$$

where the subscript $m$ indicates a property of the thermal mass. By simultaneously solving equations 4.3 and 4.4 we can predict the temperature evolution of the building shown in figure 4.1 under variations in heat load or wind speed. We begin by considering the case in which there is no wind and ventilation is driven only by buoyancy forces.

## 4.3. Buoyancy driven ventilation

Here we explore how, with ventilation driven only by buoyancy forces, the building temperature is likely to respond to discrete changes in the building state, by considering two such discrete changes as case studies. The work in this section provides theoretical insight into how thermal mass can affect the evolution of building temperatures, and also acts as analytical background for the next section, in which the effects of wind are introduced. Later, we support the predictions of this section with experimental models.

In the absence of wind we scale our dimensionless model on the heat load, such that

$$\frac{d\Theta}{d\hat{t}} = \left(1 - \Theta|\Theta|^{\frac{1}{2}} - \mu(\Theta - \Theta_m)\right) \tag{4.5}$$

where $\Theta = (\frac{\sqrt{\rho\beta gh}C_p c^* A}{\sqrt{2}H})^{\frac{2}{3}}\Delta T$, $\hat{t} = (\frac{\sqrt{\beta ghH}c^* A}{\sqrt{2C_p}\rho V^{\frac{3}{2}}})^{\frac{2}{3}}t$, and $\mu = (\frac{\sqrt{2}S^{\frac{3}{2}}\chi^{\frac{3}{2}}}{\sqrt{\rho\beta ghH}C_p c^* A})^{\frac{2}{3}}$, and

$$\frac{d\Theta_m}{d\hat{t}} = M(\Theta - \Theta_m) \tag{4.6}$$

where $M = \frac{\rho C_p V}{\rho_m C_{pm} V_m}\mu$. $\mu$ characterises the rate of heat exchange between the interior fluid and the thermal mass, and is typically of order 1. A building with $\mu \gg 1$ has a thermal mass which dominates the transient behaviour, while in a building with $\mu \ll 1$ the thermal mass can be seen to have little effect on the transient behaviour. $M$ represents the ratio of the mass of the fluid to the thermal mass, and $M \ll 1$ for buildings with large thermal mass. In this case the thermal mass response timescale will be much slower than the building response to variations in external conditions.

### 4.3.1. Cool exterior with increase in ventilation

In winter in the UK, outside temperatures are usually colder than a comfortable working environment. Thermal mass can help to retain heat while maintaining a comfortable ventilation rate. Typically, naturally ventilated office buildings

might have a reduced ventilation rate (i.e. reduced window openings) during the night, when occupation rates, and hence ventilation rate requirements, are low. This reduced ventilation helps to maintain the temperature of the interior thermal mass. In the morning the ventilation rate is then increased to accommodate a higher occupancy level. The building then cools to a new equilibrium temperature. In order to maintain a comfortable interior, it is important to be able to predict how the internal temperature will vary as the building cools to equilibrium.

We can model this cooling by considering a building with a heat supply and a relatively low ventilation rate, such that the interior is relatively warm. At time $t = 0$ we increase the ventilation rate, by increasing the window opening areas, and observe how the temperature changes.

Figure 4.2 shows a dimensionless model of possible building evolution over time, beginning at the time when ventilation is increased. Plot (a) shows the temperature evolution as a function of time, while plot (b) shows the evolution as a function of log time. The plots show interior temperatures (as solid lines) and thermal mass temperatures (as dotted lines) for three cases, as marked on the figure: i) a heavyweight building, with $M = 0.01$ (ii) an intermediate case, with $M = 0.1$, and (iii) a lightweight building, with $M = 1$. In all cases the thermal mass parameter $\mu = 1$. In all cases the building begins at a relatively warm temperature ($\Theta = 5$) and cools to a new equilibrium ($\Theta = 1$). At the end of this section we discuss the separation of timescales which is observed in this model. In section 4.5 we test this model experimentally.

### 4.3.2. Warm exterior with increase in heat load

In summer in the UK, it is frequently desirable to maintain a cool interior. One possible scheme to reduce the interior temperature is to use night cooling, in which the building is thoroughly ventilated at night, when the exterior temperature is lowest, so that the thermal mass is cooled and will absorb more heat during the warmth of the day. In the morning, the building starts relatively cool, and warms to a new equilibrium. In this case, the initial temperature may

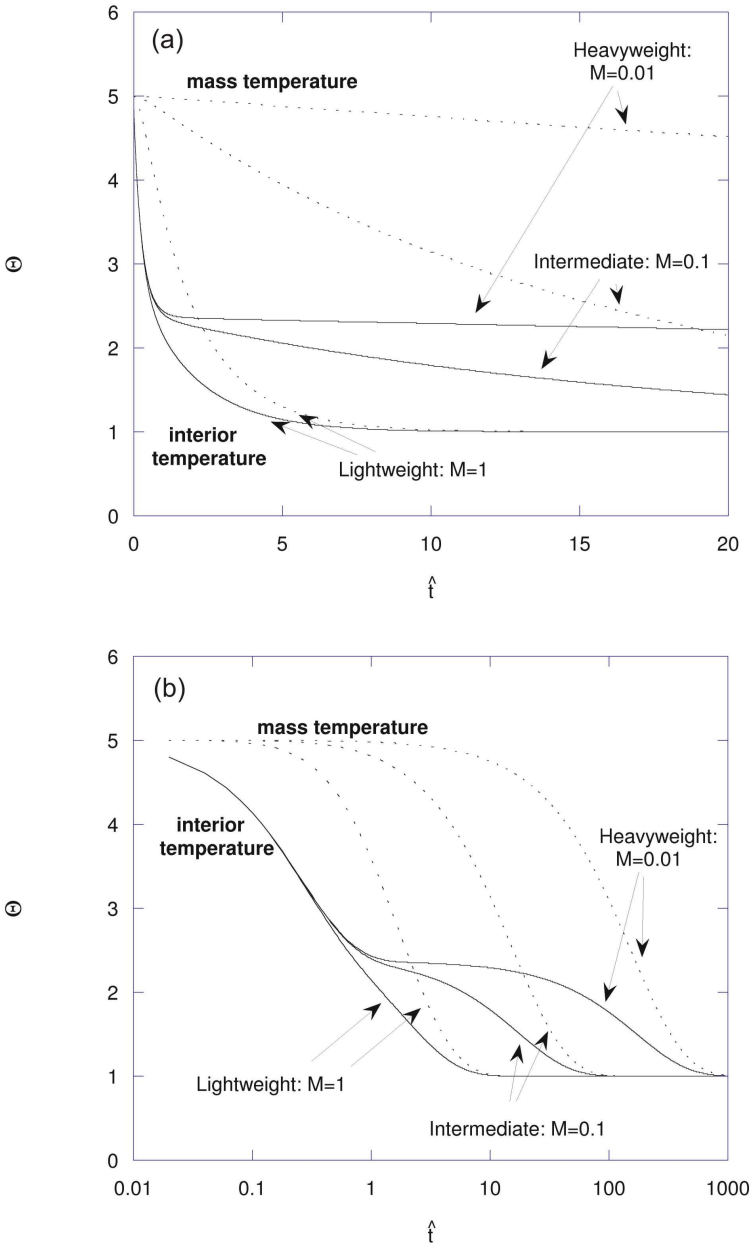


Figure 4.2.: *Temperature evolution over time for a typical naturally ventilated building on a winter day, shown as a function of time (plot (a)) and log time (plot (b)). The plot shows interior temperatures (as solid lines) and thermal mass temperatures (as dotted lines) for three cases, as marked on the figure: i) a heavyweight building, with* $M = 0.01$ *(ii) an intermediate case, with* $M = 0.1$*, and (iii) a lightweight building, with* $M = 1$*. In all cases the thermal mass parameter* $\mu = 1$*.*

be lower than the exterior temperature, due to night cooling, while the final equilibrium temperature is likely to be higher than the exterior, due to heating from, for example, people and electrical equipment. The flow direction in the building will therefore change from downflow, as the relatively dense cold fluid vents, to upflow, as the relatively buoyant warm fluid vents.

We can model the daytime evolution of the system by considering a building which is initially cooler than the exterior (due to night cooling), with no heating. At t=0 a heat load is introduced, reflecting the heat load caused by people and electrical appliances at the beginning of the day. Figure 4.3 shows a dimensionless model of building evolution over time (plot (a)) and log time (plot (b)), beginning from such a cold interior. This plot shows interior temperatures (as solid lines) and thermal mass temperatures (as dotted lines) for the same three cases as previously: (i) a heavyweight building, with $M = 0.01$, (ii) an intermediate case, with $M = 0.1$, and (iii) a lightweight building, where $M = 1$. In all cases the thermal mass parameter $\mu = 1$. The building begins at a relatively cold temperature ($\Theta = -3$) and warms to a new equilibrium at $\Theta = 1$, with the rate of change of temperature again determined by the heat transfer between the thermal mass and the interior.

### 4.3.3. Discussion of timescales

In both examples given above, when the thermal mass is large ($M \ll 1$), we see clearly that the temperature evolves on two separate timescales. First, the interior temperature evolves on a fast timescale to a pseudo-equilibrium, and then the building state evolves on a slower timescale as the thermal mass equilibrates with the interior fluid. One way of understanding the separation of these timescales is by considering the system forcing and response: if we set equation 4.5 to zero and rearrange, we obtain the relation

$$1 + \mu\Theta_m = \Theta|\Theta|^{\frac{1}{2}} + \mu\Theta \tag{4.7}$$

where the left hand side represents the forcing, and varies slowly according to

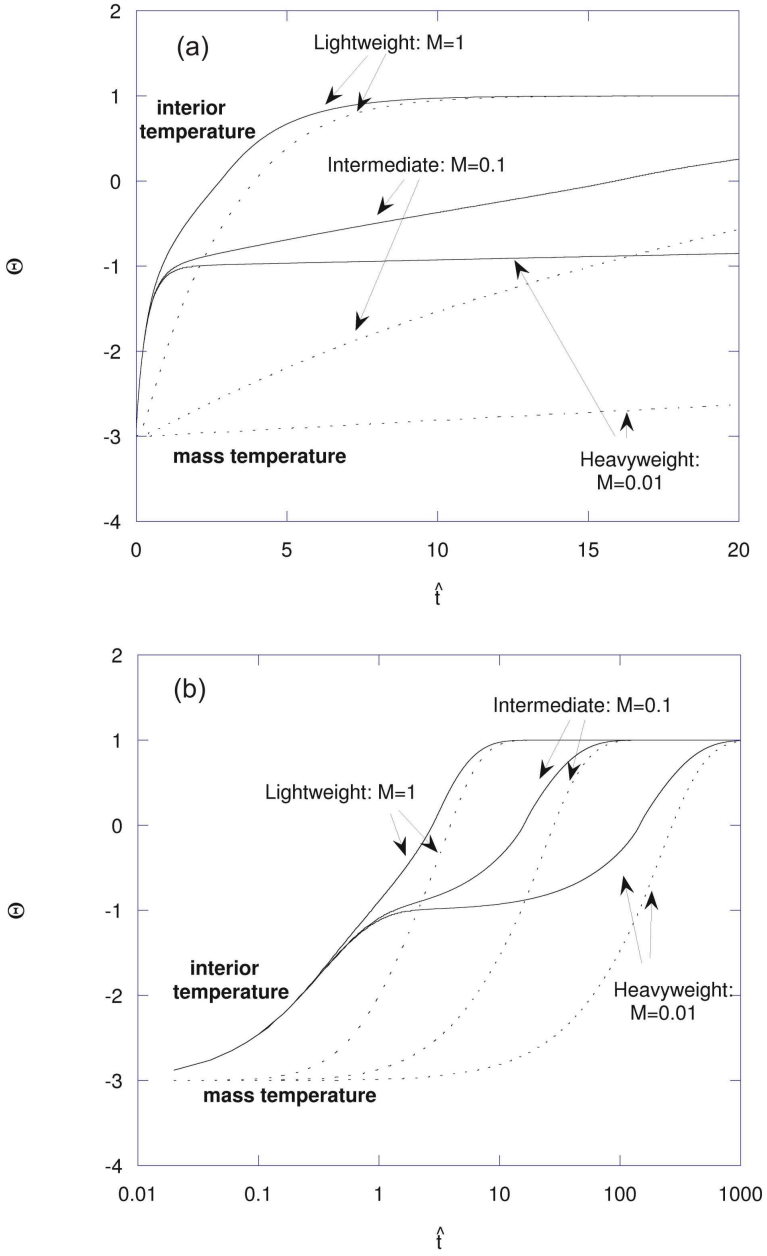


Figure 4.3.: *Temperature evolution over time for a typical naturally ventilated building on a summer day, shown as a function of time (plot (a)) and log time (plot (b)). The plot shows the interior temperatures (solid lines) and thermal mass temperatures (dotted lines) for three cases: (i) a heavyweight building, with* $M = 0.01$*, (ii) an intermediate case, with* $M = 0.1$*, and (iii) a lightweight building, where* $M = 1$*. In all cases the thermal mass parameter* $\mu = 1$*.*

equation 4.6, while the terms on the right hand side represent the response, and vary quickly to match the forcing.

Typical evolutions, assuming very large thermal mass, are illustrated in figure 4.4, which shows the system forcing $1 + \mu\Theta_m$, as a function of $\Theta_m$, as a dotted line, and the system response $\Theta|\Theta|^{\frac{1}{2}} + \mu\Theta$, as a function of $\Theta$ as a thin solid line, for $\mu = 1$. The system is in overall equilibrium when the forcing equals the response and $\Theta_m = \Theta$. However, the system is in quasi-equilibrium, i.e. the fast-varying equation 4.5 is in equilibrium, when the forcing equals the response, even if $\Theta_m \neq \Theta$. In this case, variations in temperature occur slowly along the quasi-equilibrium curve described by equation 4.7 as $\Theta_m$ varies according to equation 4.6. A typical evolution of the interior temperature $\Theta$ is shown as a thick solid line: the building temperature begins at $\Theta = \Theta_m = -1$, at the point $P_1$, and then evolves quickly (transition (a)) to the manifold at point $P_2$. During transition (a), the thermal mass temperature remains constant, and $\Theta$ varies until equation 4.5 is in equilibrium. After this transition, therefore, the interior temperature is $\Theta = 0$ (point $P_2$), while the thermal mass temperature is unchanged at $\Theta_m = -1$. The system temperature then evolves along the quasi-equilibrium to overall equilibrium on a slow timescale (transition (b)) as the thermal mass temperature tends towards the interior temperature, according to equation 4.6. As the thermal mass temperature varies, so does the interior temperature $\Theta$ at which the forcing and response of equation , until the system reaches overall equilibrium at point $P_3$, where equations 4.5 and 4.6 are both in equilibrium.

In chapter 3 we showed that with opposing wind and buoyancy, the relation between temperature, heating load and wind forcing is non-monotonic. In the next section of this chapter, we consider how thermal mass affects the timescales on which transient evolutions occur in such cases.

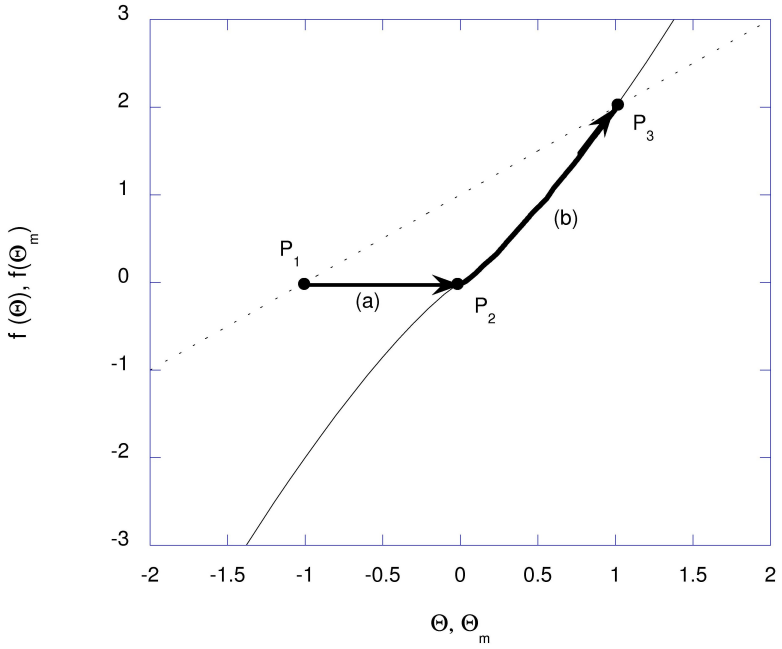


Figure 4.4.: *Plot showing system forcing (dotted line), as a function of* $\Theta_m$*, and response (thin solid line), as a function of* $\Theta$*, for a building with temperature dynamics as in equations 4.5 and 4.6, with* $\mu = 1$*. The solid arrows show the evolution of the system beginning with* $\Theta = \Theta_m = -1$*: the system evolves on a fast timescale to the manifold (transition (a)) and then on a slow timescale to equilibrium (transition (b)).*

## 4.4. Wind and buoyancy driven ventilation

The previous case studies have illustrated the typical behaviour of a building with large internal thermal mass under changes in external condition. In particular, we have highlighted the separation of timescales: the building state evolves on a relatively fast timescale to the manifold as the interior air equilibrates, and then on a relatively slow timescale to overall equilibrium as the thermal mass temperature tends to the interior temperature. When we investigate the interactions between wind and buoyancy in buildings with large internal thermal mass, we therefore expect a similar separation of timescales. However, the interaction between wind and buoyancy can lead to more complicated non-monotonic manifolds, and multiple steady states, and so our model must be extended.

With a non-zero wind we scale as before to give:

$$\frac{d\Theta}{d\hat{t}} = 1 - \Theta\sqrt{|W - \Theta|} - \mu(\Theta_m - \Theta) \tag{4.8}$$

where the wind forcing $W = (\frac{\sqrt{\rho}C_p c^* A}{\sqrt{2}H\beta gh})^{\frac{2}{3}}\Delta p_w$, and

$$\frac{d\Theta_m}{d\hat{t}} = M(\Theta - \Theta_m) \tag{4.9}$$

as before.

Again, we can rearrange equation 4.8 to compare a forcing term, given by the heat provided from the heat source and the thermal mass, to a response term, given by the heat vented out of the building and the heat transmitted to the thermal mass. At equilibrium, therefore,

$$1 + \mu\Theta_m = \Theta\sqrt{|W - \Theta|} + \mu\Theta \tag{4.10}$$

where the left hand side of the equation represents the forcing, which varies slowly, governed by equation 4.9 and the right hand side the response, which varies quickly according to equation 4.8.

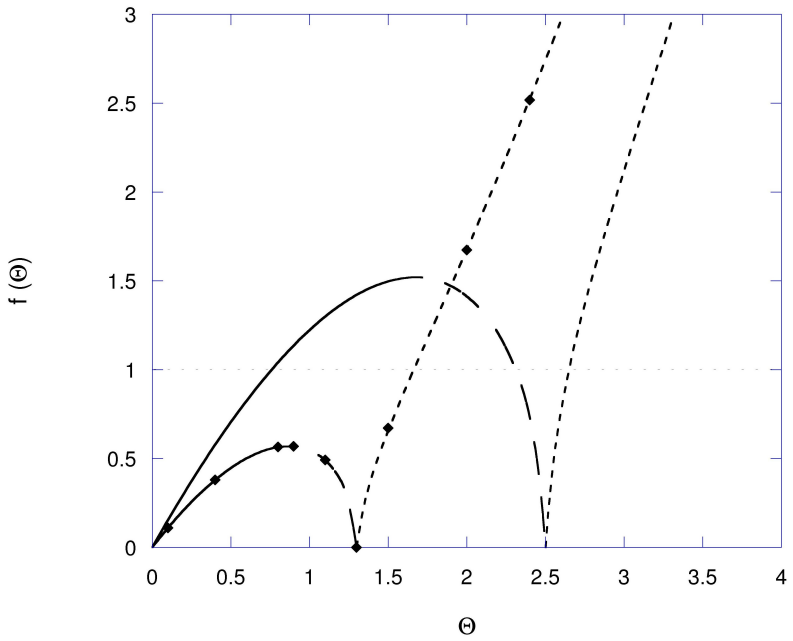


Figure 4.5.: *Plot showing the ventilation term* $\Theta\sqrt{|W-\Theta|}$ *as a function of* $\Theta$*, for wind forcing* $W = 2.5$ *(unmarked line) and* $W = 1.3$ *(with diamond markers). In both cases, the solid line represents the stable wind dominated regime; the long dashed line the unstable wind dominated regime; and the short dashed line the buoyancy dominated regime. The dotted line represents* $f(\Theta) = 1$*).*

### 4.4.1. Initial and final states of the system

To interpret equation 4.10, we examine figure 4.5, which shows the variation of $\Theta\sqrt{|W-\Theta|}$ with $\Theta$ for $W = 2.5$ (unmarked line) and $W = 1.3$ (with diamond markers). We note first that the curves are non-monotonic, and that the slope of the curve tends to $-\infty$ at $\Theta = W$, so that the response term given by the right hand side of equation 4.10 is non-monotonic for all finite $\mu$. Secondly, we note that the long-dashed sections of the curves corresponds to an unstable branch of equation 4.8, while the solid lines represent the stable wind driven regime and the short-dashed lines the stable buoyancy driven regime. Equation 4.10 gives that the system tends to one of the stable equilibria where $f(\Theta) = 1$ (since at equilibrium, $\Theta = \Theta_m$). As can be seen from figure 4.5, in the case where $W = 1.3$, this must be the buoyancy dominated regime, while if $W = 2.5$, this

may be either the buoyancy dominated regime or the stable wind dominated regime. The critical wind, above which a wind dominated equilibrium exists, is $W_* = 3\left(\frac{1}{2}\right)^{\frac{2}{3}}$ (see previous chapter). In this section we consider only cases with a positive heat load (i.e. no air conditioning systems), and so a buoyancy dominated regime exists for all winds. There are therefore two critical cases (cf. chapter 3):

- **case 1:** if the building has a wind $W < 3\left(\frac{1}{2}\right)^{\frac{2}{3}}$, only a stable buoyancy driven equilibrium exists, and;
- **case 2:** if the building has a wind $W \geq 3\left(\frac{1}{2}\right)^{\frac{2}{3}}$, there exist a stable wind driven equilibrium, an unstable wind driven equilibrium, and a stable buoyancy driven equilibrium

For case 1, therefore, we can predict the final state of the system independent of the current state. In case 2, the system can evolve to either of two stable equilibria, with the unstable regime separating the two behaviours: if the system begins with the interior colder than the unstable regime, for a given wind $W$, it will cool to the stable wind driven regime, while if the initial temperature is greater than that of the unstable regime, the building state will heat to the buoyancy driven equilibrium. The final equilibrium state can therefore be predicted for any given current state.

### 4.4.2. Transient evolution to final equilibrium

Transient evolutions along the manifold are quantitatively similar to those described in the previous section with no wind. However, when wind is introduced, transient evolutions can occur in which the system begins in the wind driven regime (see previous subsection), the heat load is increased, and the system changes flow regime during the evolution. This is illustrated on figure 4.6, which shows the system forcing $1 + \mu\Theta_m$ (the thin dotted line) as a function of $\Theta_m$, and the system response $\Theta\sqrt{|W - \Theta|} + \mu\Theta$ (the solid line shows the stable wind driven branch; the long-dashed line the unstable wind driven branch; and

the short-dashed line the stable buoyancy driven branch) as a function of $\Theta$. The plot shown is for the case of $W = 1.7$ and $\mu = 0.5$. Superimposed onto the plot are a series of arrows which indicate how the system will evolve from an initially cold equilibrium; such a scenario might occur after a night cooling strategy, or as a result of a sudden increase in heating.

The building begins with $\Theta = \Theta_m = 0$ at point $P_1$. Since $W > \Theta$, the building is in the wind driven regime. In this state the system forcing is greater than the response, and so the interior temperature heats quickly to the manifold, at point $P_2$ (transition (a)). The forcing and response are now equal, and so the evolution is governed by the slow convergence of the interior and thermal mass temperatures, equation 4.9. The system slowly heats along the manifold (transition (b)) to point $P_3$. Point $P_3$ represents the limit of the stable wind dominated solution. Once the system reaches this point, then given any increase in the thermal mass temperature, equation 4.8 no longer has a wind driven solution, and so the interior temperature increases rapidly, governed by equation 4.8 (transition (c)). Once the temperature reaches the manifold at point $P_4$ equation 4.8 is in equilibrium, and the system adjusts slowly to its final equilibrium at point $P_5$ as the mass temperature and interior temperature converge (transition (d)).

Overall, then, the system shows two separate fast temperature evolutions (transitions (a) and (c)) in which the interior temperature equilibrates according to equation 4.8, and two slow evolutions (transitions (b) and (d)) in which the thermal mass temperature gradually increases towards the interior temperature, governed by equation 4.9. This in turn leads to a gradual increase in the interior temperature, governed by equation 4.8. In the next subsection, we illustrate these evolutions numerically, and show how the results change as we relax the assumption of effectively infinite thermal mass.

Further, we can predict the maximum temperature of the stable wind driven regime (i.e. the temperature of point $P_3$ on figure 4.6) by finding the maximum value of the right hand side of equation 4.10. This maximum $\Theta_*$ is plotted in

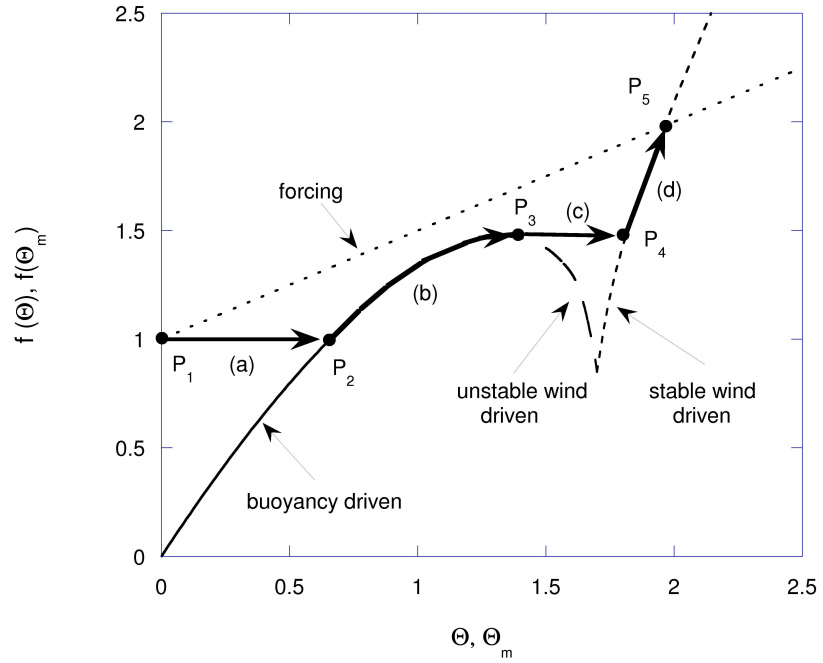


Figure 4.6.: *Temperature evolution of a heavyweight building, subject to wind opposing buoyancy, from an initial state colder than equilibrium. The thin lines show the forcing (as a dotted line) as a function of $\Theta_m$ and the response (as a solid line for the stable wind driven state; a long-dashed line for the unstable wind driven state; and a short-dashed line for the stable buoyancy driven state) as a function of $\Theta$. The evolution of building temperature is shown as a series of thick arrows. The building temperature evolves quickly to the manifold (arrow (a)) while the thermal mass temperature remains constant. The temperature then slowly increases as the interior and thermal mass temperatures converge (transition (b)). At point $P_3$, the wind driven solution ceases to exist, and so the the interior temperature evolves to that of the buoyancy driven solution. This transition (marked as transition (c)) occurs at a constant thermal mass temperature, and hence in a heavyweight building it occurs relatively quickly. Finally, the building temperature and thermal mass temperature converge to overall equilibrium in the buoyancy driven regime (transition (d)).*

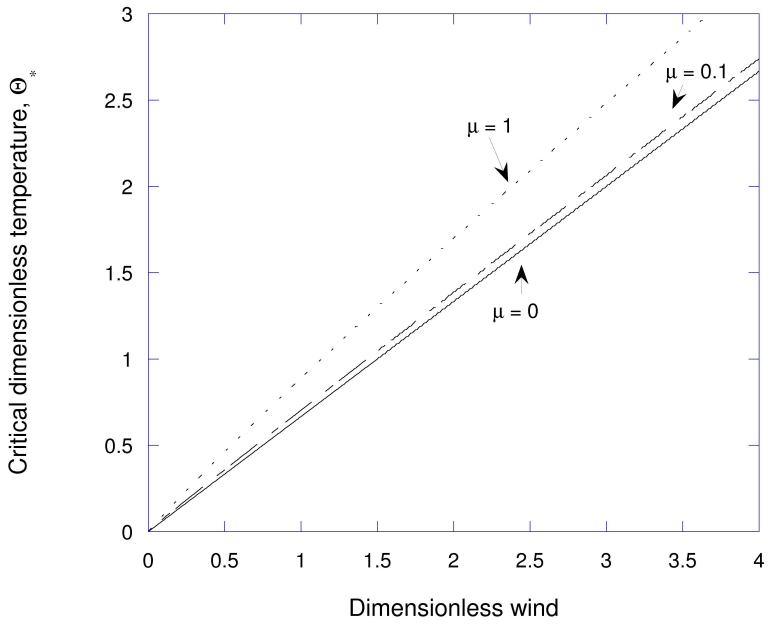


Figure 4.7.: *The maximum temperature of the wind driven regime, $\Theta_*$, plotted as a function of W, for three thermal mass cases: (1) $\mu = 0$, plotted as a solid line; (2) $\mu = 0.1$, plotted as a dashed line, and; (3) $\mu = 1$, plotted as a dotted line.*

figure 4.7 as a function of W, for $\mu = 0$, $\mu = 0.1$, and $\mu = 1$. In the $\mu = 0$ case, the thermal mass has no effect, and we find the maximum temperature of the wind driven regime is $\Theta_* = \frac{2W}{3}$ (cf. equation 3.5). The thermal mass then has the effect of slightly increasing this temperature, as the excess temperature is absorbed by the mass. Given this $\Theta_*$, we can predict the temperature of the thermal mass from equation 4.10.

### 4.4.3. Numerical models

#### Varying mass of thermal mass $M$

Figure 4.8 shows the temperature evolution of the interior and thermal mass, as a function of time (plot (a)) and log time (plot (b)), for three different cases: (1) M = 1, shown as a solid lines; (2) M = 0.1, shown as dashed lines, and (3) M = 0.01, shown as dotted lines. In all cases $W = 1.7$ and $\mu = 0.5$. In the case where $M = 1$ the thermal mass has little effect, and so the system heats almost

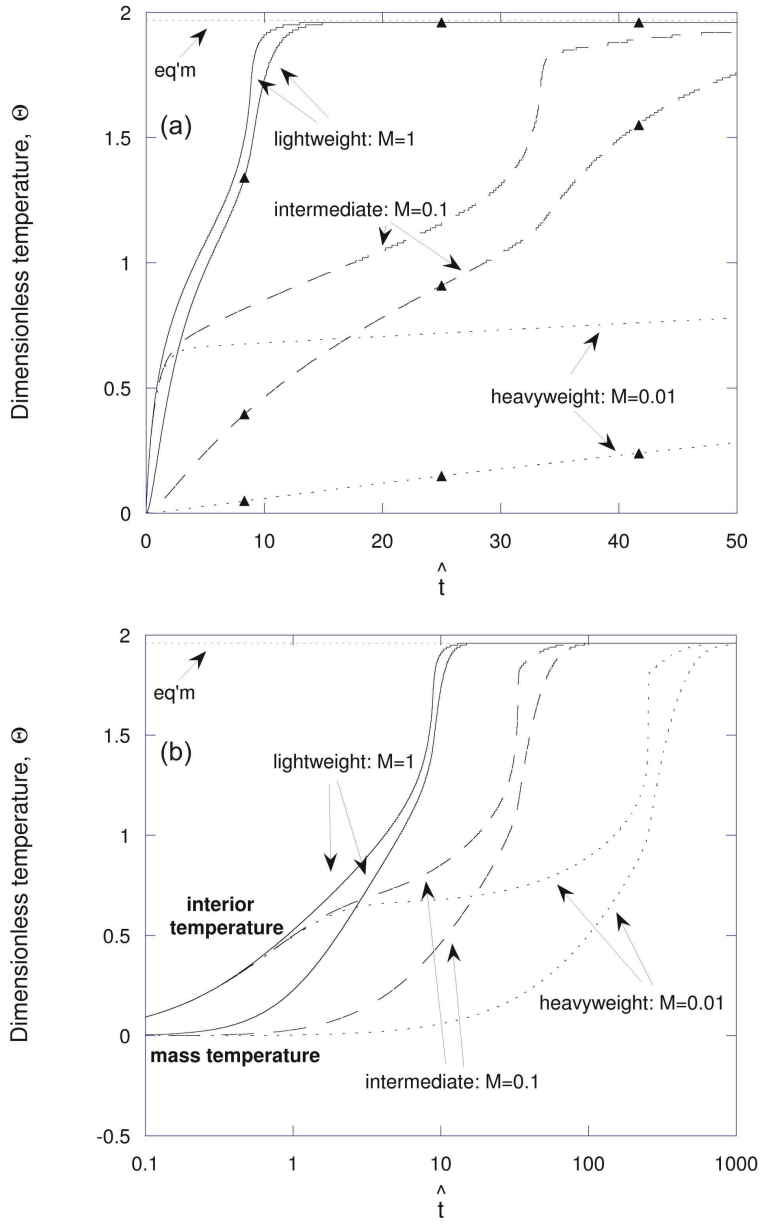


Figure 4.8.: *Temperature evolution of a naturally ventilated building, subject to wind opposing buoyancy, from an initial state colder than equilibrium, as a function of time (plot (a)) and log time (plot (b)), for three cases. In each case the the interior temperature and thermal mass temperature are shown as marked. The three cases are: (1) $M = 1$, shown as solid lines; (2) $M = 0.1$, shown as dashed lines; and (3) $M = 0.01$, shown as dotted lines. The case shown here is for $W = 1.7$, $\mu = 0.5$. All three systems tend towards the marked equilibrium at $\Theta \sim 1.96$.*

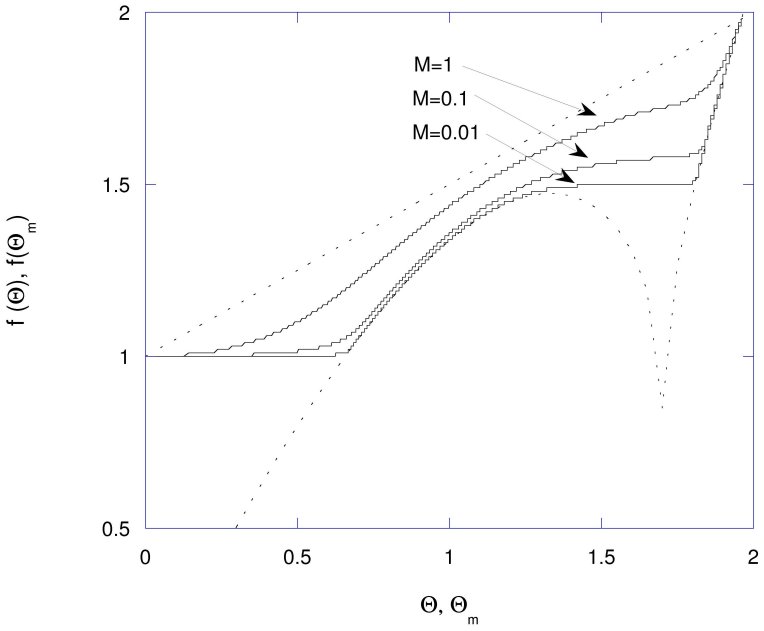


Figure 4.9.: *Temperature evolution marked on a plot of forcing and response. The solid lines show* $1 + \Theta_m$ *as a function of* $\Theta$ *for M=1, M=0.1 and M=0.01 as marked. The dotted lines show the forcing and response.*

in an almost linear fashion; by comparison, the case with $M = 0.1$ is clearly divided into two fast interior temperature evolutions (at $\hat{t} = 0$ and $\hat{t} \sim 30 - 35$) and two slower evolutions, and the separate timescales of evolution are yet more distinct when $M = 0.01$.

Figure 4.9 shows $1 + \Theta_m$ as a function of $\Theta$ and allows direct comparison to figure 4.6. The forcing and response are shown as thin dotted lines, while the three evolutions are shown as solid lines: M=1, M=0.1 and M=0.01 as marked. Here we see that in the heavyweight building (M=0.01) the temperature evolves as described in the previous section, while in the lightweight building (M=1) the thermal mass heats on a comparable timescale to the interior air, and so the distinction between evolutions to the manifold and evolutions along the manifold is less clear.

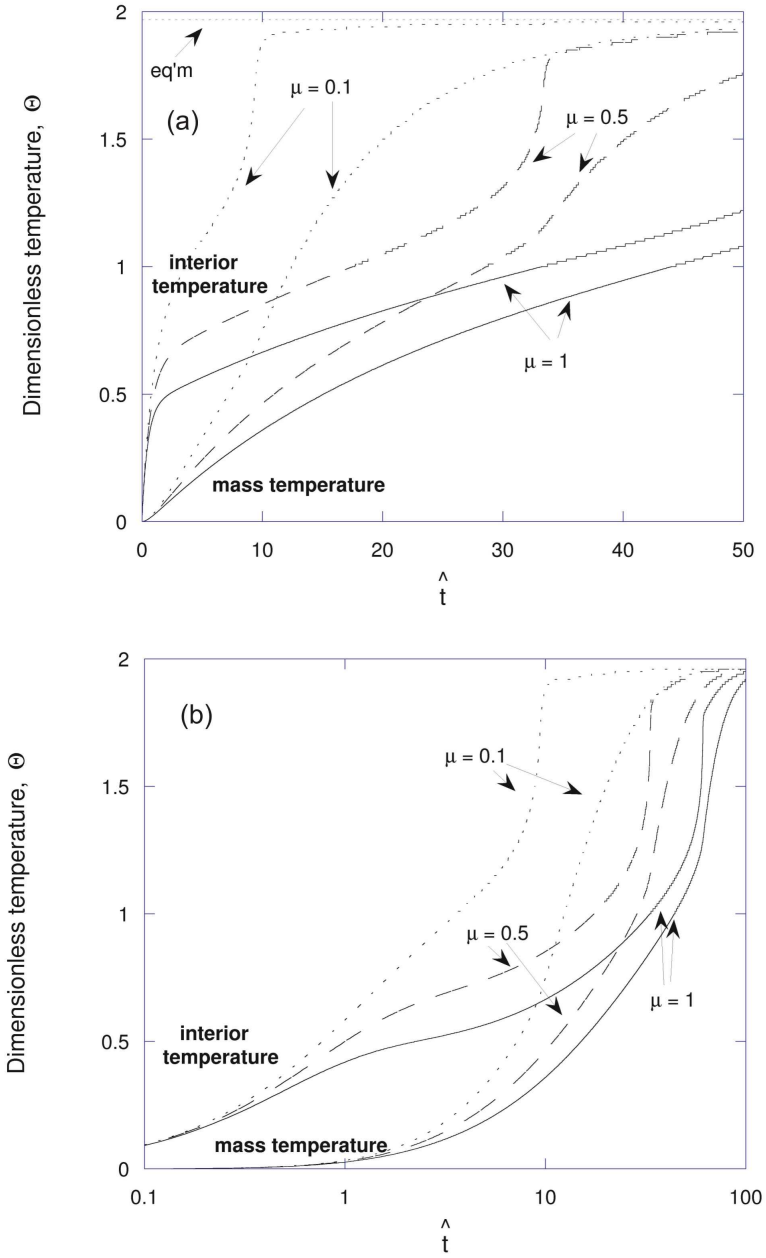


Figure 4.10.: *Plot showing the evolution of the temperature of a heavyweight building, subject to wind opposing buoyancy, from an initial state colder than equilibrium, as a function of time (plot(a)) and log time (plot (b)), for three cases. In each case interior temperature and thermal mass temperature are shown, as marked. The three cases are: (1)* $\mu = 0.1$*, shown as dotted lines; (2)* $\mu = 0.5$*, shown as dashed lines, and (3)* $\mu = 1$*, shown as solid lines. The case shown here is for* $W = 1.7$*,* $M = 0.1$*. All three systems tend towards the marked equilibrium at* $\Theta \sim 1.96$*.*

#### Varying rate of heat exchange $\mu$

Figure 4.10 shows the temperature evolution of the interior and thermal mass, as a function of time, for three different cases: (1) $\mu = 0.1$, shown as dotted lines; (2) $\mu = 0.5$, shown as dashed lines, and (3) $\mu = 1$, shown as solid lines. In all cases $W = 1.7$ and $M = 0.1$. $\mu$ determines the extent to which the temperature difference between the interior and the mass affects the interior temperature evolution (i.e. the importance of the final terms in equation 4.8). We see therefore that with small $\mu$, as in the dashed line, the temperature behaviour of the interior is almost independent of the thermal mass temperature, while with larger $\mu$ (i.e. the solid line) the temperature behaviour of the interior is slaved to the thermal mass.

#### Summary of time-dependent behaviours

The numerical models presented in this section provide clear support for the intuition presented in the previous section: that in thermally massive buildings, evolution between flow regimes will occur on a much faster timescale than evolution along flow regimes. This is because the evolutions between flow regimes are governed only by the internal temperature dynamics, as exemplified by equation 4.8, while the evolutions along flow regimes occur only as the thermal mass heats, as exemplified by the more slowly changing equation 4.9. In the next section we present a series of analogue experiments which demonstrate this separation of timescales: first, we describe our analogue experimental apparatus, and test the theory of section 4.2.

## 4.5. Experimental method

As in previous chapters, we complement the theoretical conclusions with a series of analogue water bath experiments. First, we describe the experimental apparatus used. We then provide experimental data showing how the building evolves with only heating under two separate cases: one in which the building state is initially warmer than the exterior, and one in which the building states

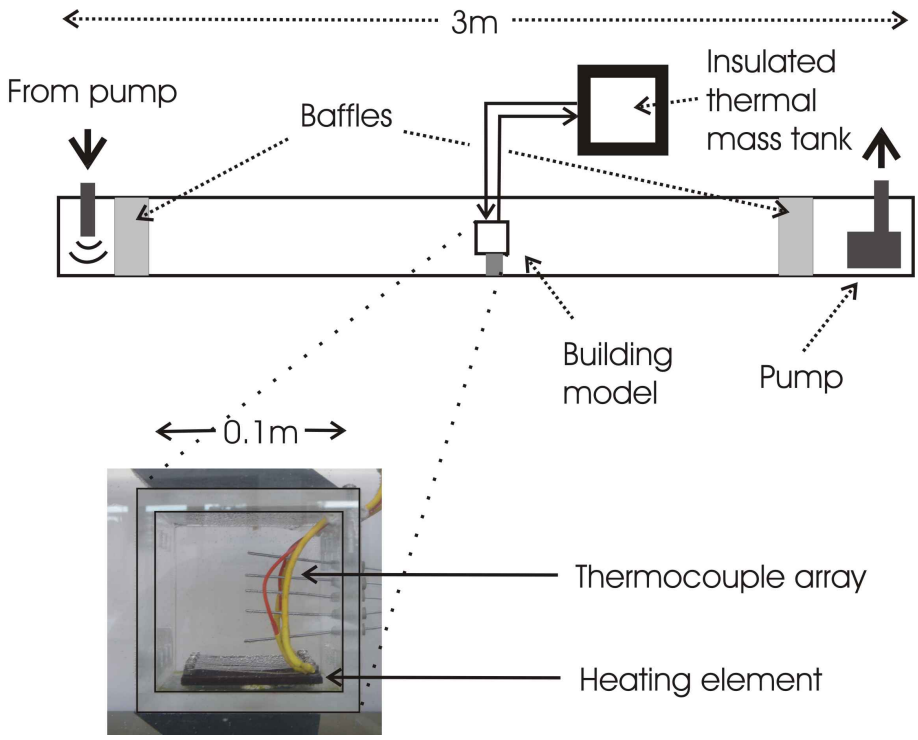


Figure 4.11.: *The experimental apparatus.*

is initially colder than the exterior. Finally, we introduce a wind and show experimental data supporting the conclusions of section 4.4, in which the building is seen to evolve slowly in one regime, and then evolve rapidly to another regime.

### 4.5.1. Apparatus

We use a similar apparatus, with a flume tank and a distributed hotwire, to the one in the previous chapter. Figure 4.11 shows an overview of the experimental apparatus and a closeup of the building model.

The building model has interior dimensions 0.1m x 0.1m x 0.1m. The model has three circular openings, on the upwind side, of diameter 0.01m, and these openings are located 0.08m higher than an equivalent set of openings on the downwind side. The building model was raised approximately 0.1m from the bottom of the flume. The flume is made of perspex and is 3m long, 0.3m high and 0.15m wide. A series of honeycomb lattices act as baffles at either end and

straighten the flow: dye tests find the flow to be very close to straight in the body of the tank. Typical flow speeds in the flume are $\sim 0.01\text{ms}^{-1}$. The effective wind pressure acting on the face of the tank is found using a series of calibration experiments with forced ventilation. For the experiments in this work, the wind pressure was found to be 4Pa$\pm$0.5Pa. A similar series of calibration experiments with no wind determined the fitting parameter $c^* = 0.65 \pm 0.03$.

The heating plate is made of a series of high-resistance metal coils attached to a power supply with variable power output (Gladstone and Woods, 2001). The maximum heating power which can be achieved is $480W$.

The thermal mass tank has dimensions 0.2m $\times$ 0.2m $\times$ 0.25m, and is connected to the main tank via two hoses of inside diameter 0.01m. These hoses are connected to two peristaltic pumps, and to a flow meter which allows the flow rate to and from the thermal mass to be measured. The entire thermal mass system is insulated. Typical flow rates to and from the thermal mass are $10^{-5}\text{m}^3\text{s}^{-1}$.

Temperatures were measured using five type-K thermocouples vertically distributed within the building, two thermocouples distributed within the exterior fluid, and one thermocouple measuring the thermal mass temperature. Temperature measurements were made every second, using Picolog software via a TC-08 cold junction. Typically the exterior temperature was around $15^o$C, and the temperatures of the thermal mass and interior ranged from around $5^o$C, initially cooled using ice, to around $35^oC$, initially filled with hot water or heated using the heating element. Temperature differences within the building were found to be small ($\pm 0.1^o$C) compared to internal-external temperature differences, which suggests that the interior was well mixed.

Other experimental parameters used were $\beta = 0.36\text{kgm}^{-3}\text{K}^{-1}$, $\rho = 1000\text{kgm}^{-3}$, $C_p = 4184\text{Jkg}^{-1}\text{K}^{-1}$ and $g = 9.81\text{ms}^{-2}$. Qualitative observations about the flow patterns were made using dye streaks.

The experimental procedure was as follows. The interior building fluid and thermal mass were initially set to the same temperature, by adding either warm

or cold water, with the building model sealed by bungs. At the start of the experiment, the bungs were removed from the building, and heating and exchange with the thermal mass were begun. Experiments were then left to run for 2000s. The experimental data presented here is averaged over ten-second intervals, to eliminate high frequency noise, and the interior data is also averaged spatially (although little spatial variation was observed in the temperature measurements).

With the thermal mass modelled as described above, equations 4.3 and 4.4 can be rewritten as

$$\rho C_p V \frac{d\Delta T}{dt} = H - \rho C_p c^* A \Delta T \sqrt{\frac{|\Delta p_w - \beta g h \Delta T|}{2\rho}} + \rho C_p q_{tm} (\Delta T_m - \Delta T) \quad (4.11)$$

and

$$\rho C_p V_m \frac{d\Delta T_m}{dt} = \rho C_p q_{tm} (\Delta T - \Delta T_m) \quad (4.12)$$

where $q_{tm}$ is the flow rate to and from the thermal mass.

### 4.5.2. Results: no wind

Figure 4.12a shows experimental data validating the model of section 3.1. In the experiment, the building and thermal mass temperatures were initially set to around $12^o$C greater than the exterior fluid, and the ventilation was begun at time $t = 0$ by removing stoppers from the window openings. The dotted lines show the theoretical temperatures for the interior (square markers) and the thermal mass (circular markers), while the solid lines show experimental measurements. In this experiment, the heating load was set to 120W, while the flow rate to and from the thermal mass was measured at $1 \times 10^{-5}\mathrm{m}^3\mathrm{s}^{-1}$. The dashed line shows the equilibrium temperature. The figure shows good agreement between theory and experiment. Figure 4.12b shows the same data plotted on a log axis for comparison to figure 4.2b.

Figure 4.13a shows the results of an experiment testing the theory of section 3.2. The building and thermal mass temperatures were initially set to around

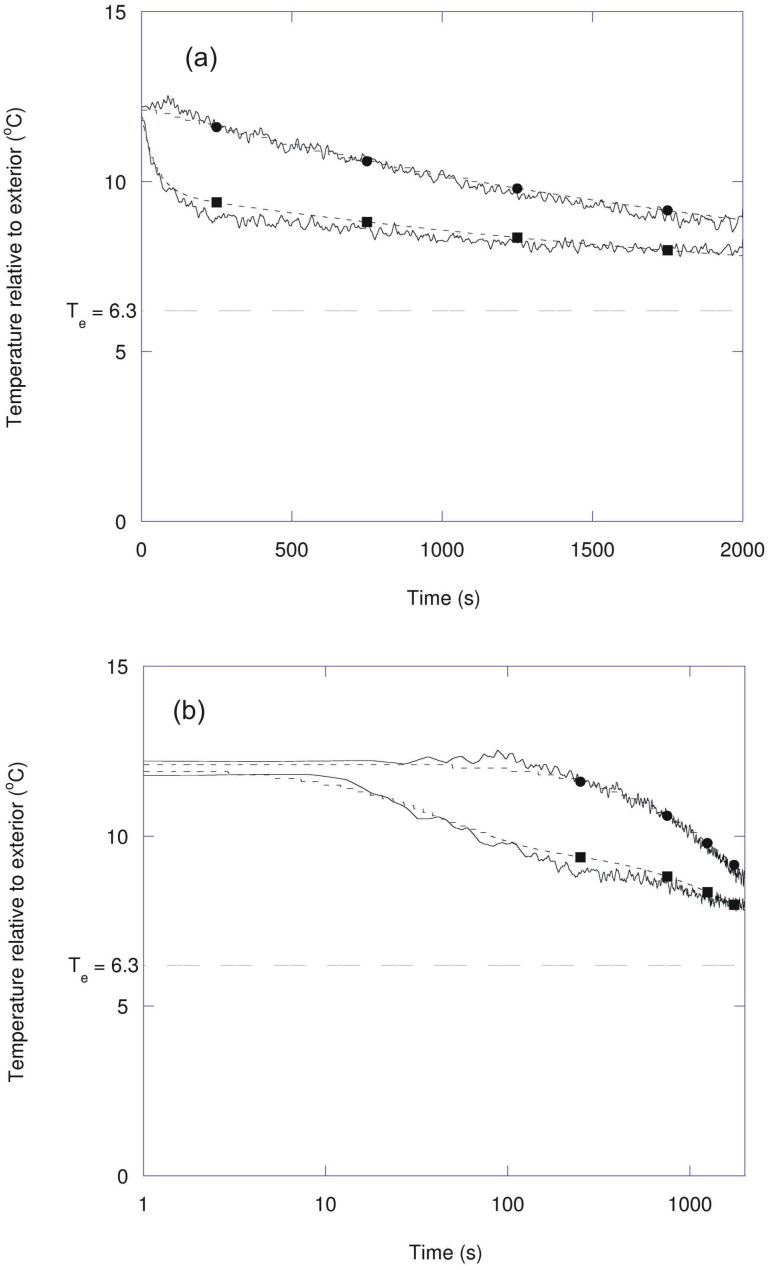


Figure 4.12.: *Comparison of theory and experimental data from a model of a typical winter morning in a building with interior thermal mass. The dotted lines show the theoretical temperatures for the interior (square markers) and the thermal mass (circular markers), while the solid lines show experimental measurements. The data is plotted twice: in figure (a), on a linear time axis, and in figure (b), on a log time axis.*

$4^oC$ less than the exterior fluid, and the ventilation was begun at time $t = 0$ by removing stoppers from the window openings. The heating load was 175W while the flow rate to and from the thermal mass was $1 \times 10^{-5} m^3 s^{-1}$. The dashed line shows the equilibrium temperature which the system tends towards. Again, the experimental data is in good accord with the theory. Figure 4.13b shows the same data plotted on a log axis for comparison to figure 4.3b.

### 4.5.3. Results: wind interacting with buoyancy

Here we test the theory of section 4.4 experimentally. Figure 4.14a shows two evolutions of an experiment modelling the transient evolution under opposing wind and buoyancy. The graph shows experimental data as solid lines and numerical predictions as dotted lines. In one experiment, the exchange flow rate with the thermal mass was $0.65 \times 10^{-5} m^3 s^{-1}$ (thermal mass temperature shown as an unmarked line; interior temperature marked by circles), while in the other the exchange flow rate with the thermal mass was $1 \times 10^{-5} m^3 s^{-1}$ (thermal mass temperature marked by squares; interior temperature marked by triangles). In both experiments, the system was initiated with the interior and thermal mass about three degrees warmer than the exterior. At $t = 0$ the ventilation is commenced, by removing bungs, and the heat load is set to 375W. In both experiments, therefore, the system begins in the wind driven regime, but the heat load is sufficient that the system tends to the buoyancy driven regime. The results are in excellent accord with the theory.

Our experiments are somewhat limited: our ratio of $\frac{M}{\mu}$ is fixed at 0.1 due to the relative sizes of our experimental thermal mass and building models. By varying the flow rate to and from the thermal mass, we effectively present evolutions for two different values of $\mu$ (cf. figure 4.10). The experimental results clearly show that the system undergoes a slow evolution along the manifold and a fast evolution to the manifold (both initially, and as the system evolves between flow regimes). This is particularly clear in the experiment with the higher exchange with the thermal mass (interior temperature marked by triangles): the system evolves quickly to the wind driven regime ($\sim 0 - 200$s);

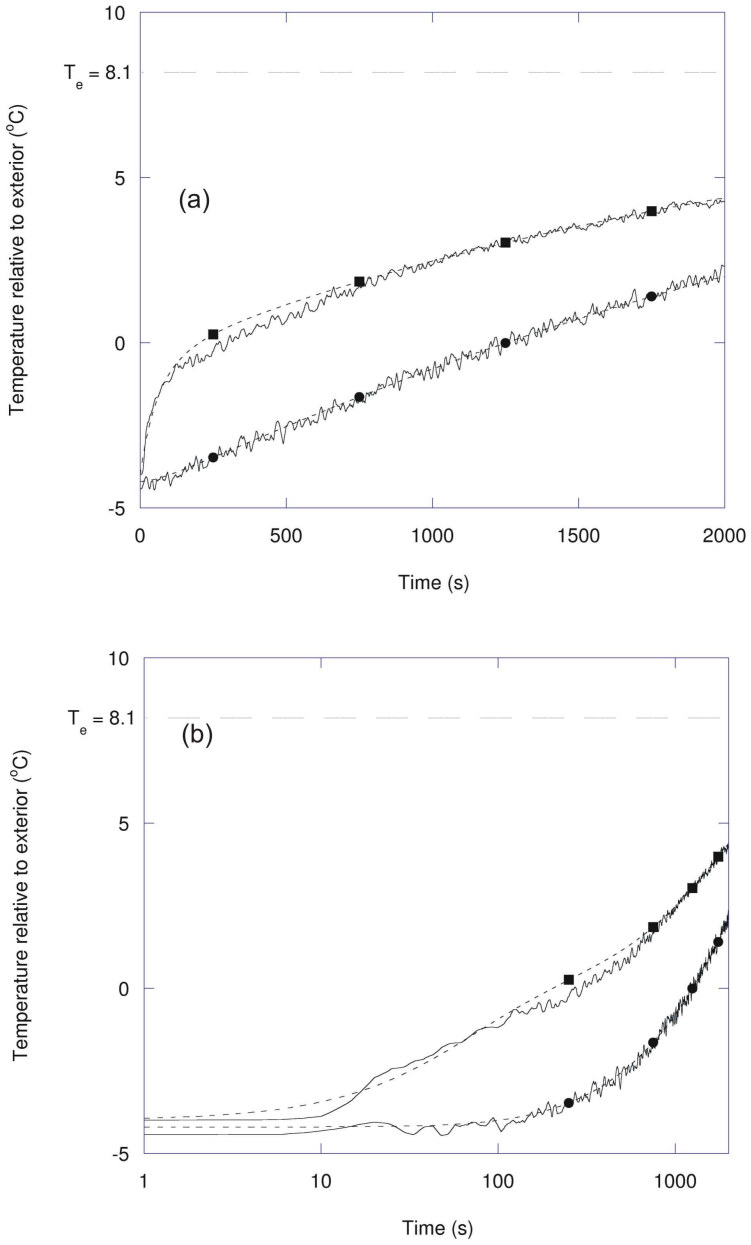


Figure 4.13.: *Comparison of theory and experimental data from a model of a typical summer morning in a building with interior thermal mass. The dotted lines show the theoretical temperatures for the interior (square markers) and the thermal mass (circular markers), while the solid lines show experimental measurements. The data is plotted twice: in figure (a), on a linear time axis, and in figure (b), on a log time axis.*

then slowly along the wind driven regime ($\sim 200 - 800$s); then quickly to the buoyancy driven regime ($\sim 800 - 1100$s); and then slowly along the buoyancy driven regime. This effect would be more pronounced in a system with a larger thermal mass, as indicated by figure 4.8. The results also show that the time at which the system evolves to the thermal mass is strongly controlled by the nature of the temperature exchange between the mass and the interior. The data are replotted on a log axis in figure 4.14b for comparison to figure 4.10b. The data are also plotted on a dimensional plot of forcing and response, for comparison to figure 4.9.

## 4.6. Further analysis

In the previous chapter we showed that some changes in flow regime are governed by variations in the wind, and are thus difficult to incorporate into a general control system. Here we extend the model of the previous chapter to investigate how thermal mass affects the possible range of building behaviours under varying wind. For simplicity we consider only buildings with extremely large interior thermal mass, for which $M \ll 1$. We can therefore consider the thermal mass temperature as fixed, $M = 0$ and examine the behaviour of the building in this case.

First, we consider a thermal mass temperature $\Theta_m = 1$ and investigate the effects of changing $\mu$, which represents the rate of exchange of heat between the mass and the room. The building behaviour is shown in figure 4.16, which shows the equilibria for two cases; $\mu = 0$, with the lines marked by circles; and $\mu = 1$, with the lines marked by triangles. In each case the solid line represents the stable wind driven regime, the dashed line the stable buoyancy driven regime, and the dotted line the unstable wind driven regime. The case where $\mu = 0$ represents the system without thermal mass. In this case, as shown in chapter 3, the buoyancy driven regime and wind driven regime do not converge for finite wind speeds, and so the buoyancy driven regime can be sustained indefinitely as the wind increases, provided the increase in wind is sufficiently slow. However,

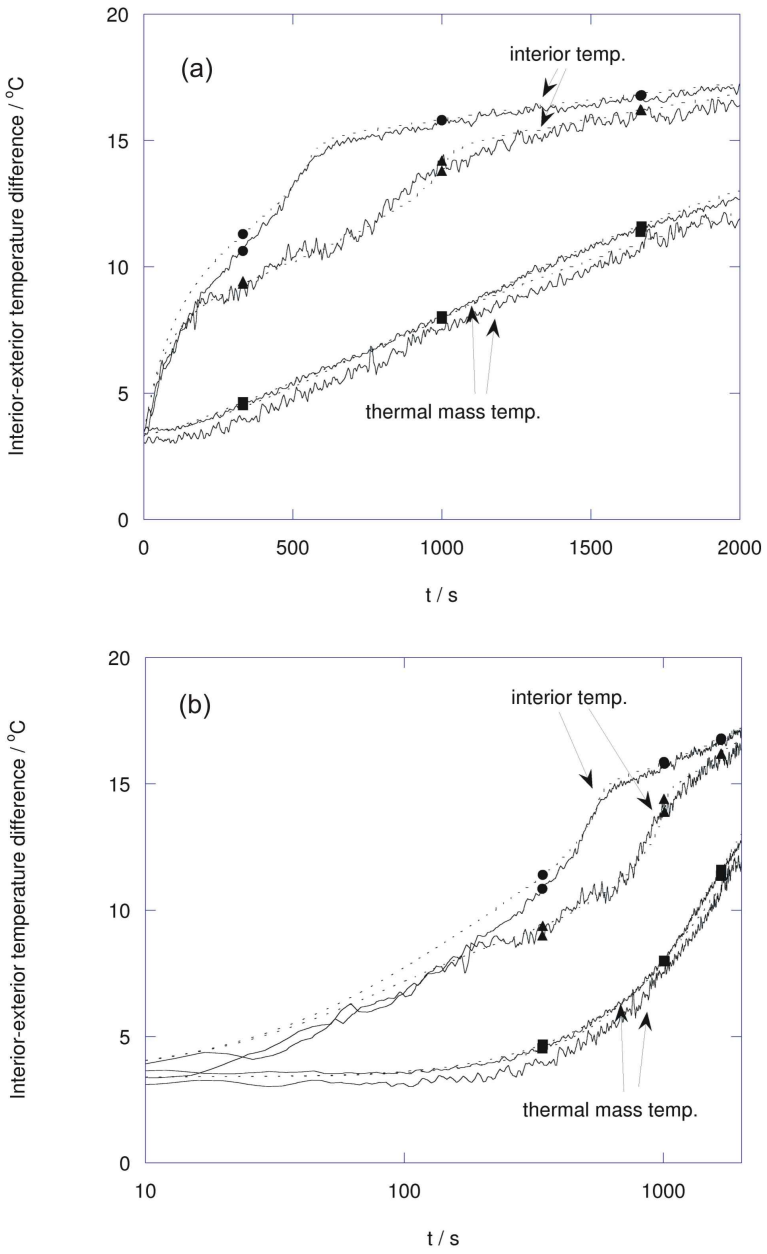


Figure 4.14.: *Plot showing experimental (solid line) and theoretical (dotted line) time evolution with (a) an exchange flow rate of* $0.65 \times 10^{-5}\mathrm{m}^3\mathrm{s}^{-1}$ *(thermal mass temperature as an unmarked line; interior temperature marked by circles), and (b) an exchange flow rate of* $1 \times 10^{-5}\mathrm{m}^3\mathrm{s}^{-1}$ *(thermal mass temperature marked by squares; interior temperature marked by triangles). The data is plotted twice: in figure (a), on a linear time axis, and in figure (b), on a log time axis. Of particular note is the interior temperature evolution on figure (a) marked by triangles: here we clearly observe two fast transitions (*$\sim 0 - 200s$ *and* $\sim 800 - 1000s$*), while the rest of the evolution is slower. This effect would be more pronounced in a system with a larger thermal mass.*

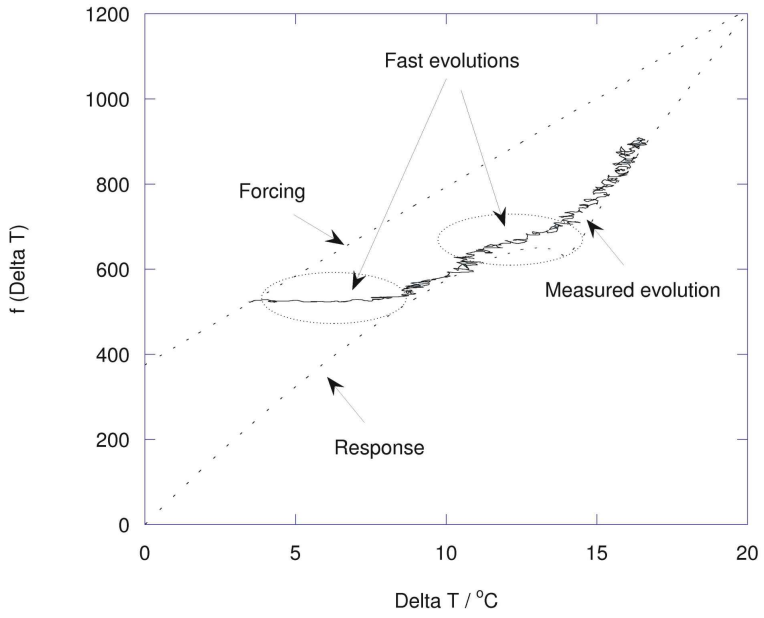


Figure 4.15.: *A plot showing the data of figure 4.14 compared to the dimensional forcing and response terms, which are shown as dotted lines (cf. figure 4.9).*

in the case where $\mu = 1$, the buoyancy driven and wind driven regimes converge, and so if the wind increases above the wind at which the two regimes converge, the system must move to the right of the unstable wind driven curve, and hence the building will cool to the stable wind driven regime.

Similarly, we plot the equilibria of the system for various thermal mass temperatures $\Theta_m$ with $\mu = 1$ in figure 4.17. Again, the buoyancy driven regime and wind driven regime intersect, with the location of the intersection dependent on $\Theta_m$.

To establish the point at which the buoyancy driven regime and wind driven regime intersect, we set $\Theta = W$ in equation 4.8, which gives the temperature at the intersection

$$\Theta_{int} = \frac{1}{\mu} + \Theta_m \tag{4.13}$$

and the wind at the intersection $W_{int} = \Theta_{int}$. If the exchange between the

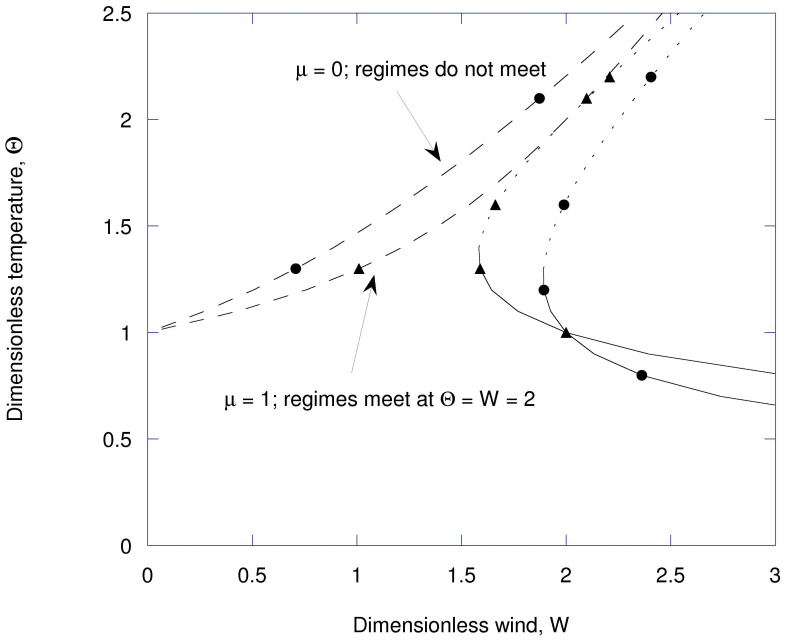


Figure 4.16.: *A plot of temperature $\Theta$ as a function of wind speed $W$, showing the system equilibria for a fixed thermal mass temperature $\Theta_m = 1$ and two values of $\mu$: $\mu = 0$, with the lines marked by circles; and $\mu = 1$, with the lines marked by triangles. In each case the solid line represents the stable wind driven regime, the dashed line the stable buoyancy driven regime, and the dotted line the unstable wind driven regime.*

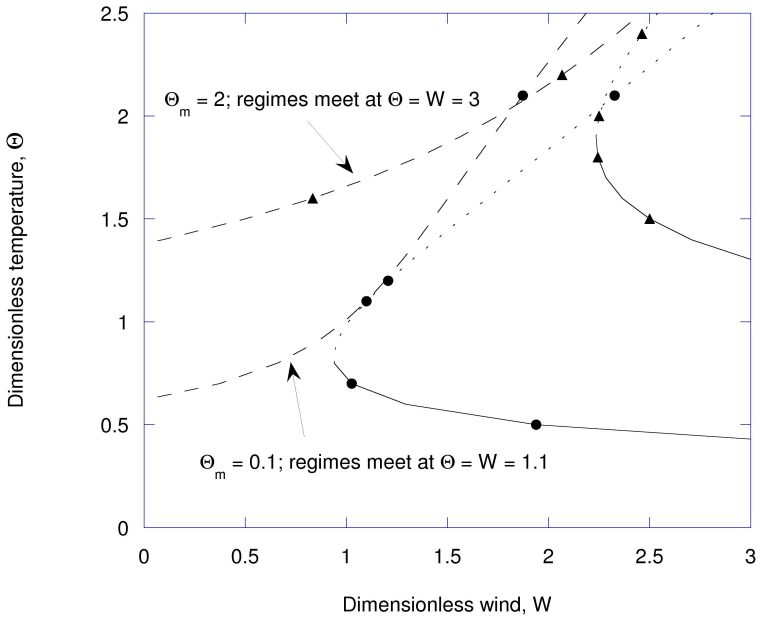


Figure 4.17.: *A plot of temperature* $\Theta$ *as a function of wind speed* $W$*, showing the system equilibria for a fixed thermal mass parameter* $\mu = 1$ *and two values of* $\Theta_m$*:* $\Theta_m = 0.1$*, with the lines marked by circles; and* $\Theta_m = 2$*, with the lines marked by triangles. In each case the solid line represents the stable wind driven regime, the dashed line the stable buoyancy driven regime, and the dotted line the unstable wind driven regime.*

thermal mass and the interior is small, $\mu \ll 1$, and the buoyancy driven regime can be sustained under increasing wind up to high winds and temperatures. However, if the heating to the room from the thermal mass is of comparable order to that from the heat load ($\mu \sim 1$) the system will evolve to the wind driven regime when the wind increases above $W_{int}$. Note that equation 4.13 holds true for all thermal mass conditions, and not just for the limiting case of infinite thermal mass: the maximum temperature which the building can reach in the buoyancy driven regime is therefore fixed for any given thermal mass temperature.

To illustrate the evolution of the system under increasing winds, consider figure 4.18, which shows how the temperature in the building varies under winds of the form

$$W = W_0 + \lambda \hat{t} \tag{4.14}$$

Figure 4.18 is plotted with $\mu = 1$ and $\Theta_m = 1$, and the dotted lines show the equilibria of this system. The dashed line shows the temperature evolution for $\lambda = 0.1$ and the solid line shows the evolution for $\lambda = 1$, calculated numerically from equation 4.8. In both cases $W_0 = 0$ and $\Theta_0 = 1$. We see that under a rapidly changing wind, the system evolves directly to the wind driven regime without heating along the buoyancy driven curve. However, under a slowly changing wind (i.e. $\lambda = 0.1$) the system evolution approximately traces out the buoyancy driven curve until the wind reaches close to $W_{int}$. At this point, the increasing wind causes the system to evolve across the unstable wind driven curve and hence cool towards the stable wind driven equilibrium.

The thermal mass in very heavyweight buildings therefore prevents the system reaching high temperatures in the buoyancy driven regime, and in doing so buffers the system against unbounded temperature variations if the system oscillates between the wind driven and buoyancy driven regimes.

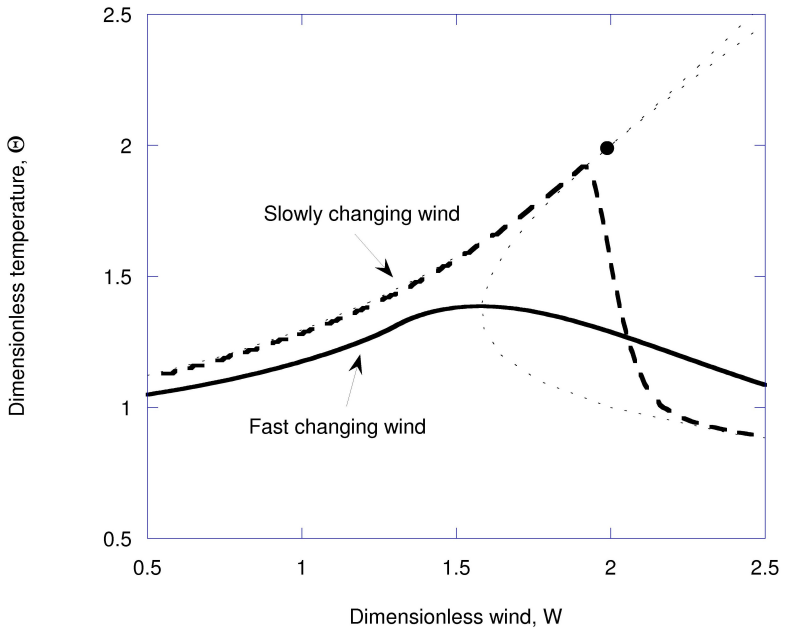


Figure 4.18.: *A plot of temperature $\Theta$ as a function of wind speed $W$, showing numerical predictions of two possible temperature evolutions under varying wind, for $\mu = 1$ and $\Theta_m = 1$. The dotted lines show the equilibria of the system. The dashed line shows the temperature evolution under a slow increase in wind ($\lambda = 0.1$) while the solid line shows the evolution under a rapid increase in wind ($\lambda = 1$). The intersection of the wind driven and buoyancy driven regimes, at $\Theta = W = 2$, is also marked.*

## 4.7. Applications and Conclusions

We now investigate how the predictions of this study might apply to a real building. Consider an open plan office, theatre or classroom of dimensions 8m × 8m × 5m. The space has two ventilation openings: one at ground level on the downwind face, and one at a height of 5m on the upwind face. Both openings have effective openings area $1\text{m}^2$. There is a heat load in the space of 2kW, representing, perhaps, 20 people. A wind pressure difference of 1Pa acts between the upwind and downwind openings, corresponding to an external wind speed of $\sim 2 - 3\text{ms}^{-1}$. $60\text{m}^2$ of the ceiling is covered in exposed thermal mass, corresponding to a value of 150 for $S\chi$. Figure 4.19 shows how the temperature in the buildings varies over the course of a typical working day, assuming the building begins at the exterior temperature at 9am.

The figure shows three separate cases. In the first case, marked by solid lines, $M = 10\mu$: the thermal mass stores ten times less heat than the interior air. This case corresponds to a very lightweight building. Here, the building temperature increases almost linearly over the first hour of the day, with little distinction between the transitions along the regime and between regimes, and then remains constant. This strategy has the advantage of simplicity, although it does little to maintain a cold interior.

The second case, shown by dashed lines and corresponding to $M = 0.1\mu$, is the most problematic. This case corresponds to an intermediate amount of thermal mass. Here, the building temperature appears to be levelling out at around $6^o$C warmer than the exterior, until suddenly the flow regime changes and the building warms rapidly after around 3 hours. This case is difficult to predict or control, since slight variations in conditions will change the time at which the flow regime changes. This case is also likely to cause occupant discomfort, as the temperature rapidly changes from its established level.

The third case, shown by dotted lines and corresponding to $M = 0.01\mu$, represents a heavyweight building. Here, the thermal mass provides sufficient buffering to the system that the building flow regime does not change over the

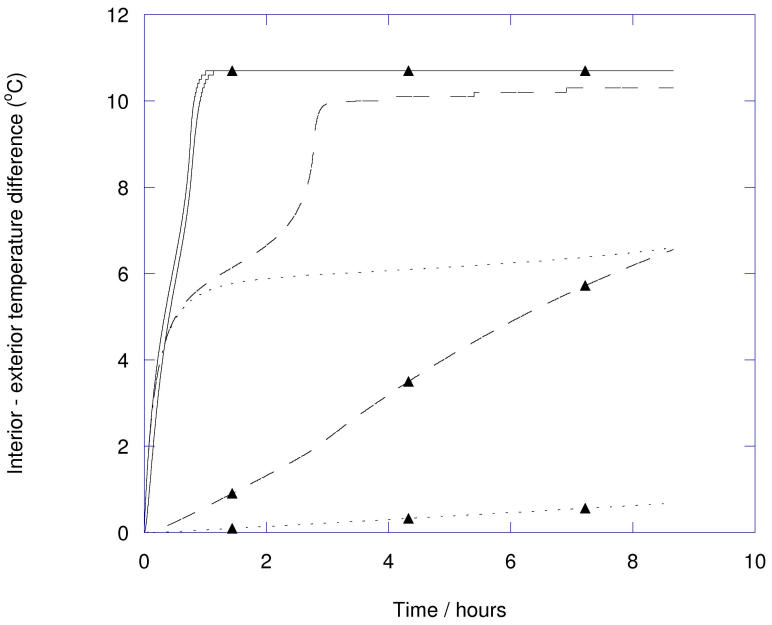


Figure 4.19.: *A plot of interior-exterior temperature difference, in* $^o$C*, as a function of time, in hours, for a typical office building. The unmarked lines represent interior temperatures, and the triangle-marked lines represent thermal mass temperatures, for three cases: (1) a lightweight building, with* $M = 10\mu$*, shown as a solid line; (2) an intermediate case, with* $M = 0.1\mu$*, shown as a dashed line, and (3) a heavyweight building, for which* $M = 0.01\mu$*, shown as a dotted line.*

course of the day. This case is relatively simple to control, and provides the most buffering against the warm exterior. Building designers aiming for this control strategy should take care to incorporate sufficient thermal mass that the building remains in the wind driven regime and case (2) does not occur.

This chapter has considered how the interaction between wind and buoyancy is affected by the thermal mass in heavyweight buildings. Two preliminary case studies, involving buoyancy driven flow, showed how thermal mass can slow the rate at which the system tends to equilibrium. When the nonlinear interaction between wind and buoyancy is considered, the problem becomes more complicated, and evolution occurs on two separate timescales: one controlled by the thermal mass, and one controlled by the building dynamics. These theoretical predictions were supported by new laboratory experiments, and implications for real buildings were discussed.

# 5. The control of multiple steady states through building geometry

*The previous chapters have investigated the building behaviour with two openings, and opposing wind and buoyancy. Here, we investigate whether further openings cause qualitative differences in the range of flow regimes which can occur in the building. We introduce a new opening, and find that if this third opening exceeds a critical area, then the multiple steady states are eliminated, and the transition from buoyancy to wind dominated flow is continuous. This critical area is shown to be a function of the relative heights of the three windows. The predictions of the model are in accord with new laboratory experiments, discussed and presented in section 5.4, and the implications for building design are discussed.*

## 5.1. Introduction

The previous chapters have discussed the nature of multiple steady states in buildings with two openings. However, many buildings are, in reality, of more complex geometry, and include three or more openings to the exterior. In this chapter we show that this may lead to a fundamental difference in the flow regime as compared to a building with just two openings. In particular, the research presented in this chapter shows that in a building with three openings, if the upper downwind window is sufficiently large, then as the internal heat load increases there may be a smooth adjustment from the wind-dominated to the buoyancy-dominated flow regime, with no intermediate regime in which there are multiple steady states.

Before commencing a description of quantitative modelling and laboratory

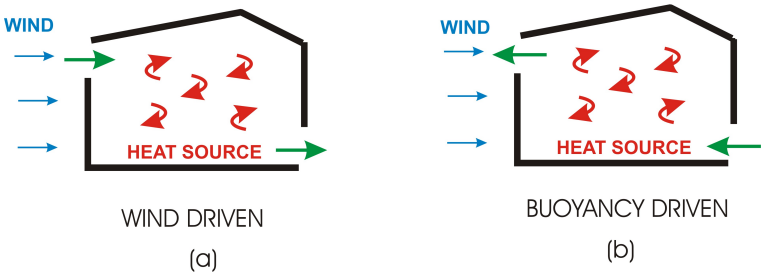


Figure 5.1.: *With two openings, two regimes are possible: a wind dominated regime, shown on the left, and a buoyancy dominated regime, shown on the right.*

experiments, it is useful to contrast how wind and buoyancy forces compete in a theoretical simplified open-plan building with three openings.

In chapter 3 we discussed the transitions between flow regimes in a building with two openings, and deduced that no smooth transition was possible between the stable flow regimes. This is because in order for the flow regime to change, the ventilation rate must drop to zero. In this chapter we show that if there is a further opening, of similar size, at a high level on the downwind face, then the flow may adjust continuously through a series of steady state solutions from the wind driven to the buoyancy driven flow. To illustrate this difference, we consider in detail the inclusion of a new high level opening on the downwind face of the building (figure 5.2). The transition from buoyancy to wind driven flow may be understood by considering in detail the flow through the three vents as the wind speed increases from small to large values. At small wind speeds, the heating within the space leads to a pure upward displacement mode of ventilation, with inflow at the base and outflow through both high level vents (figure 5.2a). As the wind increases, the flow through the high level upwind vent falls to zero and then reverses, while the flow through the two downwind vents remain of finite value, thereby venting the heat load from the space (figure 5.2b). As the wind increases further, the flow through the low level, downwind vent reverses to become an outflow; at this second critical wind speed, there is still a finite in/out flow through the two high level vents which acts to ventilate the heat generated within the space (figure 5.2c).

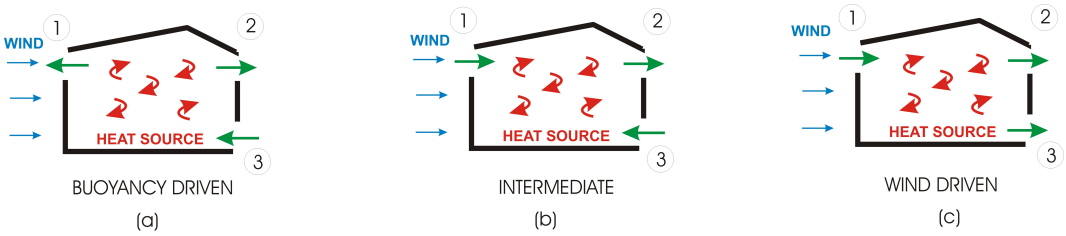


Figure 5.2.: *With three openings, three regimes are possible: a buoyancy dominated regime, shown as (a), with inflow through the low downwind vent, and outflow through both upper vents; an intermediate regime, (b), with inflow through the upwind and low downwind vents, and outflow through the upper downwind vent; and a wind-dominated regime, (c), with inflow through the upwind vent and outflow through the downwind vents.*

Real buildings are likely to have three or more openings, and so for a given heat load and wind speed, it should be possible to ensure that for each pair of values of wind speed and flow, there is a unique flow regime. However, with two openings, we have seen that there is a set of conditions for which the flow is non-unique, and so the transition between flow regimes is discontinuous. By continuity, it follows that in a building with three openings, but in which the upper downwind opening is rather small, there may be a range of conditions for which the flow is non-unique and hence the transitions in flow regime may again be discontinuous.

The main purpose of this chapter is to identify the key factors which control whether, in a building with three openings, the flow is uniquely determined in terms of the wind speed and heat load. This situation (uniquely determined flow) leads to much simpler control of the natural ventilation, and smooth rather than discontinuous transitions in flow regime.

In section 3 a model is developed of the natural ventilation within an open plan building with three openings (figure 5.2), in which there is a distributed heating system at low level. We examine the controls on the flow regime and flow rate as both the heat load and the size of the high-level downwind opening change for a given size of the other openings. We compare the predictions of the model with a series of new analogue laboratory experiments in which a

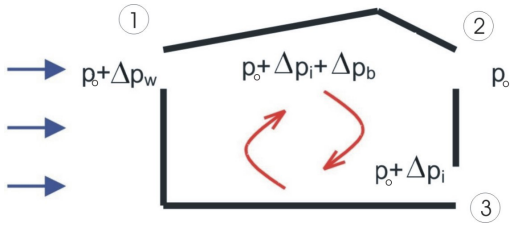


Figure 5.3.: *Pressures acting on the building. We assume a background pressure $p_0$, and note that three further pressures need to be considered: the wind forcing $\Delta p_w$, which is positive from exterior to interior at the upper upwind opening, the hydrostatic pressure difference between the exterior cold air and interior warm air, $\Delta p_b$, which is positive from interior to exterior at the upper openings, and the pressure difference between the lower interior and exterior, $\Delta p_i$, which is positive from interior to exterior at all openings. The sign of $\Delta p_i$ varies with the flow regime.*

heated rectangular tank of water, with three ventilation openings, is placed in a steady background flow within a flume. We then explore how the size and height of the upper downwind opening affects the uniqueness of the flow as the heat load and wind speed vary. Using these results, we map out a bifurcation diagram of the different flow regimes as a function of opening area and height of the opening. Finally, we discuss the implications of these results for design and control of naturally ventilated buildings.

## 5.2. Analysis

### 5.2.1. Modelling Approach

We develop a simplified theoretical model of the overall ventilation flow and heat budget within a building. Figure 5.3 illustrates the geometry of the theoretical model building we consider. We assume the building has high-level openings at the same height on the upwind and downwind faces, and a further low-level opening on the downwind face (below the other two openings). In section 5, we will generalise the analysis to allow the height of the upper downwind opening to differ from that of the upper upwind opening. We use the suffices 1, 2 and 3 to represent the upper upwind opening, upper downwind opening and lower downwind opening respectively (see figure 5.3). For simplicity we consider the

case when the areas of the upper upwind and lower downwind openings are the same, i.e. $A_1 = A_3$.

We assume that the underfloor distributed heating leads to high Rayleigh number convection and hence a well-mixed interior (cf. Gladstone and Woods (2001)). We also assume that each opening is of sufficiently small vertical extent compared to the depth of the room that the flow is purely in- or outflow, as controlled by the pressure difference across the mid-height of that opening (cf Linden, Lane-Serff, and Smeed (1990)). This implies that the volume flow through each opening is (see Linden, Lane-Serff, and Smeed (1990)):

$$q_x = c^* A_x \sqrt{\frac{\Delta p_x}{\rho}} \tag{5.1}$$

where $q_x$ is the volume flow through an opening, $A_x$ is the area of that opening, $\Delta p_x$ is the pressure difference across the opening, $c^*$ is a loss coefficient and $\rho$ is the fluid density. For convenience we assume the the loss coefficient $c^*$ is the same for each opening of our model building.

The pressure difference between the upwind and downwind face of the building associated with the wind is taken to have the constant value $\Delta p_w$. We use $\Delta p_b$ to represent the hydrostatic pressure difference between the exterior cold air and interior warm air, measured between the mid-heights of the high-level and low-level openings, a vertical distance $h$ apart. $\Delta p_b$ is given by (see e.g. chapter 3)

$$\Delta p_b = \rho g' h \tag{5.2}$$

Finally, we denote the magnitude of the pressure difference across the lower downwind opening by $\Delta p_i$. Note the actual difference in pressure on the inner and outer surfaces of this opening changes sign depending on the flow regime.

For each flow regime (fig 5.2 a-c) the system is described by an overall mass balance and an energy balance, combined with the law for the volume flow through each of the three openings (equation 5.1). This gives us five equations for the five unknown quantities $\Delta p_i$, $\Delta T$, $q_1$, $q_2$ and $q_3$, in terms of the wind

forcing $\Delta p_w$, the internal heat load $H$, and the fluid properties and building geometry.

We first consider the wind-driven regime (figure 5.2c). Since the changes in density associated with the temperature changes are small, we can write the mass balance in the approximate form (Batchelor 1967)

$$q_1 = q_2 + q_3 \tag{5.3}$$

Combining equations 5.1 and 5.3 and noting the pressure differences across each opening, we find:

$$A_1\sqrt{\Delta p_w - \Delta p_b - \Delta p_i} = A_2\sqrt{\Delta p_b + \Delta p_i} + A_1\sqrt{\Delta p_i} \tag{5.4}$$

It is convenient to use dimensionless variables. We define $\alpha = A_2/A_1$, the ratio of the area of the upper upwind opening to the area of the downwind upper opening. We scale pressure relative to the wind forcing $\Delta p_w$, setting

$$p = \frac{\Delta p_i}{\Delta p_w} \tag{5.5}$$

and

$$\theta = \frac{\Delta p_b}{\Delta p_w} \tag{5.6}$$

We can then rearrange equation 5.4 to express $p$ in terms of $\theta$ and $\alpha$:

$$p = \frac{2 - \alpha^2\theta - \alpha^4\theta + \alpha^2 - 2\theta - 2\sqrt{\alpha^2(1 - \alpha^2\theta - \theta^2)}}{4 + \alpha^4} \tag{5.7}$$

We then use an energy balance to equate heat lost (as warm air leaves the building) to heat input (from the building heat sources).

$$H = \rho C_p q_1 \Delta T \tag{5.8}$$

where $H$ is heat flux, $\rho$ is fluid density, $C_p$ is specific heat capacity, and $\Delta T$ is the temperature difference between the interior and exterior fluids. Note that $q_1$ is equal to the volume flux out of the building (see equation 5.3).

By combining equations 5.1, 5.7, and 5.8, and considering the pressure difference driving flow into the building through the upper upwind opening, we obtain the following dimensionless relationship between the internal-external temperature difference $\theta$ and the heat input to the room $q$:

$$Q = \theta\sqrt{1 - p - \theta} \tag{5.9}$$

where $Q = H\beta gh/(\sqrt{\rho}C_p c^* A_1 \Delta {p_w}^{\frac{3}{2}})$ is a dimensionless heat flux which compares actual heat flux with heat flux required to generate a ventilation flow equal to that provided by the wind, and $p(\theta)$ is given by equation 5.7.

The variation of $\theta$ as a function of $Q$ is found by solving the coupled nonlinear algebraic equations 5.7 and 5.9. The solutions will be described in section 3. First, we present equivalent relations to describe the temperature and flow in the intermediate (figure 2b) and buoyancy-driven (figure 2c) regimes.

For the intermediate regime:

$$Q = \theta\sqrt{\theta - p} \tag{5.10}$$

where

$$p = \frac{\alpha^3\theta - \alpha + 3\alpha\theta - 2\sqrt{\alpha^2\theta + 2\theta - 1 - \theta^2}}{\alpha(4 + \alpha^2)} \tag{5.11}$$

For the buoyancy-driven regime:

$$Q = \theta\sqrt{p} \tag{5.12}$$

where

$$p = \frac{\alpha^2 - 2 + 2\theta - \alpha^2\theta + \alpha^4\theta + 2\sqrt{\alpha^2(\theta^2 - \alpha^2\theta + 1)}}{4 + \alpha^4} \tag{5.13}$$

We now use these relations to describe the possible variation of the internal temperature relative to the external temperature for any given heat load.

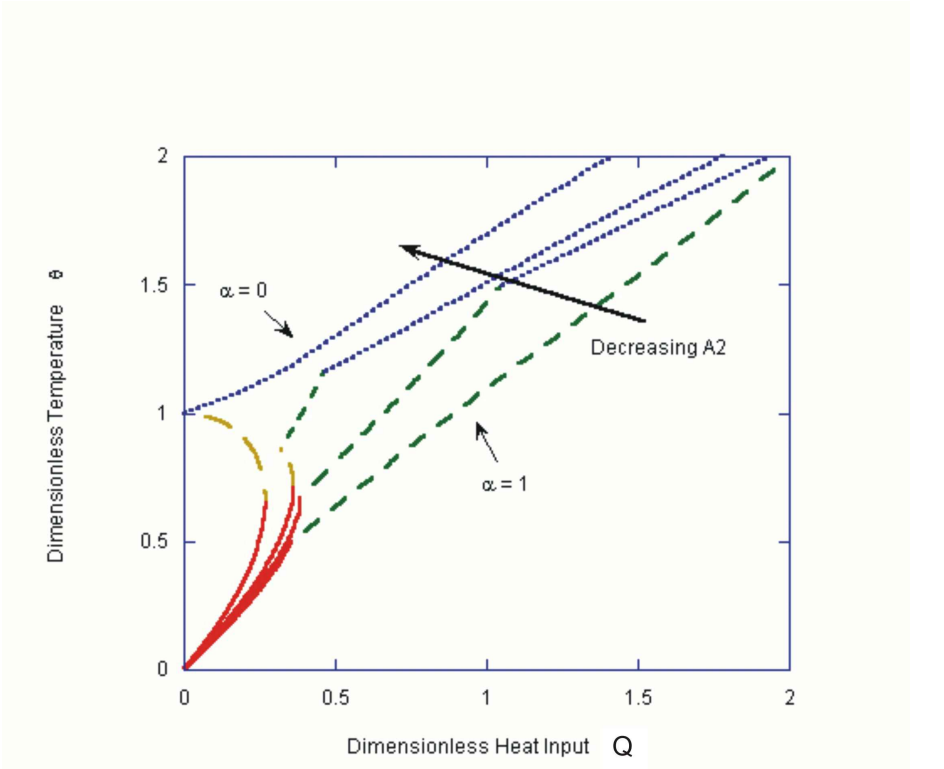


Figure 5.4.: *Temperature as a function of heat input for various area ratios $\alpha$. The four curves correspond to the parameter values, from left to right, $\alpha = 0$, $\alpha = 0.4$, $\alpha = 0.7$, and $\alpha = 1$. The solid lines represent the stable wind driven regime (figure 5.2c), the long-dashed lines represent the unstable wind-driven regime (figure 5.2c), the short-dashed lines represent the intermediate regime (figure 5.2b), and the dotted lines represent the buoyancy driven regime (figure 5.2a). At low values of $\alpha$, multiple steady states exist for certain values of $Q$.*

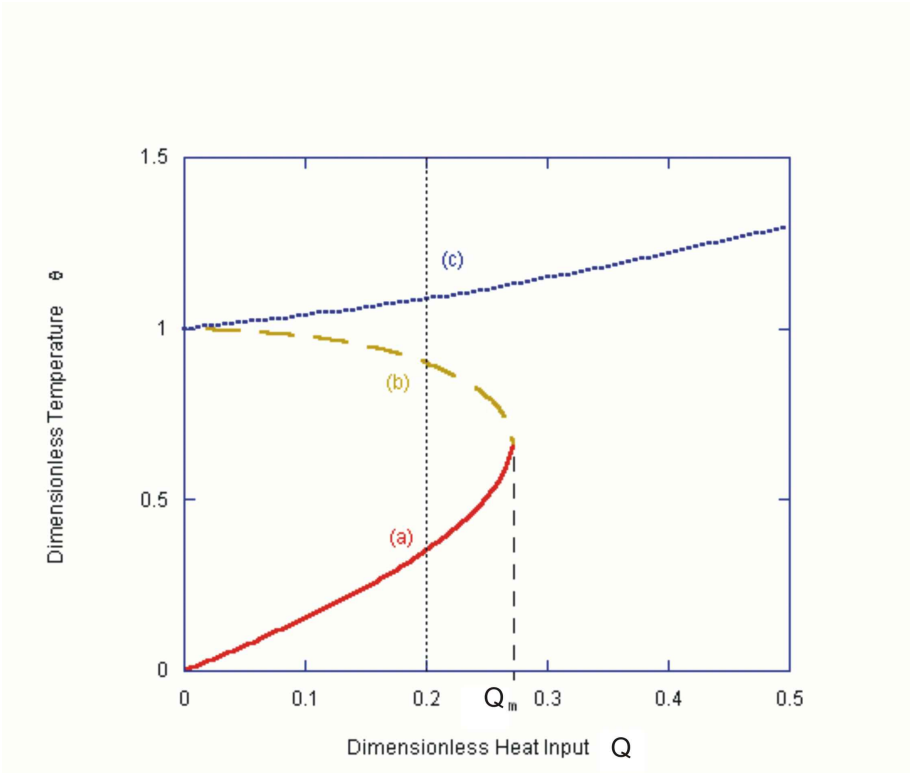


Figure 5.5.: *Temperature as a function of heat input for area ratio $\alpha = 0$. The dotted line represents the buoyancy driven regime while the dashed and solid lines represent the wind driven regime (see figure 5.1). $Q_m$ is the maximum temperature at which multiple steady states are possible. The thin dotted line represents a typical heat load for which three steady states can occur; these three states are labelled (a), (b) and (c).*

### 5.2.2. Predictions

In figure 5.4 we show how the dimensionless temperature $\theta$ varies as the dimensionless heat input $Q$ increases, for various values of the ratio of the upper and lower vent areas $\alpha$. The solid lines in figure 5.4 represent wind-driven regimes in which $d\theta/dQ > 0$. The long-dashed lines represent wind-driven regimes in which $d\theta/dQ < 0$. The short-dashed lines represent the intermediate regime (figure 5.2b), and the dotted lines represent the buoyancy-driven regime (figure 5.2a). The transitions between these regimes are plotted for four different opening ratios $\alpha$; 0, 0.4, 0.7, and 1, going from left to right on the graph.

Figure 5.5 shows temperature $\theta$ as a function of heat input $Q$ for the two-

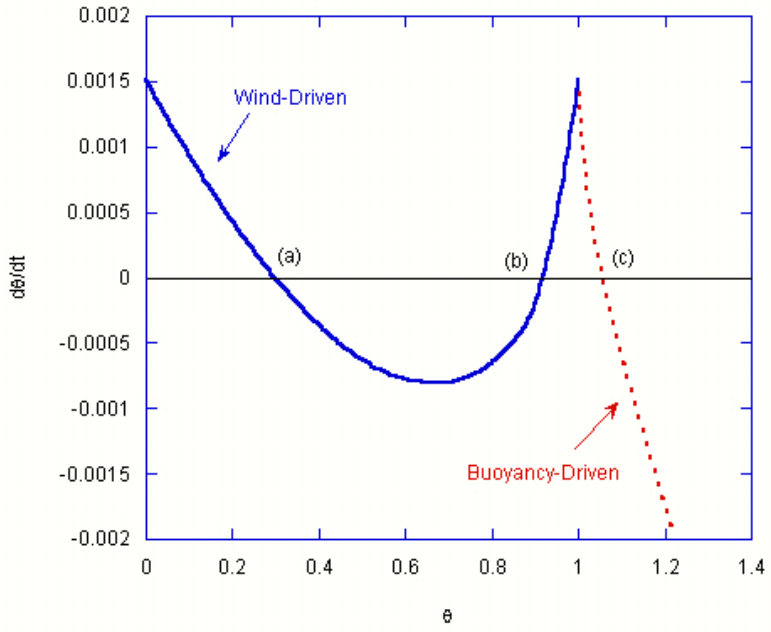


Figure 5.6.: *Graph of $d\theta/dt$ as a function of theta for a building with two openings, showing the stability of the possible regimes. The three possible steady state solutions (a), (b) and (c) correspond to the wind-driven solutions (points (a) and (b)) and the buoyancy driven solution (point (c)) as shown in figure 5.5. Near to solution (a), $\frac{d(\frac{d\theta}{dQ})}{d\theta} < 0$, and so any small deviation from the equilibrium $\theta = \theta_e$ is stable. Similarly, it may be seen that the buoyancy driven solution, (c), is stable but the second wind driven solution, (b), is unstable.*

opening case, i.e. $\alpha = 0$. The thick dotted line represents the buoyancy driven case, and the thick dashed and thick solid lines represent the wind driven case (see figure 5.1). If $Q$ is sufficiently small ($0 < Q < Q_m$) then the figure shows that three solutions exist, labelled (a), (b) and (c). To investigate the stability of each solution, we consider the transient behaviour of the system for temperature close to the steady state solutions. The overall heat balance of the system leads to heating or cooling of the interior fluid depending on whether the heat supply $H$ exceeds the heat which is convected from the space by the ventilation flow. We use this heat balance along with a mass balance for the building and equations 5.1 and 5.2 to show that:

$$\rho C_p V \frac{d\Delta T}{dt} = H - \rho C_p c^* A \Delta T \sqrt{\frac{\Delta p_w - \beta g h \Delta T}{2\rho}} \tag{5.14}$$

for the wind driven regime, and

$$\rho C_p V \frac{d\Delta T}{dt} = H - \rho C_p c^* A \Delta T \sqrt{\frac{\beta g h \Delta T - \Delta p_w}{2\rho}} \tag{5.15}$$

for the buoyancy driven regime. In dimensionless form (see equations 5.5 and 5.6) we can write:

$$C_1 \dot{\theta} = \sqrt{2} Q - \theta \sqrt{1 - \theta} \tag{5.16}$$

for the wind driven regime, and

$$C_1 \dot{\theta} = \sqrt{2} Q - \theta \sqrt{\theta - 1} \tag{5.17}$$

for the buoyancy driven regime, where $C_1 = \sqrt{2\rho} V / (\sqrt{\Delta p_w} c^* A)$ has units of time. This transient behaviour is plotted in figure 5.6, which shows a plot of $d\theta/dt$ as a function of $\theta$ for a building with two openings, i.e. $\alpha = 0$, for a typical dimensionless heat input $Q = 0.25$. The three possible steady-state solutions, (marked (a), (b) and (c) on the plot, and corresponding to points (a), (b), and (c) on figure 5.5) occur when $d\theta/dt = 0$. We see from the graph that in the wind driven solution on the left, (a), and in the buoyancy driven solution, (c),

any deviation from the steady-state will decay, but in the wind driven solution on the right, (b), any deviation will grow and the system evolves to another regime. We therefore conclude that the second part of the wind-driven regime, where $d\theta/dQ < 0$, shown on figure 5.4 as a long-dashed line, is unstable in the case with two openings, and by continuity, in the case with three openings.

Figure 5.4 reveals that at low values of $\alpha$, when the upper downwind opening area is small, there is a range of heat fluxes for which we observe multiple steady states. As $\alpha$ increases, the range of dimensionless heat fluxes for which the unstable mode (the long-dashed line) develops becomes smaller; instead the range of heat fluxes for which the intermediate mode (the short-dashed line) develops becomes larger. Eventually at a critical value of $\alpha$, $\alpha = \alpha_c$, say, multiple steady states cease to occur and for $\alpha > \alpha_c$ only one temperature is possible for any given heat input.

This information is represented in the regime diagram of figure 5.7, in which the possible flow regimes are shown as a function of the dimensionless area $\alpha$ and the dimensionless heat input $q$. In figure 5.8 we illustrate the same transitions in flow regime on a graph of dimensionless temperature $\theta$ as a function of dimensionless heat input $Q$, to complement the regime diagram of figure 5.7. The marked boundaries on figure 5.8 correspond to those of figure 5.7.

Figure 5.8 shows temperature as a function of heat input, for various values of window area ratio $\alpha$ ($\alpha = 0, 0.4, 0.7, 1$, as in figure 5.4). On figure 5.8, the triangles represent the maximum heat input for which the wind-driven regime can occur. The squares represent the transition from wind-driven to intermediate, and hence the minimum heat input for which the intermediate regime occurs. The circles represent the transition from intermediate to buoyancy-driven regimes. The lines on the regime diagram (figure 5.7) correspond to the loci of the triangles, squares and circles in figure 5.8, and this provides further insight into the conditions under which multiple steady states can exist.

The line labelled W (on figures 5.7 and 5.8) represents the maximum heat input for which a wind-driven regime can exist; line I represents the minimum

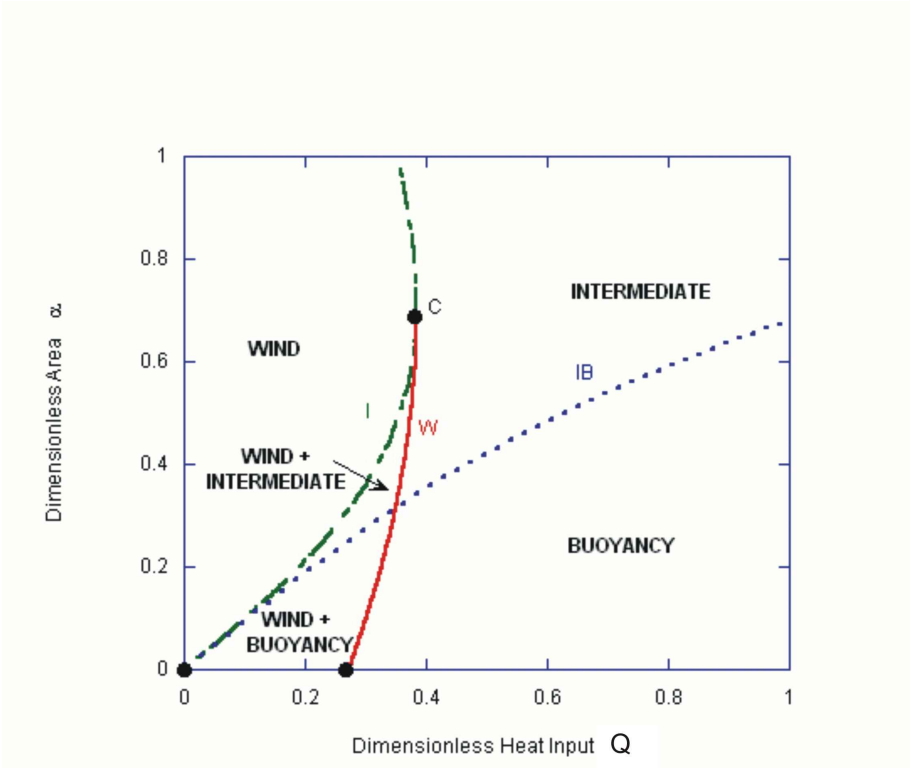


Figure 5.7.: *Regime diagram, shown on a plot of ratio of openings $\alpha$ as a function of dimensionless heat input $Q$. The solid line, labelled $W$, represents the maximum heat load for which a wind-driven solution is possible. The dashed line, labelled $I$, represents the minimum heat load for which an intermediate solution is possible. The dotted line, labelled $IB$, represents the transition from the intermediate regime to the buoyancy driven regime. In three regions of the diagram (labelled wind, intermediate and buoyancy respectively), only one flow regime is possible. In two regimes (labelled wind + intermediate and wind + buoyancy respectively) multiple steady states exist, as labelled.*

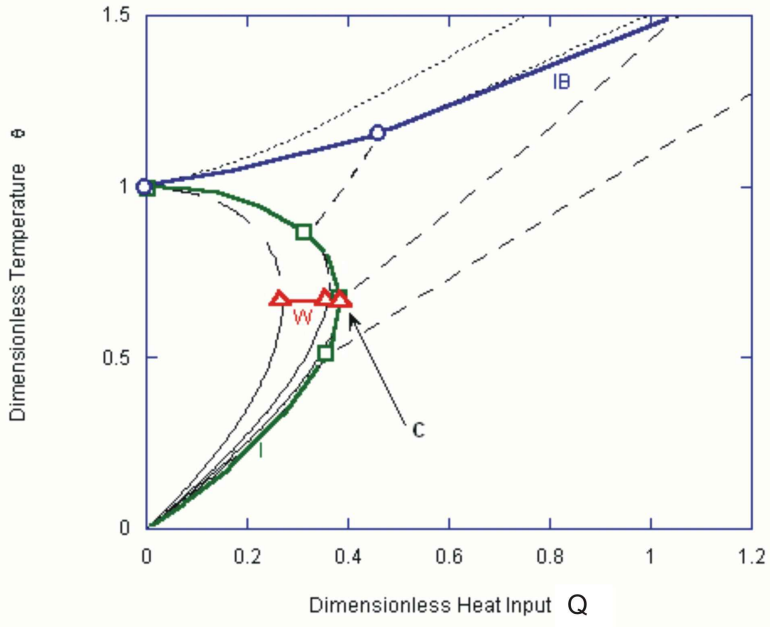


Figure 5.8.: *Graph to illustrate the regime boundaries shown in figure 5.7, in the* $(\theta, Q)$ *plane. The triangular markers represent the maximum of the wind-driven regime for each curve for a series of values of* $\alpha$*, and the line intersecting these corresponds to the solid line labelled* $W$ *on figure 5.7. The square markers represent the transitions from the wind-driven regime to the intermediate regime, and hence the minimum possible temperature at which the intermediate regime can occur, for a series of values of* $\alpha$*. The line joining these squares corresponds to the line labelled* $I$ *on figure 5.7. The circular markers represent the transition from the intermediate regime to the buoyancy-driven regime for a series of values of* $\alpha$*, and the line joining these markers corresponds to line* $IB$ *on figure 5.7. In this figure we have also included a series of thin lines to illustrate the solutions* $\theta(Q)$ *for a series of values of* $\alpha$ *as shown in figure 5.4.*

heat input for which an intermediate regime can occur; and line IB represents conditions under which there is a transition from the intermediate to the buoyancy-driven flow regimes.

This figure illustrates that as $\alpha$ increases, the range of values of heat input $Q$ for which multiple steady states exist becomes smaller. Eventually, when $\alpha = \alpha_c$ there is a unique solution for all values of $Q$.

The minimum area ratio at which multiple steady states cease to exist corresponds to the situation in which the point of transition from the wind to the intermediate mode corresponds to the maximum heat load for which a wind-driven regime arises.

From equation 5.9, the maximum value of $Q$ for which a wind-driven regime exists occurs when

$$\frac{d}{d\theta}(\theta\sqrt{1-p-\theta}) = 0 \tag{5.18}$$

where $p$ is given by equation 5.7.

At the transition between wind-driven and intermediate regimes, there is no flow through the lower opening, and hence

$$\Delta p_i = 0 \tag{5.19}$$

Combining equations 5.19 and 5.4 gives a relationship between $\theta$ and $\alpha$ at the transition point:

$$\theta = \frac{1}{1+\alpha^2} \tag{5.20}$$

Combining equations 5.7, 5.18 and 5.20 and solving for $\alpha$, we find the critical area ratio;

$$\alpha_c = \frac{1}{\sqrt{2}} \tag{5.21}$$

We deduce that if the area of the upper downwind opening is at least $1/\sqrt{2}$ times that of the other two window openings, multiple steady states will not occur.

There is also a critical heat input, say $Q_c$, above which multiple steady states cannot occur. To find this, we define the critical point C, at which the transition from the wind-driven regime to the intermediate regime changes from going through multiple steady states to switching directly (marked C on figures 5.7 and 5.8).

Returning to equation 5.20, we can find a value for the dimensionless temperature at C:

$$\theta_c = \frac{2}{3} \tag{5.22}$$

and from equation 5.9 we find the dimensionless heat flux,

$$Q_c = \frac{2\sqrt{3}}{9} \tag{5.23}$$

at the critical point. For heat loads in excess of $Q_c$ there exists a unique steady solution at all times.

## 5.3. Experiments

The theory was tested empirically using an analogue building model contained in water in a recirculating flume, shown diagrammatically in figure 5.9. The analogue experimental system consists of a small Perspex tank, the model building, of dimensions 0.1765m x 0.1765m x 0.1765m, with seven circular openings (radius 0.0075m) at the top and bottom of each face. During the experiments, rubber bungs were used to seal different sets of openings. As an analogue experimental model of the two opening flow regime, $\alpha = 0$ (figure 5.1), the tank was set up with a row of openings at a high level on the upwind side and a row of openings at a low level on the downwind side. To model the case $\alpha = 1$ (figure 5.2) a further row of openings was used at a high level on the downwind side. The model building was placed in a flume of dimensions 2m x 0.5m x 0.5m, which pumps water across the building and acts as a simple analogue of the wind, in that it produces a pressure decrease from the upflow face to the downflow face of the building. The flume contained honeycomb lattices to

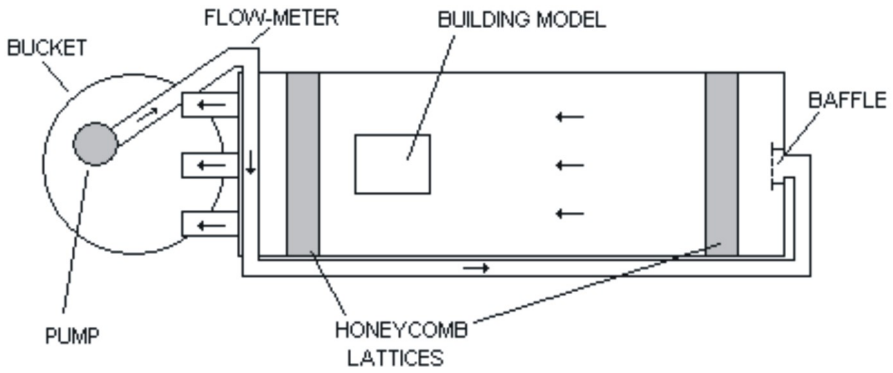


Figure 5.9.: *Experimental layout: the building model is placed in a flume tank, and water is pumped along the flume tank as an analogue to wind. Honeycomb lattices ensure uniform flow.*

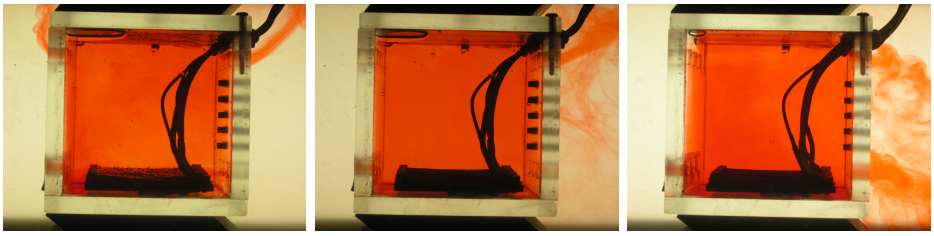

Figure 5.10.: *Experimentally observed regimes, for a building with three openings ($\alpha = 1$). From left to right, the photographs show: (a) the buoyancy driven regime, with outflow from both upper vents; (b) the intermediate regime, with outflow from the upper downwind vent, and (c) the wind driven regime, with outflow through both downwind vents.*

ensure a uniform flow as confirmed by observing the transport of dye streaks. Typical flow speed in the flume was around $0.01\text{ms}^{-1}$. The building model was raised from the floor of the tank. The building model had a heating plate on its floor which represents a distributed heat source. The heating plate is made with a series of high resistance metal coils attached to a power supply with variable power output (Gladstone and Woods 2001).

Temperatures were measured using four type-K thermocouples vertically distributed within the building interior, and three thermocouples distributed in the exterior flume, to measure external temperature and ensure uniform conditions were maintained. Temperature measurements were made every five seconds, using Picolog software via a TC-08 cold junction, until the system reached steady

state. The external temperature was around $35^oC$, since the pump supplied a significant amount of heat to the system. It was ensured that the exterior fluid was in equilibrium before any data points were taken. Temperature measurements were taken every second over 100s and averaged to minimise the effects of fluctuations in the flume. Temperature differences within the building were found to be small ($\pm 0.1^o$C) compared to internal-external temperature differences (up to $7^o$C), and did not increase with the heating load, suggesting that the interior was, to good approximation, well mixed. As well as quantitative temperature measurements, qualitative information about flow patterns was obtained from dye and shadowgraph techniques (for example, dye can be injected on either side of an opening to investigate flow direction through that opening). The fitting parameter $c^*$ was measured for the building model using a calibration experiment with no wind, where $c^*$ is the only parameter not independently measured, and found to be $c^* = 0.95$ (see e.g. Appendix A). The pressure difference across the building associated with a given flow in the flume was measured using a series of calibration experiments in which the flow induced pressure acted in parallel with the buoyancy (see appendix A for an example of such calibration: also c.f. Hunt and Linden (2004)). The wind pressure was found to be $p_w = 1.9$Pa at the pump's maximum flow rate (again, see calibrations in Appendix A). Also, by performing calibration experiments testing the upper and lower openings independently it was found that the pressure variation across each face was only a small percentage of the pressure difference between the upwind and downwind faces. All other parameters (i.e. building geometry) were independently measured. Other experimental values used were $\beta = 0.36\text{kgm}^{-3}\text{K}^{-1}$, $\rho = 1000\text{kgm}^{-3}$, $C_p = 4184\text{Jkg}^{-1}\text{K}^{-1}$, and $g = 9.81\text{ms}^{-2}$.

First, experiments were performed in which there was one row of openings at a high level on the upwind side, and one row of openings at a low level on the downwind side, in order to test the prediction that multiple steady states can occur with $\alpha = 0$ (figure 5.1). Experimental results with $\alpha = 0$ are presented in dimensional form in figure 5.11. The solid line represents the stable wind-driven

theory, while the circles represent data points corresponding to the wind-driven regime. These data points were obtained by starting with zero heat input and gradually increasing the heat input between measurements. Eventually a transition to the buoyancy driven regime occurred. The dashed line shows the unstable wind-driven solution. The dotted line shows the buoyancy-driven solution, and the squares show data points obtained in the buoyancy-driven regime. These were obtained by starting with the maximum achievable heat load and gradually decreasing until the mode changed. For all data points, the error bars represent the tolerance of the thermocouples used to measure temperature ($\pm 0.1^o$C, from the manufacturer's specification) and the vertical stratification in the tank (measured as $< 0.1^o$C).

Next, a third row of openings was included on the upper part of the downwind face of the tank to test the predictions of the model developed in section 2 and presented in section 3 (figure 5.2). Theoretical and experimental results, for the case with three equal windows, (i.e. $\alpha = 1$) are presented in dimensional form in figure 5.12. Initially the heat input was set at zero. Each successive data point was then found by increasing the heat input and waiting for the system to reach steady state. Similar results were also obtained by starting with a high heat input and gradually reducing it for each data point. Shadowgraph and dye techniques were used to observe the flow regimes. Of the data points on the graph, circles represent the wind-driven regime, squares the intermediate regime, and triangles the buoyancy driven regime. The experimental data are shown alongside the theory: the solid line represents the wind-driven theory, the dashed line the intermediate, and the dotted line the buoyancy driven regime (as in figure 5.2). Photographs of the experiments, showing the buoyancy-driven, intermediate, and wind-driven regimes, are shown in figure 5.10.

In both cases, experimental results are in good accord with the theory. The two-opening results show the hysteresis associated with multiple steady states and an unpopulated area associated with the unstable regime. There is a slight systematic discrepancy between the theory and experiment in the buoyancy

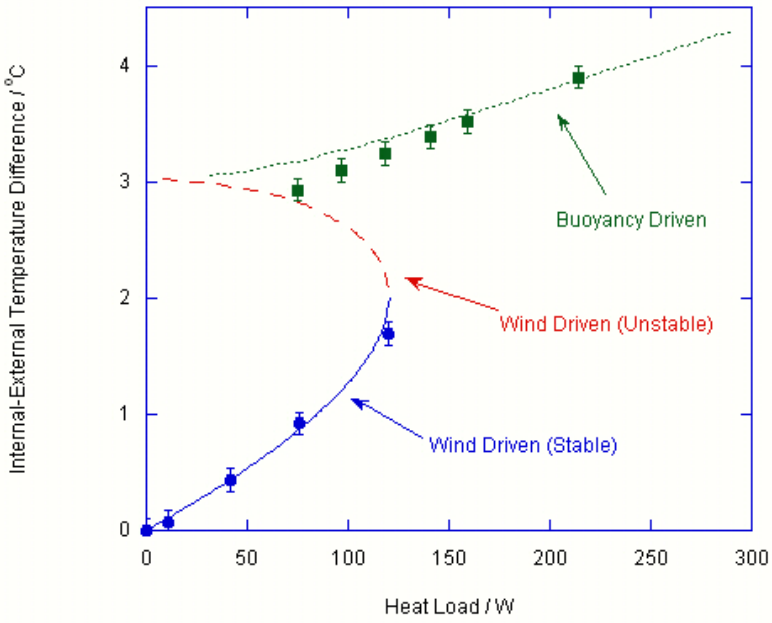


Figure 5.11.: *Graph of internal-external temperature difference $\Delta T$ (in $^oC$) as a function of heat load $H$ (in $W$), showing theory and experiment, for a building model with two openings of equal area (see figure 5.1). The solid line represents the theoretical stable wind-driven solution, the dashed line the unstable wind-driven solution, and the dotted line the buoyancy-driven solution. The circular markers show experimental data points in the wind-driven regime, and the square markers represent experimental data points in the buoyancy-driven regime. The error bars represent the tolerance of the thermocouples used to measure temperature ($\pm 0.1^oC$) and the vertical stratification in the tank ($< 0.1^oC$).*

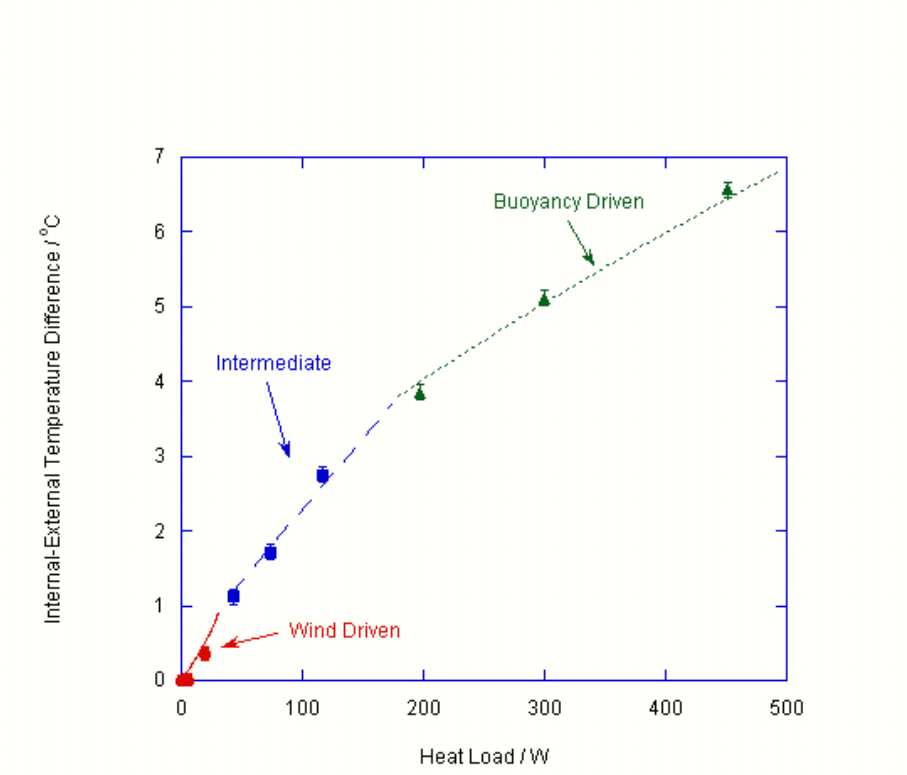


Figure 5.12.: *Graph of internal-external temperature difference $\Delta T$ (in $^oC$) as a function of heat load $H$ (in $W$), showing theory and experiment, for a building model with three openings of equal area (see figure 5.2). The solid line represents the theoretical wind-driven solution, the dashed line the intermediate solution, and the dotted line the buoyancy-driven solution. The circular markers correspond to experimental data points in the wind-driven regime, the square markers to experimental data points in the intermediate regime, and the triangular markers to experimental data points in the buoyancy-driven regime. The error bars represent the tolerance of the thermocouples used to measure temperature ($\pm 0.1^oC$) and the vertical stratification in the tank ($< 0.1^oC$).*

driven regime for the two-opening case (figure 5.11), as the difference between the unstable wind-driven regime and the stable buoyancy-driven regime becomes small.

The experimental system in fact has seven openings on the upwind face and fourteen openings on the downwind face, with seven located at the upper elevation and seven at the lower elevation. Near the point of transition between the wind and buoyancy dominated flow, the pressure change across one set of these openings becomes small. As a result, any small horizontal pressure fluctuations within the tank, which can lead to a gradient in the pressure difference across the openings at a given height, may become dominant. Indeed, this may then lead to inflow through some openings and outflow through other openings at the same elevation. Such three-dimensional effects are not included in the present model, but may account for the difference between the model prediction and the data. This interpretation is supported by the observation that near the point of transition in flow regime, the flow reverses through each of the openings at a given elevation in sequence, rather than occurring en masse.

## 5.4. Further analysis: the effect of varying the height of the new opening

The analysis presented so far in this chapter has assumed the height of the upper downwind opening is the same as that of the upper upwind opening. We now show how the analysis may be generalised to account for situations in which the new opening is at a different height. We define the height of the upper upwind opening as $h_1$, the height of the upper downwind opening as $h_2$, and the ratio $h_2/h_1 = \omega$ (see figure 5.13). In the case that the height of the upper downwind opening lies at a position $h_2 < h_1$, the three flow regimes described earlier are possible, but a new fourth buoyancy-driven regime can also develop in which there is inflow through both of the downwind openings and outflow from the upwind opening (figure 5.14). In the case of zero wind, the flow through the intermediate-elevation vent can be either in- or outflow depending on its height

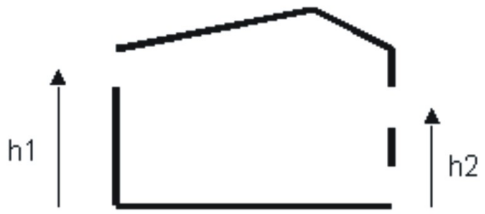


Figure 5.13.: *The new building model with the upper downwind opening at a variable height: the height ratio* $\omega = h2/h1$.

in relation to the neutral pressure level in the room (Fitzgerald and Woods 2004). This neutral pressure level is given for the case with no wind by

$$h_n = \frac{A_u^2}{A_l^2 + A_u^2} h = \Gamma h. \tag{5.24}$$

where $h$ is the the vertical distance between the top and bottom openings, $A_u$ is the opening area of the top opening, and $A_l$ is the area of the bottom opening. If $\omega > \Gamma$ the flow through the upper downwind opening will be outflow, whereas if $\omega < \Gamma$ the flow will be inflow. If a wind pressure gradient develops across the building, then the neutral height will move to some new level, say $\Gamma_w h_b$. For $\omega > \Gamma_w$, as the heat load increases the flow will evolve in a similar fashion to that shown in figure 5.2, from a wind-driven regime through an intermediate regime to a buoyancy dominated regime. If $\omega < \Gamma_w$, then, as the heat load increases the flow will go through wind-driven, intermediate and buoyancy-driven regimes as before, but now with increasing heat load a fourth regime becomes possible, in which flow is inwards through the downwind openings and outwards through the upwind opening (see figure 5.14 a-1).

To further investigate the effects of varying $\omega$, we use equation 5.2, and note that $\Delta p_b$ is proportional to height, $h$. Therefore, the ratio of two heights above the lower opening will equal the ratio of pressures due to density difference, i.e. the ratio of $\Delta p_b$ at those two different heights. We can therefore adapt equation 5.4 to give, for the wind-driven regime:

$$\sqrt{1 - \theta - p} = \alpha \sqrt{\omega\theta + p} + \sqrt{p} \tag{5.25}$$

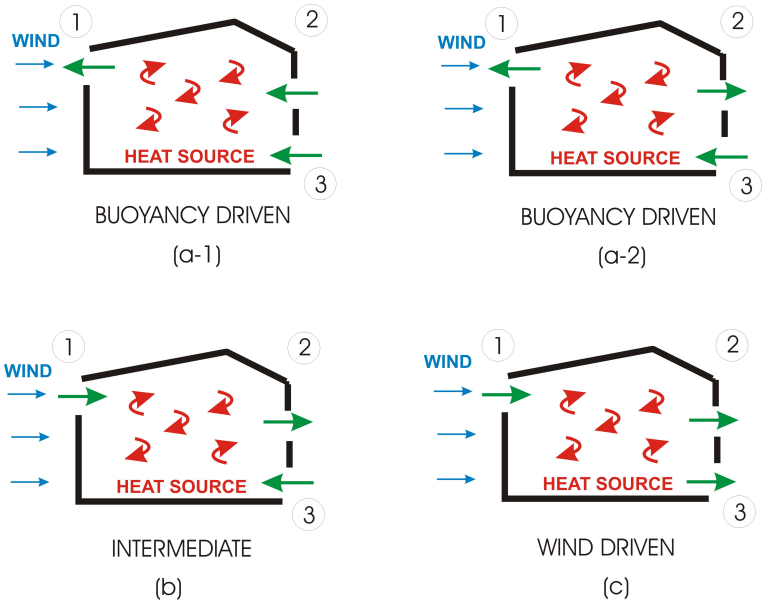


Figure 5.14.: *Possible flow regimes: when the height of the upper upwind opening is varied, a new buoyancy-driven regime (shown here as a-1) can exist*

where $p(\theta)$ is calculated using a mass balance as in section 2. Similarly, for the intermediate and buoyancy driven regimes, we find

$$\sqrt{1-\theta+p}+\sqrt{p}=\alpha\sqrt{\omega\theta-p} \tag{5.26}$$

and

$$\sqrt{1-\theta+p}+\alpha\sqrt{\omega\theta-p}=\sqrt{p} \tag{5.27}$$

respectively.

As before, we can then use equation 5.8 to find an expression for $Q$ as a function of $\theta$ for each regime. Figure 5.15 shows the predictions of this model for varying $\omega$. For this figure, all openings are assumed to be of the same size, i.e. $\alpha = 1$. We see that raising the height of the new window can eliminate multiple steady states in much the same way as an increase in area did. Again the figure shows a wind-driven regime (solid line), an intermediate regime (short-dashed line) and a buoyancy-driven regime (dotted line). Note the new fourth regime, with inflow through both downwind openings, which is shown by the

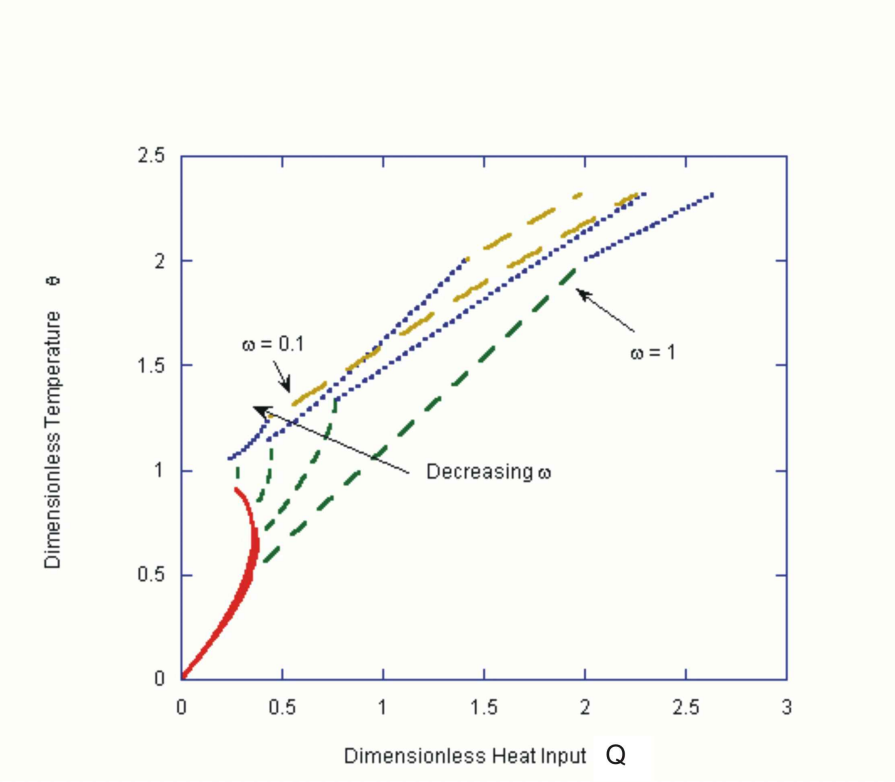


Figure 5.15.: *Temperature $\theta$ as a function of heat input $Q$ for various height ratios $\omega$ (with area ratio $\alpha = 1$). From right to left, the four curves represent $\omega = 0.1$, $\omega = 0.25$, $\omega = 0.5$ and $\omega = 1$. The long-dashed line shows the new buoyancy-driven regime (figure 5.14 a-1), the dotted line shows the original buoyancy-driven regime (figure 5.14 a-2), and the short-dashed line shows the intermediate regime (figure 5.14b). The solid line represents the wind-driven regime (figure 5.14c) (here, both the stable and unstable modes are shown as a solid line).*

long-dashed line. In this regime a lower value of $\omega$ will actually lead to more ventilation, since the flow through the upper downwind opening is now inwards.

Figure 5.16 shows a regime diagram for the case when $\omega = 0.4 < \Gamma$, i.e. the upper downwind opening is below the neutral pressure level, and hence the flow through this opening can be inward as in figure 5.14 a-1. Figure 5.16 shows, on a plot of $\alpha$ as a function of log $Q$, a long-dashed line (labelled I) which represents the minimum heat input for which the intermediate solution can exist, a solid line (labelled W) which represents the maximum heat input for which the wind-driven regime can exist, and a dotted line (labelled IB) which represents the transition from the intermediate regime to the first buoyancy regime, as in figure 5.7. Also shown on the graph is the transition between the two buoyancy regimes (figure 5.14 a-2 to 5.14 a-1), which occurs at a constant value of $Q = 7.07$ for $\omega = 0.4$, independent of $\alpha$, and is labelled $B1/B2$.

To find the critical point $\alpha_c$ such that for $\alpha > \alpha_c$ there is a unique solution for all heat loads $Q$, as before, we consider the wind driven regime, combine equation 5.25 with a heat balance to give a relation between $Q$ and $\theta$, and differentiate. At the critical point, then,

$$\frac{dQ}{d\theta} = 0 \tag{5.28}$$

This gives us one condition for the critical point C. The other condition is found by considering the transition from the wind-driven regime to the intermediate regime: we now find that when the flow through the lower opening is zero,

$$\theta = \frac{1}{1 + \alpha^2 \omega} \tag{5.29}$$

Combining these two conditions, we find the relationship between the height ratio $\omega$ and the area ratio $\alpha$ at the critical point:

$$\alpha_c = \frac{1}{\sqrt{2\omega_c}} \tag{5.30}$$

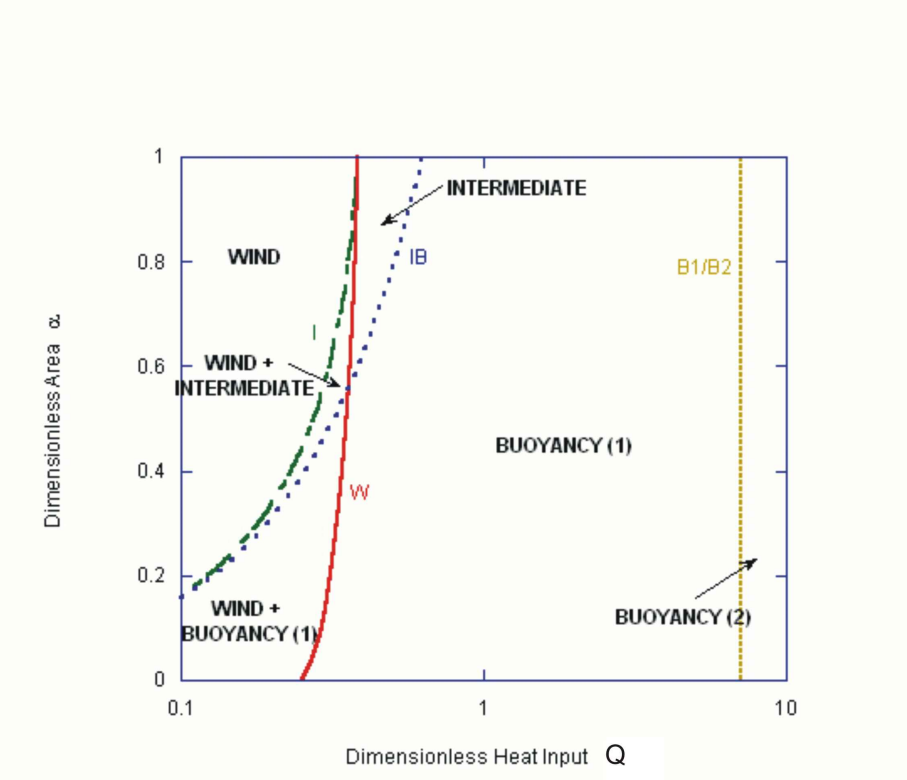


Figure 5.16.: *Regime diagram, shown on a plot of ratio of openings $\alpha$ as a function of the log of dimensionless heat input $Q$, with height ratio $\omega = 0.4$ (compare this figure with figure 5.7, which shows a similar plot for $\omega = 1$). The solid line, labelled $W$, represents the maximum heat load for which a wind-driven solution is possible. The long-dashed line, labelled $I$, represents the minimum heat load for which an intermediate solution is possible. The dotted line, labelled $IB$, represents the transition from the intermediate regime to the buoyancy driven regime. The short-dashed line, labelled $B1/B2$, represents the transition between the two buoyancy regimes. In four regions of the diagram (labelled wind, intermediate, buoyancy (1) and buoyancy (2) respectively), only one flow regime is possible. In two regimes (labelled wind + intermediate and wind + buoyancy (1) respectively) multiple steady states exist, as labelled.*

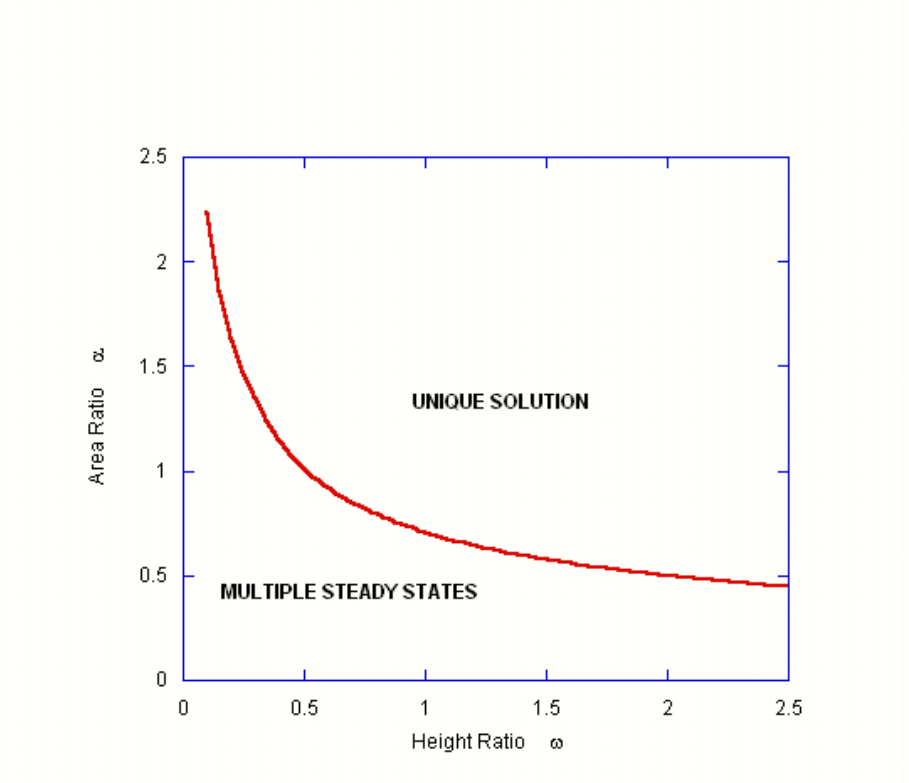


Figure 5.17.: *Plot of area ratio $\alpha$ as a function of height ratio $\omega$ summarising regions of unique solutions and multiple steady states.*

This relationship is plotted in figure 5.17, and summarises our findings of the geometrical conditions under which there is always a unique flow regime, irrespective of the heat load.

## 5.5. Applications and conclusions

We now explore the predictions of the model in the context of a typical building. We consider a meeting room with an upwind window located 3m above the floor, and a downwind opening at ground level, both of area $1\text{m}^2$. We then examine the flow regime in the case that there is an additional opening 1, 2, or $3m$ above the floor on the downwind side of the building, and of size $0.8\text{m}^2$. We assume that there is a pressure difference across the building of 0.8Pa associated with the wind, perhaps corresponding to a wind speed of $2 - 3\text{ms}^{-1}$. Figure 5.18 illustrates the predictions of the model for these three

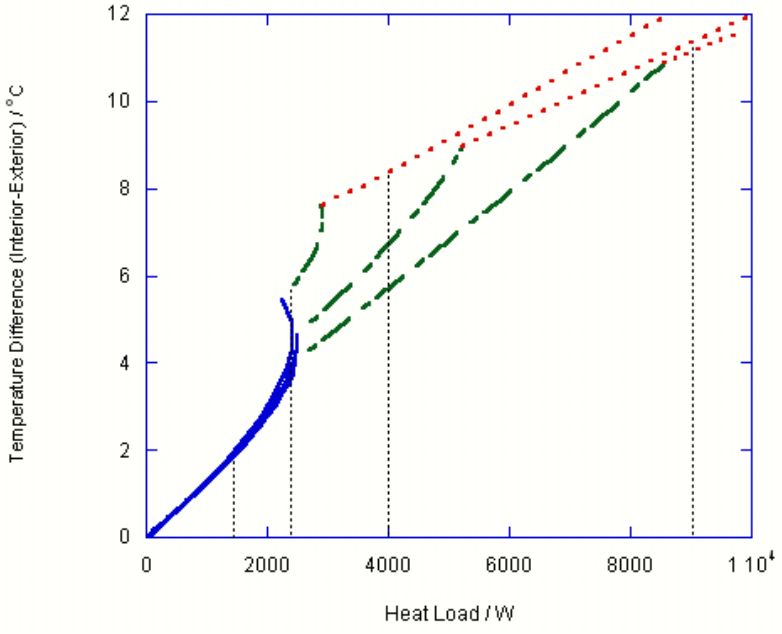


Figure 5.18.: *Dimensional plot of temperature difference (interior-exterior) in degrees celsius as a function of heat load in watts. The building considered has an upwind opening at a height of 3m, and a downwind opening at 0m (ground level) as well as an upper downwind opening at height $h_d$; plots are shown for (from left to right) $h_d = 1m$, $h_d = 2m$ and $h_d = 3m$, i.e. $\omega = 0.33$, $\omega = 0.66$ and $\omega = 1$. The upper upwind and lower downwind windows have an area of $1m^2$; the upper downwind opening has an area of $0.8m^2$, i.e. $\alpha = 0.8$. A typical wind pressure of 0.8 Pa acts on the face of the building. On each curve, the solid line represents the wind-driven regime, the dashed line the intermediate regime, and the dotted line the buoyancy-driven regime. The thin, vertical dotted lines represent possible operating heat loads: 1.5kW, 2.4kW, 4kW, and 9kW.*

different configurations. The solid lines represent the wind-driven regime, the dashed lines the intermediate regime, and the dotted lines the buoyancy-driven regime. Note that when $\alpha = 0.8$ and $\omega = 0.33$ or $\omega = 0.66$, figure 5.17 predicts multiple steady states, but when $\omega = 1$ (the rightmost curve) we find a unique solution for all heat inputs.

Four possible heating loads are marked on the graph by thin dotted lines. The first (in the wind-driven regime) heat load has value 1.5kW, equivalent to 15 people producing 100W each, with no extra heating, which causes a temperature increase of around $2^oC$. This might be a typical summer load. The second heat load has value 2.4kW; at this heat load multiple steady states can occur when $\omega = 0.33$ or $\omega = 0.66$. The third heat load marked is 4kW, which might represent a typical spring load, with some additional heating. At this heat load, with $\omega = 0.66$ or $\omega = 1$, the building will be in intermediate mode. Finally in the winter, a high heat load will generate a buoyancy-driven flow as shown for the case with an internal heat load of 9kW.

By designing the building such that multiple steady states cannot occur, each heat load can be mapped to a corresponding internal temperature (given the external temperature and wind), and hence temperature control in the building is simplified.

In the previous two chapters, we have investigated multiple steady states in buildings with two openings. This chapter has shown both theoretically and with new laboratory experiments that for a building with a distributed heat source in the presence of wind, the flow behaviour with three openings is fundamentally different. With three openings, it is possible for the flow direction through any opening to change while building ventilation continues through the other two openings. The transition between states may therefore be smooth (figure 5.2), and the multiple steady states associated with two openings (figure 5.1) may be eliminated. However, by continuity, if the area of the new opening is very small, the flow behaviour will be similar to the two-opening case, and exhibit multiple steady states; only as the area is increased to match the

areas of the other two openings does the flow regime become uniquely defined. We have also shown that the critical size of the new opening, above which multiple steady states are no longer possible, increases as the elevation of the new opening above the lower downwind opening decreases.

# 6. Conclusions and Further Work

*The aim of this thesis was to investigate the occurrence and control of multiple steady states in naturally ventilated buildings subject to wind and buoyancy forces. Here, we first summarise the work which has been presented. We then describe how the results of the research undertaken may be useful for building designers and controllers, and how practical steps may be taken to integrate our research into natural ventilation strategies, providing more comfortable and more efficient building environments. We conclude by outlining potential avenues for further research.*

## 6.1. Summary of work and implications for building design and control

The literature review of chapter two described problems of multiple steady states in natural ventilation, which complicate control and can lead to uncomfortable, inefficient naturally ventilated buildings. In particular, the literature review highlighted work on multiple steady states due to the interaction between wind and buoyancy. It was shown from the literature that, in buildings with two openings, subject to wind and buoyancy, there exist both a stable wind driven regime and a stable buoyancy driven regime.

The research presented in this thesis focusses on the limited case of idealized buildings with distributed heat sources, leading to well mixed interiors. Within these limitations, in this thesis we have furthered the understanding of these multiple states in three key ways:

- chapter 3 quantified the nature of transient evolutions between the multiple states under varying winds;

- chapter 4 extended the analysis to the control of multiple states in buildings with significant internal thermal mass; and
- chapter 5 showed that by understanding the equilibria of the system, it is possible to modify building design to avoid multiple states;

In each chapter we began with a theoretical model, from which the key building behaviour, flow patterns and control parameters can be determined. These theoretical models were then validated by comparison to the results of new, small-scale laboratory experiments. The theoretical models were then applied to real buildings to show how design and control might be improved.

In chapter 3, we investigated how changes in external conditions can lead to changes between the flow regimes, focussing specifically on changes in wind speed. We showed initially that the wind driven regime only exists for a given range of conditions, so the transition to the buoyancy driven regime will occur at the point when the wind driven regime ceases to exist. However, we also showed that for a well mixed interior the buoyancy driven regime exists for all wind speeds and heat loads, and hence the transition from the buoyancy driven regime to the wind driven regime is fundamentally different to the reverse transition. We showed that sufficiently large changes in wind speed can cause the building to evolve to the wind driven regime. Further, we showed that the final steady state of the system was dependent on the rate of change of the wind, and that a critical rate of change of wind speed exists, above which the building state will evolve to the wind driven regime.

In chapter 4, we introduced the effects of thermal mass, and investigated the transient evolutions which occur in naturally ventilated buildings. We began by considering ventilation driven only by buoyancy, and showed how the transient evolution could be interpreted intuitively by considering the dynamics as governed by a slow-varying forcing and a fast-varying response. For pure buoyancy-driven flow, the forcing and response are both monotonic, and so the evolution is relatively simple. The system behaviour becomes more complex when the effects of wind are introduced, since the nonlinear interaction

between wind and buoyancy leads to a non-monotonic response term. In this case, the system temperature evolves slowly along regimes, but rapidly between regimes. This can lead to unpredictable sudden jumps in temperature. We also investigated how the conclusions of chapter 3 might be modified for heavyweight buildings, and found that, under variations in wind, thermal mass causes the wind and buoyancy driven regimes to intersect for finite winds, and hence prevents unbounded temperatures in the buoyancy driven regime.

In chapter 5, we investigated whether the understanding of multiple states changes qualitatively when the building has more than two openings. We examined the differences between a building with two openings, subject to wind and buoyancy, and a building with three openings. We suggested that these two cases are fundamentally different. With two openings, it is not possible that the equilibrium flow through any opening reaches zero for a finite heat load, since this would indicate zero ventilation, and the building would heat. There is therefore no smooth transition between regimes. However, with three openings, the flow across one opening can reach zero while the building continues to ventilate through the other two openings, and so a series of smooth transitions between regimes is possible. Theoretical and experimental modelling of a building with three openings confirmed the smooth transition between regimes. The dependence on building geometry was then further investigated: specifically, we modelled the effects of varying the height and the size of the new opening. From this modelling we concluded that the existence of multiple steady states can be determined based solely on building geometry.

How, then, do these conclusions affect building design and control, and what conclusions are most relevant to architects and building systems engineers? Firstly, we note that a building in which the flow regime oscillates between a warm buoyancy driven regime and a cold wind driven regime is likely to be uncomfortable to live or work in. Designers could therefore, most obviously, work with the conclusions of chapter 5, which outline building designs for which the building state is uniquely determined by the heat load. In situations where such

a design is not possible, designers should refer to chapter 3, which shows that, if multiple states are possible, the building controller is hostage to variations in the wind. Control over window opening areas, and even heating load, may not be enough to adequately control the building environment. Chapter 3 provides some guidelines which enable the designer to determine the extent to which the building is likely to oscillate between regimes under varying winds. Analysis based on these guidelines may show that oscillation is unlikely. Alternatively, the designer might need to modify the design to give some control over the effective wind; for example, by adding maneuverable cowls onto stacks. Chapter 4, meanwhile, shows that uncomfortable temperature swings may be prevented by incorporating thermal mass into the building, but that this thermal mass must be carefully considered such that evolutions between flow regimes are predictable.

Alternatively, the research in this thesis may be applied to existing buildings. Some buildings are routinely found to be 'gusty' and uncomfortable. In such cases, it seems sensible to investigate whether the building is oscillating between steady states (for example using temporary flow sensors at windows), and then, if necessary, to implement some design change as suggested in the previous paragraph.

## 6.2. Further work

A number of important avenues for further research remain, of which the following are examples.

### 6.2.1. Building data

The research in thesis has focussed on theoretical models, supported by small-scale experiments. It would be extremely useful now to confirm the findings for real buildings. Several studies have obtained useful natural ventilation data from real buildings (e.g. (Fitzgerald, Lomakina, Livermore, Lishman, Walker, Norford, Gladstone, and Woods 2004)). Two main avenues of research seem

clear: first, to confirm the findings of the theoretical models presented here; and second, to conduct sociological experiments to find the human perceptions of wind-buoyancy oscillations and hence to target control strategies to avoid discomfort. However, it may prove difficult to show the existence of multiple states in real buildings, as changes in interior temperature could be due to a variety of factors. For example, as shown in chapter 5, the flow behaviour in the building is fundamentally different when there are three openings, so opening a single door will disguise the multiple states. This thesis has therefore attempted to elucidate the key principles of the multiple states to ease control problems.

### 6.2.2. Wind management

Further useful real-world data could be collected on typical wind speeds and rates of variation. This could then be combined with current technology for wind cowls, along with the theory of chapter 4, to produce a complete integrated system to manage changes in wind, and hence avoid large temperature variations in buildings.

### 6.2.3. Multiple rooms

This research has considered only a single large room, which might be a useful model of a lecture theatre, a classroom, or an open-plan office. However, many buildings are made up of multiple interconnected spaces. Li, Delsante, Chen, Sandberg, Andersen, Bjerre, and Heiselberg (2001) provide an interesting analysis of the multiple states problem for a two-zone interior, which clearly might be extended to model multi-zone interiors. In a simple form, the two-zone problem might incorporate a large open space and a connected entrance lobby. The level of complexity rises rapidly as multiple openings and heat sources are introduced, and hence thought is required as to how to generalise the simple models of this thesis to more complicated building geometries.

### 6.2.4. Cooling

This thesis has considered only buildings with positive heat loads. This is typical for the UK, where the outside temperature is rarely uncomfortable high, and so few buildings have air conditioning systems installed. However, in other countries, and in particular in the US, a warm climate and relatively cheap fuel means that air conditioning is fitted as standard. It would be useful to consider how the conclusions of this thesis need to be adapted for buildings with both heating and cooling systems.

### 6.2.5. Economics

The introduction to this thesis mentioned the importance of using theoretical ventilation models to inform practical and economic decisions. One area of research which might lead to widespread benefits is to apply appropriate costings and limitations on power inputs and then determine the optimum economic ventilation strategy over, say, a typical day. This problem is significantly complicated by the inclusion of multiple states in the model.

### 6.2.6. Overall

The overall aim of natural ventilation research is to create building control systems which create a comfortable interior environment at minimal cost and without dependence on fossil fuels. Such control systems would need to respond to changes in external conditions, such as fluctuations in the wind speed; changes in internal conditions, as people come and go, and hence the heat load changes; and changes in flow regime, in more complicated buildings, as described here. There is clearly still a great deal of work to be done to produce a general artificially intelligent controller. The theoretical and experimental research in this thesis has helped move us closer to this ideal controller.

# Bibliography


Action Energy (2003). Energy use in offices. Energy Consumption Guide 19.

Aynsley, R., W. Melbourne, and B. Vickery (1977). *Architectural Aerodynamics*. Applied Science Publishers.

Batchelor, G. (1967). *An Introduction to Fluid Dynamics*. Cambridge University Press.

Chenvidyakarn, T. and A. Woods (2004). The control of precooled natural ventilation. *Building Services Engineering Research and Technology 25*, 127–140.

Chenvidyakarn, T. and A. Woods (2005). Multiple steady states in stack ventilation. *Building and Environment 40*, 399–410.

CIBSE (2006). Guide A: Environmental design. The Chartered Institution of Building Services Engineers.

Dalziel, S. (1993). Rayleigh-Taylor instability: experiments with image processing. *Dynamics of Atmospheres and Oceans 20*, 127–153.

Department of Trade and Industry (2004). The renewables innovation review: longer term options. UK Department of Trade and Industry. `http://www3.dti.gov.uk/renewables/policy/longertermoptions.pdf` [Accessed 27th March 2007].

Energy Saving Trust (2006). Energy efficient ventilation in dwellings - a guide for specifiers. Energy Saving Trust.

Energy White Paper (2003). Our energy future - creating a low carbon economy. Department for Trade and Industry.

http://www.dti.gov.uk/files/file10719.pdf [Accessed 27th March 2007].

Etheridge, D. and M. Sandberg (1996). *Building ventilation, theory and measurement*. John Wiley and Sons.

Fanger, P. (1970). *Thermal Comfort*. McGraw-Hill.

Fitzgerald, S., A. Lomakina, S. Livermore, B. Lishman, C. Walker, L. Norford, C. Gladstone, and A. Woods (2004). Case study: temperature evolution and thermal mass in a passively ventilated office : Houghton Hall, England. *In proceedings of 9th International Conference on Air Distribution in Rooms, Coimbra, Portugal*.

Fitzgerald, S. and A. Woods (2004). Natural ventilation of a room with vents at multiple levels. *Building and Environment 39*, 505–521.

Fitzgerald, S. and A. Woods (2007). Transient natural ventilation of a room with a distributed heat source. In review.

Gebhart, B., Y. Jaluria, R. Mahajan, and B. Sammakia (1988). *Buoyancy-induced flows and transport*. Hemisphere publishing corporation.

Gladstone, C. and A. Woods (2001). On buoyancy-driven natural ventilation of a room with a heated floor. *Journal of Fluid Mechanics 441*, 293–314.

Heiselberg, P., Y. Li, A. Andersen, M. Bjerre, and Z. Chen (2004). Experimental and CFD evidence of multiple solutions in a naturally centilated building. *Indoor Air 14*, 43–54.

Holford, J. and A. Woods (2007). On the thermal buffering of naturally ventilated buildings through internal thermal mass. *Journal of Fluid Mechanics*. In Press.

Hunt, G. and P. Linden (1999). The fluid mechanics of natural ventilation - displacement ventilation by buoyancy-driven flows assisted by wind. *Building and Environment 34*, 707–720.

Hunt, G. and P. Linden (2001). Steady-state flows in an enclosure ventilated

by buoyancy forces assisted by wind. *Journal of Fluid Mechanics 426*, 355–386.

Hunt, G. and P. Linden (2004). Displacement and mixing ventilation driven by opposing wind and buoyancy. *Journal of Fluid Mechanics 527*, 27–55.

Kyoto Protocol (1998). Kyoto Protocol to the United Nations framework convention on climate change. `http://unfccc.int/resource/docs/convkp/kpeng.html` [Accessed 27th March 2007].

Li, Y. and A. Delsante (2001). Natural ventilation induced by combined wind and thermal forces. *Building and Environment 36*(1), 59–75.

Li, Y., A. Delsante, Z. Chen, M. Sandberg, A. Andersen, M. Bjerre, and P. Heiselberg (2001). Some examples of solution multiplicity in natural ventilation. *Building and Environment 36*(7), 851–858.

Linden, P. (1999). The fluid mechanics of natural ventilation. *Annual Review of Fluid Mechanics 31*, 201–238.

Linden, P., G. Lane-Serff, and D. Smeed (1990). Emptying filling boxes: the fluid mechanics of natural ventilation. *Journal of Fluid Mechanics 212*, 309–335.

Livermore, S. and A. Woods (2007a). Heat loss by conduction in naturally ventilated buildings. In review.

Livermore, S. and A. Woods (2007b). Natural ventilation of a building with heating at multiple levels. *Building and Environment 42*, 1417–1430.

Morton, B., G. Taylor, and J. Turner (1956). Turbulent gravitational convection from maintained and instantaneous sources. *Proceedings of the Royal Society of London A234*, 1–23.

Part F (2006). UK Building Regulations. Office of the Deputy Prime Minister. `http://www.planningportal.gov.uk/` [Accessed 27th March 2007].

Part L (2006). UK Building Regulations. Office of the Deputy Prime Minister.

http://www.planningportal.gov.uk/ [Accessed 27th March 2007].

Rousseau, J. (1995). Vents, ventilation drying and pressure moderation. *Canadian Housing Information Centre Research Highlights*. http://www.cmhc-schl.gc.ca/publications/en/rh-pr/tech/98104.htm [Accessed 19th July 2004].

Sartori, I. and A. Hestnes (2006). Energy use in the life cycle of conventional and low-energy buildings. *Energy and Buildings 39*, 249–257.

Steemers, K., T. Chenvidyakarn, and A. Woods (2002). Visualising ventilation: salt bath modelling from research to practice. *In Proceedings of Conference on Passive and Low Energy Architecture, Toulouse, France*.

Stern, N. (2006). *Review on the Economics of Climate Change*. HM Treasury.

Turner, J. (1973). *Buoyancy effects in fluids*. Cambridge University Press.

US Department of Energy (2006). The buildings energy data book. US Department of Energy. http://buildingsdatabook.eere.energy.gov/docs/1.1.3.pdf [Accessed 27th March 2007].

Woods, A., T. Chenvidyakarn, and A. Short (2003). Reversing flow in a naturally ventilated building with multiple stacks. *Proceedings of Passive and Low Energy Architecture conference, Santiago, Chile*.

Yam, J., Y. Li, and Z. Zheng (2003). Nonlinear coupling between thermal mass and natural ventilation in buildings. *International Journal of Heat and Mass Transfer 46*, 1251–1264.

# A. Experimental detail

In this appendix I will give further details on all experimental work. I hope the thoughts and examples given in this appendix will be useful to anyone trying to conduct similar wind-buoyancy experiments. First, I will outline the difficulties involved in obtaining good experimental results, and how these difficulties were overcome. I will then present full calibration data for a series of experiments.

## A.1. Complications and solutions

Some of the experimental work described in this thesis was developed by a process of trial and error. In order to save a similar process for anyone trying to repeat the results, I will outline some of the experimental complications I have faced, and the solutions to these problems.

### A.1.1. Unknown wind pressures

The wind pressure acting on the upwind face of the building in my experiments is of the order of 1 Pa greater than the equivalent pressure on the downwind face. I have not found any sensor capable of measuring such small pressure differences in water. I therefore used a series of calibration experiments to determine the wind pressure. Such experiments use forced ventilation to calibrate the wind pressure (and hence are not complicated by interactions between wind and buoyancy). The results for one such set of experiments are detailed later in this appendix. The calibrated winds used in the experiments were considered constant over a period of 2-3 weeks (roughly one set of experiments), but were expected to vary over several months (due to, for example, sediment buildup in the pumps or changes in the geometry of the hoses), and so new calibration

experiments were required for each new set of experiments.

If it were possible to measure the wind pressure directly, this would greatly speed up the experiments (since the calibration experiments could be cut out), and allow more accurate diagnosis of the causes of occasional fluctuations in the system.

### A.1.2. Fluctuations in the flow

In early experiments in one flume I found that the flow in the building was oscillating between wind driven and buoyancy driven regime with a period of roughly five seconds. Since the temperature of the fluid in the building remained approximately constant over these oscillations, and the mixing seemed thorough when viewed using dye tests, I assume that these fluctuations were caused by variations in the wind pressure.

It seemed plausible that these fluctuations might be caused by seiches (surface waves) in the tank. Since the pressure difference caused by the wind was only of the order 1 Pa, a wave of height 0.1 mm could cause a comparable pressure difference. The period of a seiche is given by the formula

$$T_s = \frac{2L}{\sqrt{gd}} \tag{A.1}$$

(see `http://www.coastal.udel.edu/faculty/rad/seiche.html`) where L is the tank length and d the depth. For a 3m long tank with a depth of 50cm, this gives a seiche period of 2.7s. Since this was comparable to the 5s oscillations observed, it was decided to add a lid to the tank to cancel the effects of any waves.

Unfortunately, this did not improve the situation. The eventual solution was to move to a different flume tank, with a different pump. Here, the wind pressure was found to be much more uniform. I suspect, therefore, that the fluctuations were caused by either variations in the pump flow rate (these were not noticeable on the pump flow meter, but the flow meter's inertia may have made the effects too small to observe) or by the structure of the flow within the

tank. If I were conducting these experiments again, I might investigate adding a flow meter in the centre of the tank and using feedback from this flow meter to control the pump speed. This would ensure constant flow speed. This could also then be developed into a fully variable controllable pump, which might offer a wider range of possible experiments involving varying wind.

### A.1.3. Pump heating

The experiments of chapter 3 were conducted in a relatively large flume with pump flow rates of the order $1l/s$. It was found that the pump acted to significantly heat the water, such that the steady state temperature of the external fluid was around $35^oC$. Since the external fluid temperature was intended to be constant, before each experiment the flume was filled with warm water (approximately $35^oC$) and then the pump was run until the external fluid temperature remained constant. Only then could experimental data be taken.

For later experiments (chapters 4 and 5) it was found that a small flume with a smaller pump could create equivalent effective wind pressures but ran at temperatures much closer to room temperature, thus allowing experiments to be undertaken more quickly and easily.

## A.2. Calibration experiments

Here I will outline one complete set of calibration experiments, used to determine the loss coefficient $c^*$ and the wind pressures for each pump configuration available. This particular set of experiments was used to calibrate the various wind pressures for the experiments outlined in chapter 4.

### A.2.1. Calibration of loss coefficient

To find the loss coefficient $c^*$ we use a series of experiments with no wind. With no wind, at equilibrium, equation 3.3 becomes

$$H = \rho C_p c^* A \Delta T \sqrt{\frac{\beta g h \Delta T}{2\rho}} \tag{A.2}$$

For the fluid properties of water, we use $\beta = 0.36kgm^{-3}K^{-1}$, $\rho = 1000kgm^(-3)$, and $C_p = 4184Jkg^{-1}K^{-1}$. For gravity, we use $g = 9.81ms^{-2}$. We know the height between openings, $h = 0.08m$ and the window opening area, $A = \pi x0.005^2 x3m^2$, since there are three openings of radius $0.005m$. $\Delta T$ and $H$ are measured during the experiment, so we find $c^*$ by comparing theoretical and experimental results.

Figure A.1 shows the results of three calibration experiments. In each experiment readings were taken at heat loads of approximately 35W, 70W, 105W, and 140W. These data points are shown with error bars of $\pm 0.1^oC$ representing the uncertainty in the thermocouple measurement. The solid line represents the theoretical curve for a value of $c^* = 0.65$, while the dotted curves represent $c^* = 0.62$ and $c^* = 0.68$.

Allowing for one outlier at 70W, from figure A.1 we conclude that the loss coefficient $c^* = 0.65 \pm 0.03$.

### A.2.2. Calibration of wind pressure

To find the wind pressure we run a series of experiments with only the upper openings on both sides open, thus eliminating buoyancy forces from the experiment.

Firstly, we need to confirm that the wind pressure difference across the top openings is equal to the wind pressure difference from the upwind top opening to the downwind bottom opening. To do this, we run an experiment with only the downwind upper and lower openings, with the pump switched on. If the results of this experiment are similar to those of the experiment in the previous subsection, with no wind, then we can assume that the wind does not cause any pressure difference between the upper and lower downwind openings.

Figure A.2 shows the results of such an experiment. Readings were taken at heat loads of approximately 35W, 70W, 105W, and 140W. Again, these data points are shown with error bars of $\pm 0.1^oC$. As in figure A.1, the solid line represents the theoretical curve for a value of $c^* = 0.65$, while the dotted curves represent $c^* = 0.62$ and $c^* = 0.68$. From this graph we conclude that, since the

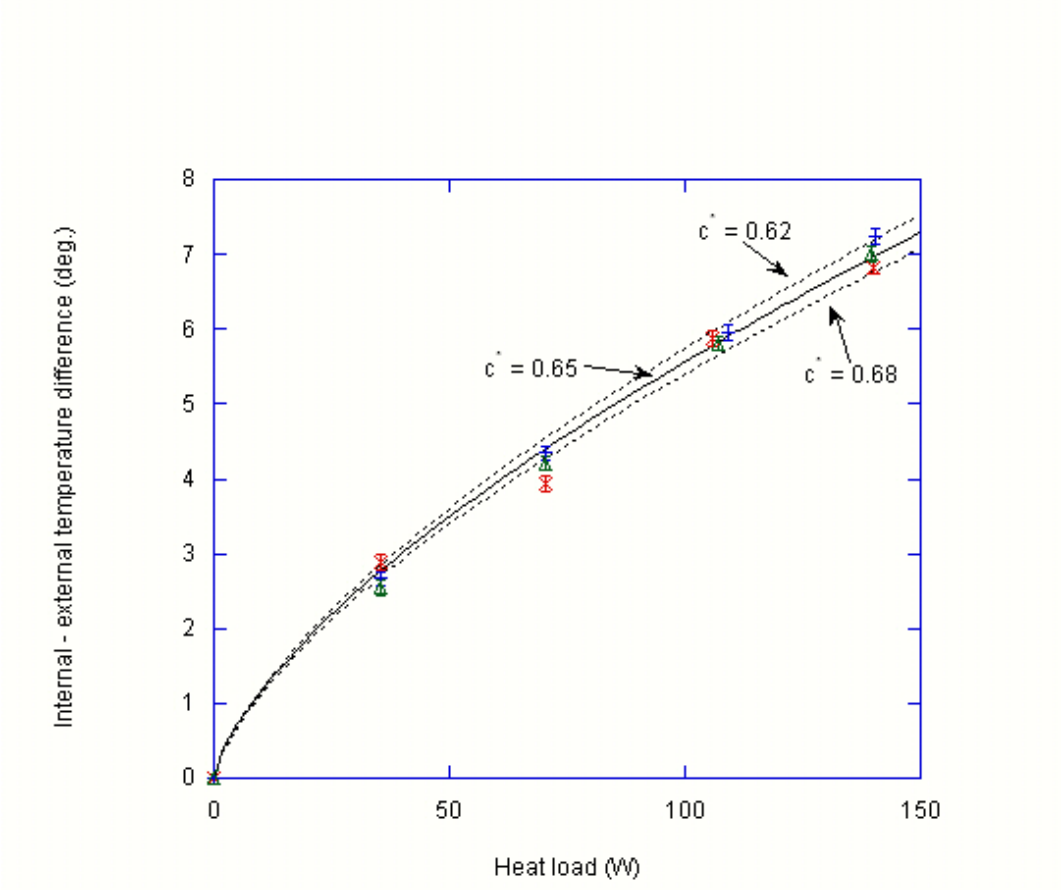


Figure A.1.: *Calibration of loss coefficient* $c^*$*. The figure shows, on a dimensional plot of interior-exterior temperature difference as a function of heat load, the theoretical curves corresponding to* $c^* = 0.65$ *(solid line),* $0.62$ *(upper dotted line) and* $0.68$ *(lower dotted line). The individual data points shown come from a series of three experiments with no wind.*

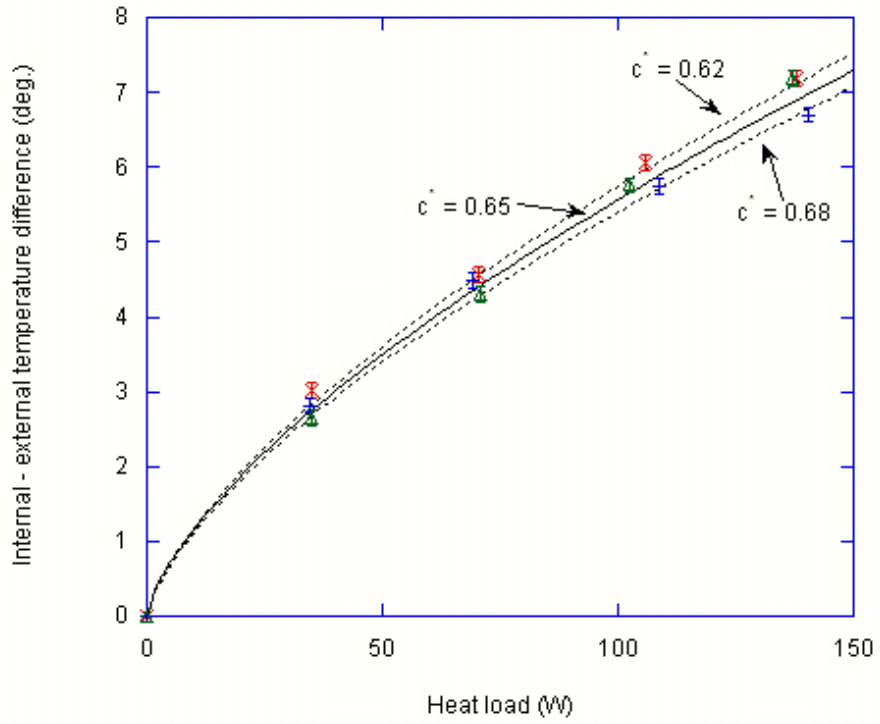


Figure A.2.: *Test for wind pressure difference between downwind openings. The figure shows, on a dimensional plot of interior-exterior temperature difference as a function of heat load, the theoretical curves corresponding to* $c^* = 0.65$ *(solid line),* $0.62$ *(upper dotted line) and* $0.68$ *(lower dotted line). The individual data points shown come from an experiment with upper and lower downwind openings open, with wind.*

experimental values fall inside the theoretical predictions, the wind does not cause a significant pressure difference between the upper and lower downwind openings. We therefore conclude that by finding the pressure difference between the two upper openings, we find the pressure difference between the upper upwind and lower downwind openings, as required.

Finally, we use forced-ventilation experiments with the top two openings open to determine the wind pressure for various pump configurations. With only the upper openings, there is no height difference between the openings, and so

buoyancy forces have no effect. Equation 3.3 then becomes:

$$H = \rho C_p c^* A \Delta T \sqrt{\frac{\Delta P_w}{2\rho}} \tag{A.3}$$

This relationship is plotted in figures A.3, A.4, A.5, A.6 and A.7 for the five possible pump configurations. These figures each show data points from three separate calibration experiments, and also theory for a calibrated value and an upper and a lower limit. The experimental data points have error bars representing the accuracy of the thermocouples ($\pm 0.1^o C$). From these we find the following calibrated pump pressures acting on the building:

| Pump configuration | Calibrated pressure / pa | Error / pa |
|---|---|---|
| Pump 2, half open | 0.9 | $\pm 0.2$ |
| Pump 2, fully open | 2.4 | $\pm 0.2$ |
| Pump 1, fully open | 3.4 | $\pm 0.3$ |
| Pump 1, fully open, and pump 2, half open | 6.5 | $\pm 0.5$ |
| Both pumps fully open | 10 | $\pm 0.5$ |

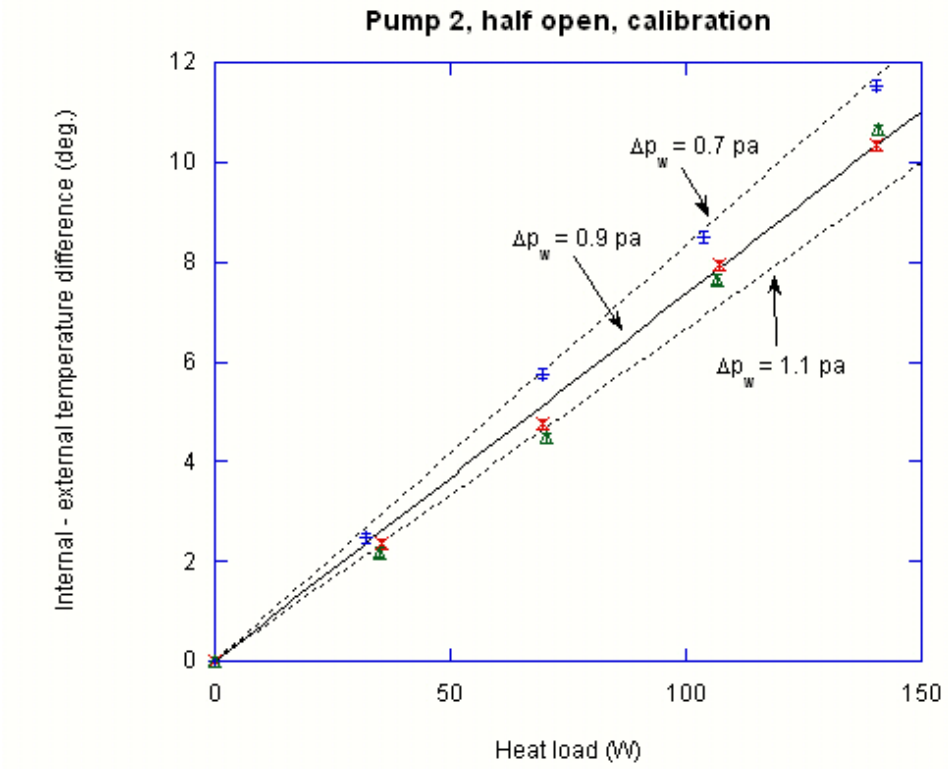


Figure A.3.: *Calibration of wind pressure on upper upwind opening. The figure shows, on a dimensional plot of interior-exterior temperature difference as a function of heat load, the theoretical curves corresponding to* $\Delta p_w = 0.9pa$ *(solid line),* $0.7pa$ *(upper dotted line) and* $1.1pa$ *(lower dotted line). The individual data points shown come from an experiment with both upper openings open, with pump two set to its half-open level.*

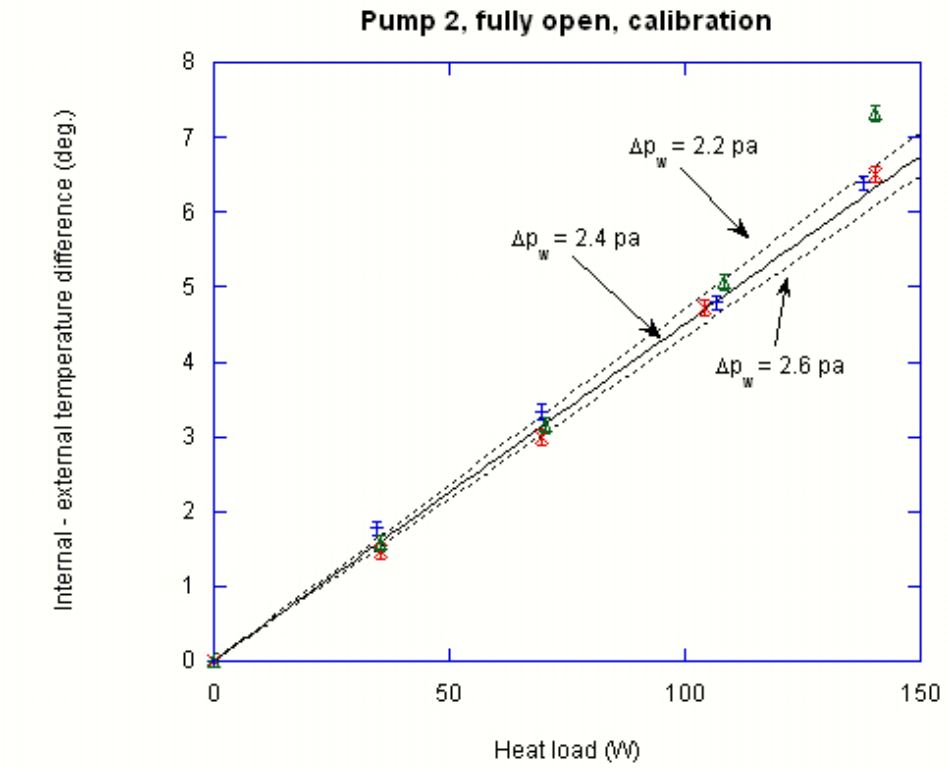


Figure A.4.: *Calibration of wind pressure on upper upwind opening. The figure shows, on a dimensional plot of interior-exterior temperature difference as a function of heat load, the theoretical curves corresponding to* $\Delta p_w = 2.4pa$ *(solid line),* $2.2pa$ *(upper dotted line) and* $2.6pa$ *(lower dotted line). The individual data points shown come from an experiment with both upper openings open, with pump two fully open.*

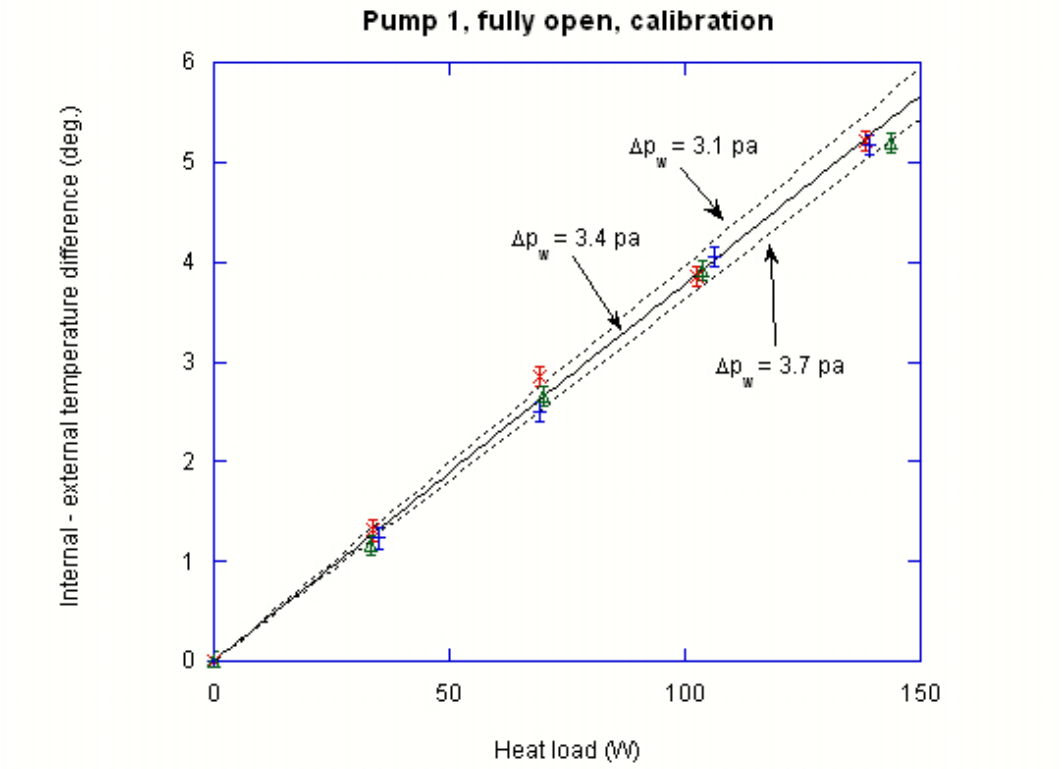


Figure A.5.: *Calibration of wind pressure on upper upwind opening. The figure shows, on a dimensional plot of interior-exterior temperature difference as a function of heat load, the theoretical curves corresponding to* $\Delta p_w = 3.4pa$ *(solid line),* $3.1pa$ *(upper dotted line) and* $3.7pa$ *(lower dotted line). The individual data points shown come from an experiment with both upper openings open, with pump one fully open.*

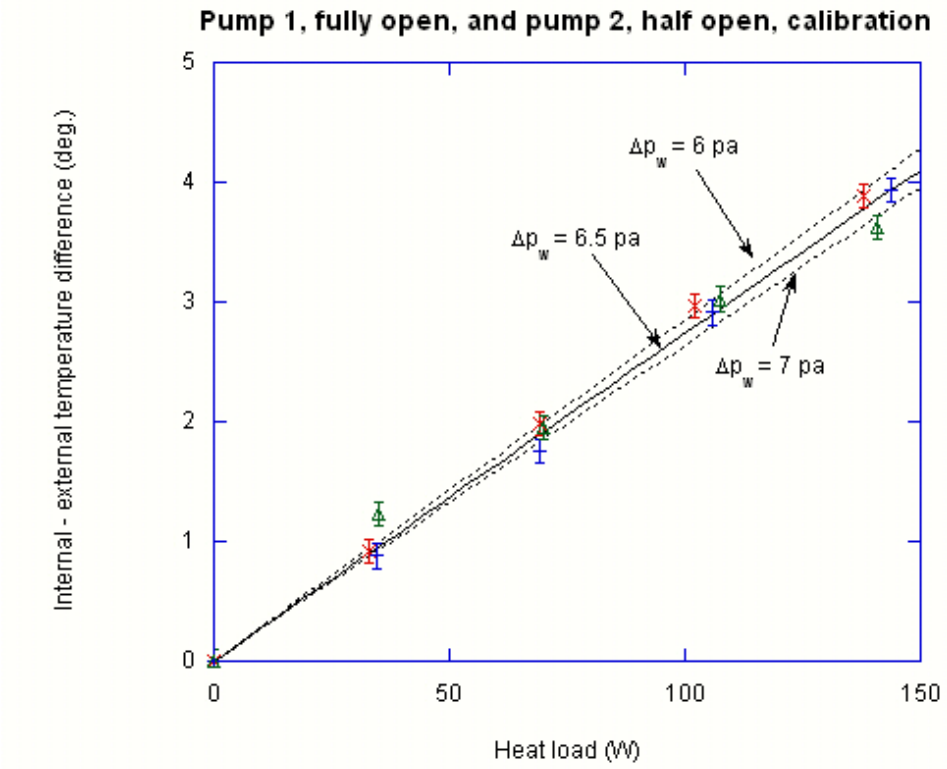


Figure A.6.: *Calibration of wind pressure on upper upwind opening. The figure shows, on a dimensional plot of interior-exterior temperature difference as a function of heat load, the theoretical curves corresponding to* $\Delta p_w = 6.5pa$ *(solid line),* $6pa$ *(upper dotted line) and* $7pa$ *(lower dotted line). The individual data points shown come from an experiment with both upper openings open, with pump one fully open and pump two half open.*

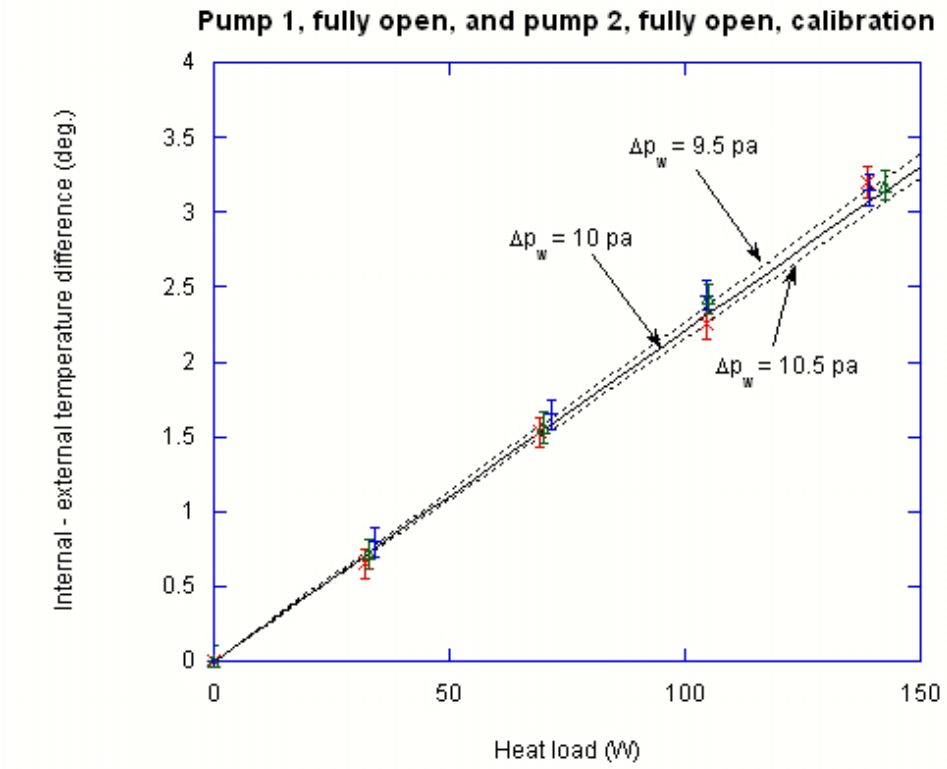


Figure A.7.: *Calibration of wind pressure on upper upwind opening. The figure shows, on a dimensional plot of interior-exterior temperature difference as a function of heat load, the theoretical curves corresponding to* $\Delta p_w = 10pa$ *(solid line),* $9.5pa$ *(upper dotted line) and* $10.5pa$ *(lower dotted line). The individual data points shown come from an experiment with both upper openings open, with both pumps fully open.*

# B. Stratification of transient flows

An understanding of the causes of transitions between regimes helps us to develop a control system which regulates building temperature, by using the actuators available to move to the most comfortable regime. However, it is also important when designing such a control system that we understand the detailed flow patterns, since these can be important in designing for local comfort, and to inform control sensor specifications.

In order to understand the basic principles determining transitions between regimes for our building with two openings, we have assumed that the distributed heat source in the building leads to a well-mixed interior environment. Gladstone and Woods (2001) discuss experiments with a distributed heat source and show that the large Rayleigh number associated with the heat source leads to turbulent convection and a well-mixed fluid at equilibrium.

However, during transitions between equilibria, the fluid in the building can stratify. To see this, consider a transition in the buoyancy-driven regime, in which the heating is reduced. The fluid in the building at the initial equilibrium temperature (say $T_i$) is warmer than the fluid in the building at the final equilibrium temperature (say $T_f$). In the transition between the two temperatures, therefore, as the initial fluid ventilates through the upper opening, the relatively warm fluid from the initial equilibrium will form a layer above the relatively cold new fluid. Since the upper layer is warmer, the only mixing between the layers will occur through penetrative convection due to warm plumes coming off the distributed heating source. This mixing is, however, a low-order effect, since it only affects the temperature of the fluid close to the interface.

In these periods of stratified transition, the ventilation is being driven by the

buoyancy forces due to the fluid currently in the building. Since the fluid was initially at a warm equilibrium, the ventilation during the transition between equilibria is faster than it will be at the final equilibrium. The heating load is therefore insufficient to heat the fluid entering the building to the equilibrium temperature, and hence the building temperatures "overshoots": that is, it drops below the final equilibrium temperature and then rises back up. Again, this can have serious implications both for control system design (since the temperature observed by the sensors may be lower than the final equilibrium temperature) and also for occupant comfort (since the overshoot may move the building out of acceptable comfortable conditions).

If we assume that the exterior fluid is cooler than the interior fluid (since we are heating the interior), then the case of cooling in the buoyancy driven regime is the only one where stratification is likely to occur. In the wind driven regime, we add cold fluid at the top of the building, which will mix without stratifying. In the buoyancy driven regime, moving to a warmer state, we add in relatively warm fluid at the bottom of the building, which again leads to mixing. The analysis presented in this chapter therefore does not contradict any of the conclusions of chapters 4 and 5.

A full description of similar transient processes, in the absence of wind, including a discussion of the importance of penetrative convection, can be found in Fitzgerald and Woods (2007).

## B.1. Numerical and experimental analysis

We have studied the stratification which can occur numerically and experimentally. To study the system numerically, we model the building as a series of layers of fluid. The average temperature in the building controls the buoyancy pressure and thus determines which flow regime the building is in, and the flow rate through the building. At each time step, a new layer is created (with volume determined by the flow rate and time step length), either at the top of the building (in the wind driven mode) or at the bottom (in the buoyancy driven

mode). The heating energy for that time step is then added to the bottom layer in the building and the new temperature of this layer calculated. Finally, any pairs of layers with colder fluid above warmer fluid are mixed to form one new layer, at the average temperature of the two previous layers, until no layer is colder than the layer below it.

To study the transitions experimentally, we use the experimental apparatus described in chapter 4: a water flume tank with a perspex building model,, which is heated by a distributed heat source, and in which temperatures can be measured using thermocouples. Our experiment was conducted at a wind pressure of 0.75pa. The heat load was initially set to 220W, and the building allowed to reach equilibrium. Some time later the heating was instantaneously reduced to 20W.

This experiment was also modelled numerically, to allow a comparison between theoretical and experimental predictions. These results are shown in figure B.1.

The numerical model provides a reasonable prediction of the experimental data. Some differences are observed due to interfacial mixing: while the numerical model predicts a sudden transition from hot to cold as the interface moves up the tank, in the experimental model we find that this transition is slightly more gradual, since there is a narrow horizontal layer which is continuously stratified due to interfacial mixing between the hot upper layer and the cold lower layer. However, the predicted stratification is observed (hence we see different temperatures at different heights in the tank during the transition), as is the temperature overshoot (the building cools to below 2 degrees warmer than the exterior, before settling at over 3 degrees warmer).

## B.2. Conclusions

In problems of multiple steady states due to interaction between wind and buoyancy, and with a distributed heat source, we have assumed a well-mixed interior at equilibrium. However, in this study we show that during transitions

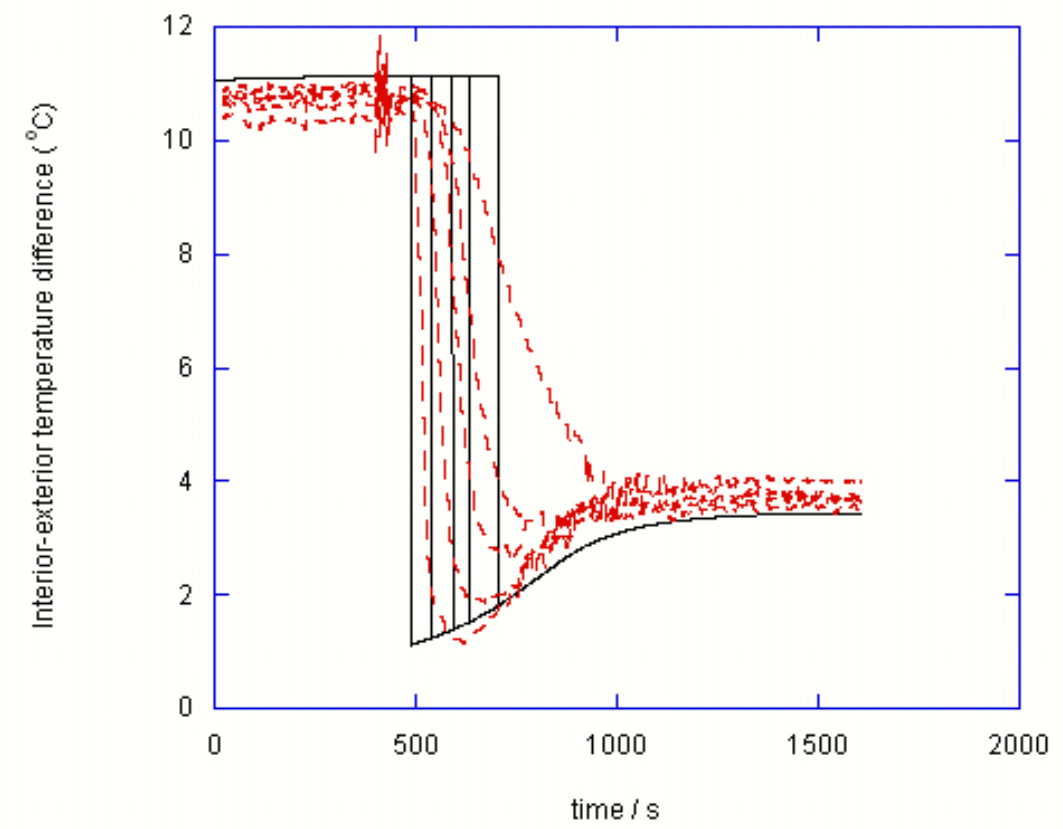


Figure B.1.: *Comparison of numerical and experimental modelling of stratification, on a plot of temperature as a function of time. The wind pressure is constant at 0.75pa. The heat load begins at 220W, and is then reduced to 20W at t = 500. The solid black lines show the numerically predicted temperatures at heights of 0, 2cm, 4cm, 6cm and 8cm. The dashed red lines show the experimental data measured at these heights.*

between equilibria (specifically when moving to a colder steady state in the buoyancy driven regime) stratification can occur. Since the flow is driven by a combination of the initial warm fluid and the new, cooler fluid, we expect the ventilation rate during transition to be faster than the final ventilation rate, and hence we predict that the temperature drop will "overshoot", before the temperature settles to equilibrium.

We have modelled these transitions experimentally and observed both the stratification and the overshoot in cooling. We have also produced a numerical model which provides a reasonable estimate of the flow behaviour and internal temperatures.

These effects are transient and unlikely to play a large part in overall building comfort. However, it is important from a control system design perspective to understand how the building flow changes when the temperature moves away from equilibrium.

# C. Temporary gusts and regime changes

## C.1. Introduction

In chapter 3 it was shown that an instantaneous change in wind can cause a building to evolve from the buoyancy driven regime to the wind driven regime. Here we consider such instantaneous changes in wind as gusts: sudden, pulse-like increases in wind. If such a gust is extremely brief, the building may well return to its original, buoyancy driven state. However, if the gust last for a longer period of time, the building may cool to the wind driven state. Here we produce a model to predict the duration of gust which will cause the building to permanently change regimes.

Such analysis has applications in lightweight buildings, where sudden gusts may cause the building flow regime to change. If the flow regime is likely to oscillate, this may cause occupant discomfort for those near windows, where cold inflow and warm outflow may alternate. Similarly, if the gusts are likely to last long enough to change the building flow regime permanently, then the building controller may wish to ensure comfortable conditions in the new, colder, wind driven regime.

## C.2. Theory

This work follows on from chapter 3, where we use an energy balance and a heat balance to produce a model of the temperature evolution in the building shown in figure C.1. We consider a fixed heating load and a varying wind, so we scale on the heating load as in chapter 4. In this model

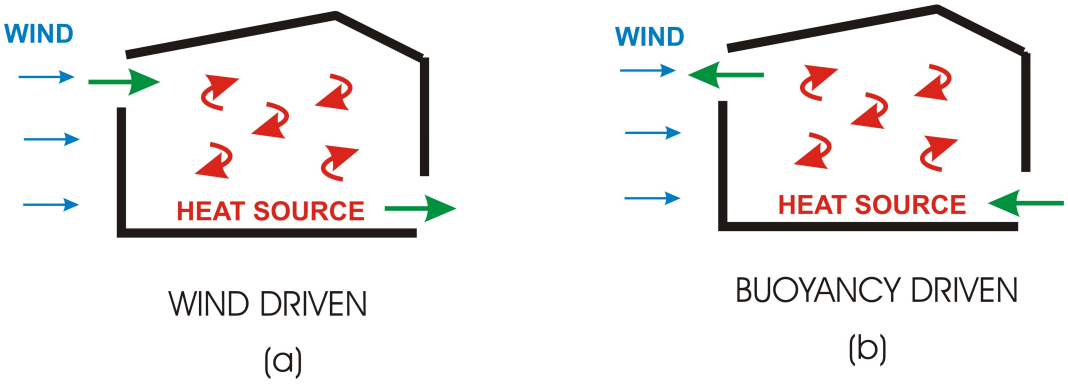


Figure C.1.: *Schematic showing the two possible regimes in our two opening case: on the left, a wind-driven solution, with flow from left to right, and on the right, a buoyancy-driven solution, with flow from right to left, upwards through the building.*

$$\frac{d\Theta}{d\hat{t}} = 1 - \Theta\sqrt{|W - \Theta|} \tag{C.1}$$

where $\Theta$ is dimensionless temperature, $\hat{t}$ is dimensionless time, and $W$ is dimensionless wind.

We now consider which variations in wind will cause a permanent transition in flow regime. First we consider occasions where the building starts in the buoyancy-driven regime, at a wind for which both flow regimes are possible ($W > W_{crit}$). We then increase the wind such that the building flow changes direction (to the wind-driven regime) and the building starts to cool. How long do we have maintain the increase in wind for, in order that the flow regime does not switch back (to the buoyancy-driven regime) when the wind changes back again?

First, consider the initial state, at wind $W_1$, in the buoyancy-driven regime. Rearranging equation C.1 we note that the initial temperature $\Theta_1$ is the real solution of the equation

$$\Theta_1{}^3 - W_1\Theta_1{}^2 - 1 = 0 \tag{C.2}$$

In order for the system to stay in the wind-driven regime, the gust must last sufficiently long that the building cools below the unstable wind-driven equilib-

rium at $W_1$. From equation C.1 we know that this final required temperature $\Theta_2$ is the largest solution of the equation

$$\Theta_2{}^3 - W_1\Theta_1{}^2 + 1 = 0 \tag{C.3}$$

The cooling occurs at a higher wind, which we call $W_2$. We express the difference between the winds as $\Delta W$, such that $W_2 = W_1 + \Delta W$. Rearranging equation C.1 we find an expression for the time $\tau_c$ to cool from $\Theta_1$ to $\Theta_2$.

$$\tau_c = \int_{\Theta_1}^{\Theta_2} \frac{1}{1 - \Theta\sqrt{W_2 - \Theta}} \tag{C.4}$$

For a given base wind $W_1$ and gust size $\Delta W$ we can therefore find the minimum gust duration $\tau_c$ which will cause the flow regime in the building to change. Figure C.2 maps out the trajectory of the system on a plot of W as a function of $\Theta$.

Figure C.3 shows typical results for the duration of wind pulse required to change regimes.

By comparing this graph to real wind data, we can find a typical range in which multiple steady states would be expected. We can also see from this graph that as the 'base' wind $W_1$ increases, the size and duration of gusts required to change from the buoyancy-dominated to the wind-dominated regime decreases.

In contrast, figure C.4 shows a typical trajectory for a system to switch from the wind-driven to the buoyancy-driven regime under gusting wind.

We observe that the minimum wind change $\Delta W$ for which the regime change is that which causes the system to reach $W_c$, i.e. $W_1 - \frac{3}{4^{\frac{1}{3}}}$. The wind must then remain sufficiently low that the building heats up past the 'nose' of the wind-driven curve, and then increase sufficiently gradually that the wind returns to its original value without the building switching back into the wind-driven regime. We deduce that, at high winds, with small or large gusts, the building is much more likely to move to the wind-driven regime than the buoyancy-driven regime.

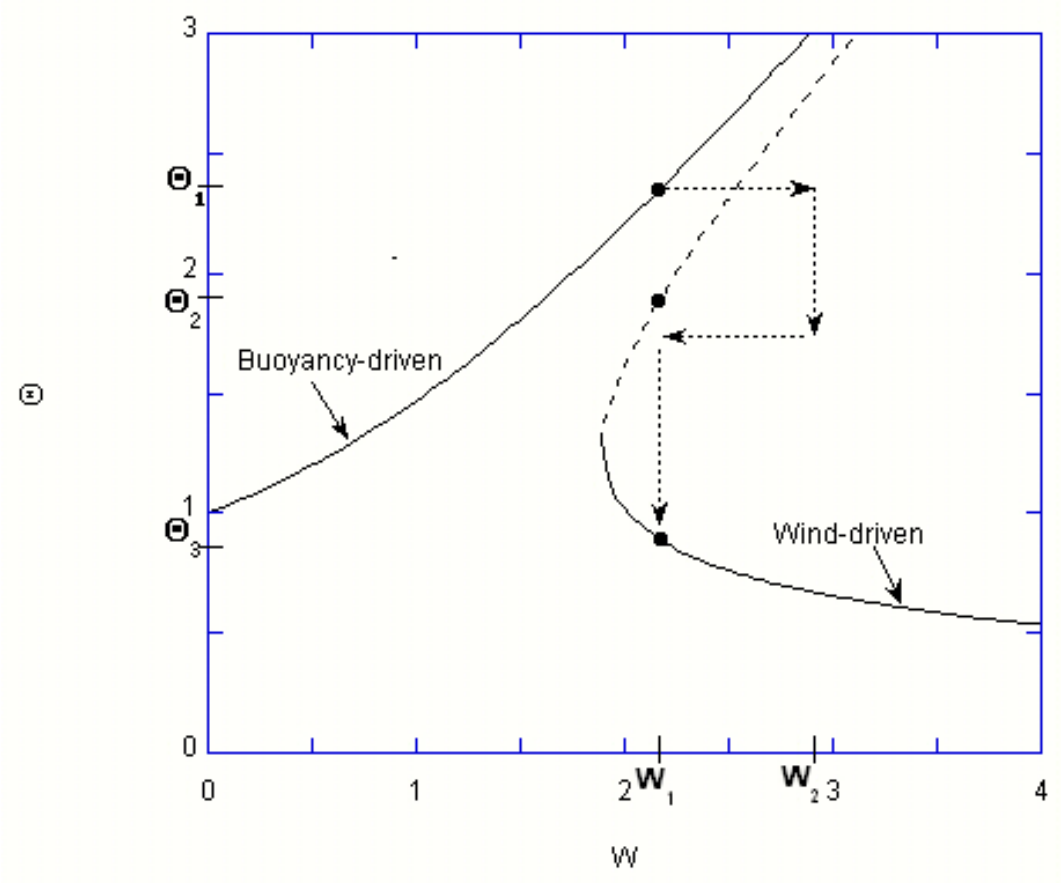


Figure C.2.: *Evolution of the building temperature under gusting wind, with the regime going from a buoyancy-dominated regime to a wind-driven regime. The building start at a buoyancy-dominated equilibrium at temperature $\theta_1$ and wind $W_1$. The wind is then increased to $W_2$, at which point the flow regime changes to the wind-driven regime and the building starts to cool. At some time the wind reverts to $W_1$. At this point, if the building has cooled sufficiently that $\theta < \theta_2$ (as shown here), then the building will cool to the wind-driven equilibrium, $\theta_3$. If, when the wind reverts to $W_1$, $\theta > \theta_2$, the building will heat up again, and the temperature will return to $\theta_1$.*

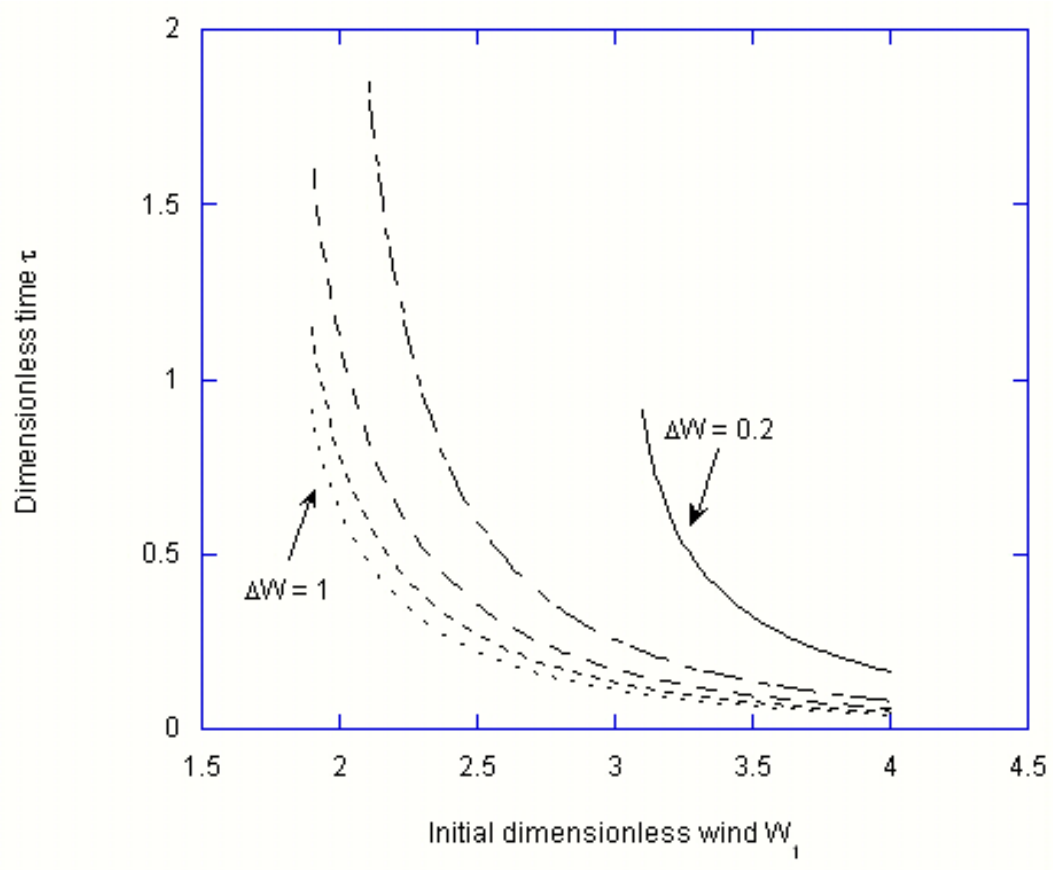


Figure C.3.: *Duration of gust $\tau$ which causes a permanent change of regimes (as illustrated in figure C.2) shown as a function of the initial wind $W_1$. The graph is plotted for various gust sizes: from left to right, these are $\Delta W = 1, \Delta W = 0.8, \Delta W = 0.6, \Delta W = 0.4, \Delta W = 0.2$. Note that at low initial winds, some values of $\Delta W$ may be too small to cause a change in regime, even after infinite time.*

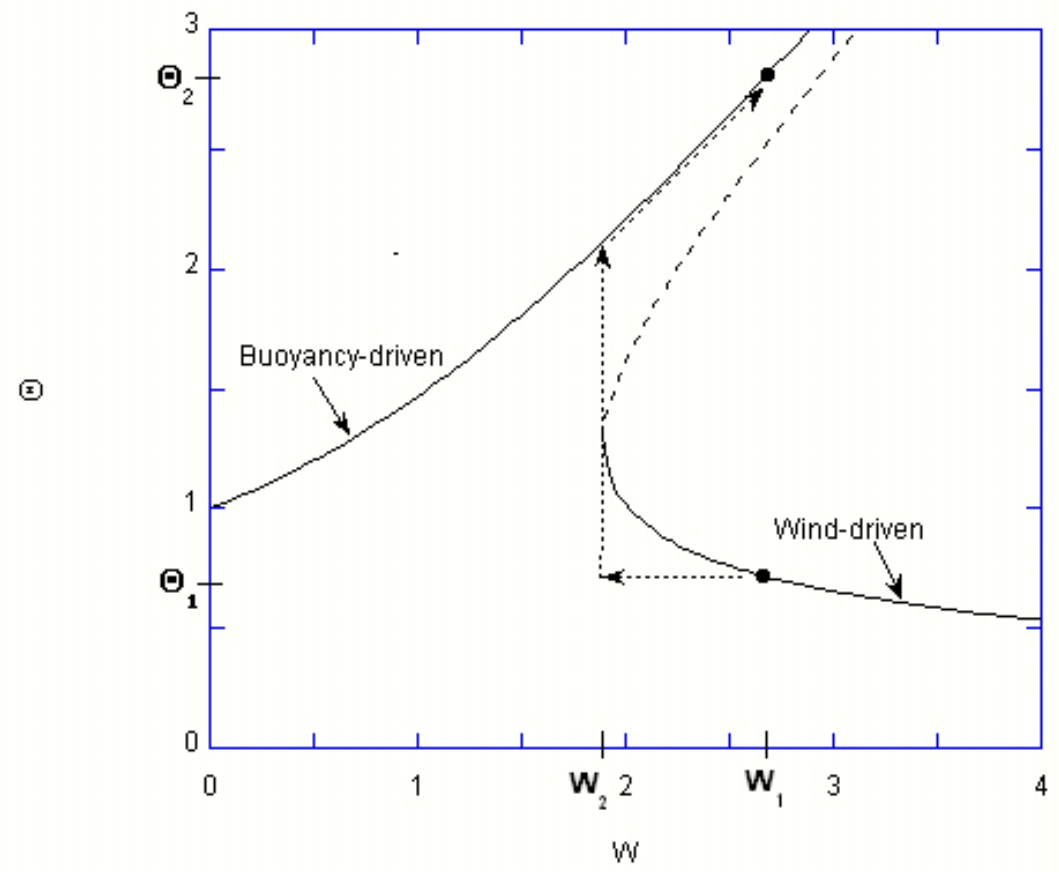


Figure C.4.: *Evolution of the building temperature under gusting wind, with the flow regime moving from wind-driven to buoyancy-driven. The building starts at a wind-dominated equilibrium at temperature* $\theta_1$ *and wind* $W_1$*. The wind is then decreased to* $W_2$*, at which point the wind-driven regime no longer exists, and the building heats towards the buoyancy-driven equilibrium. When the buoyancy-driven equilibrium is reached, the wind then slowly increases, and the building remains in the buoyancy-driven regime until the wind returns to* $W_1$*.*

### C.2.1. Experiments

We can test the theory above using the experimental setup described in chapter 4. Here we begin our experiment with pump 1 on (wind pressure of 3.4pa) and then temporarily turn pump 2 on (increasing wind pressure to 10pa), for a time interval measured by stopwatch. By numerical analysis of equation 3.3, we find that a 10s change in wind should be insufficient to cause the regime to change permanently, whereas a 30s change in wind should cause the flow to change direction, and the final steady state temperature in the building should be significantly lower.

Figure C.5 shows a comparison of the theoretical behaviour (derived numerically from equation 3.3) and our experimental observations, for an initial wind of 3.4pa, increasing to 10pa from 100s to 110s (i.e. a 10s pulse).

Similarly, figure C.5 shows a comparison of the theoretical behaviour and our experimental observations, for an initial wind of 3.4pa, increasing to 10pa from 100s to 130s (i.e. a 30s pulse).

In figure C.5 we see that the temperature returns to its initial value, and the building returns to the buoyancy driven state, while in figure C.6 the building cools sufficiently that cooling continues after the wind pulse has ended, and the building remains in the wind driven state. The results shown in figures C.5 and C.6 support the theory and clearly show that the pulse must last sufficiently long in order for the flow to permanently change direction.

### C.2.2. Conclusions

Using the simplified model of a square-wave pulse of wind, we are able to determine the length of pulse required for the flow regime in the building to change. This, in turn, demonstrates that at high winds, the building is very likely to evolve from the buoyancy driven to the wind driven regime under fluctuating wind, and far less likely to undergo the reverse transition. Further, this model gives an illustration of how typical wind data might be used to predict whether uncomfortable changes of flow direction are likely to occur.

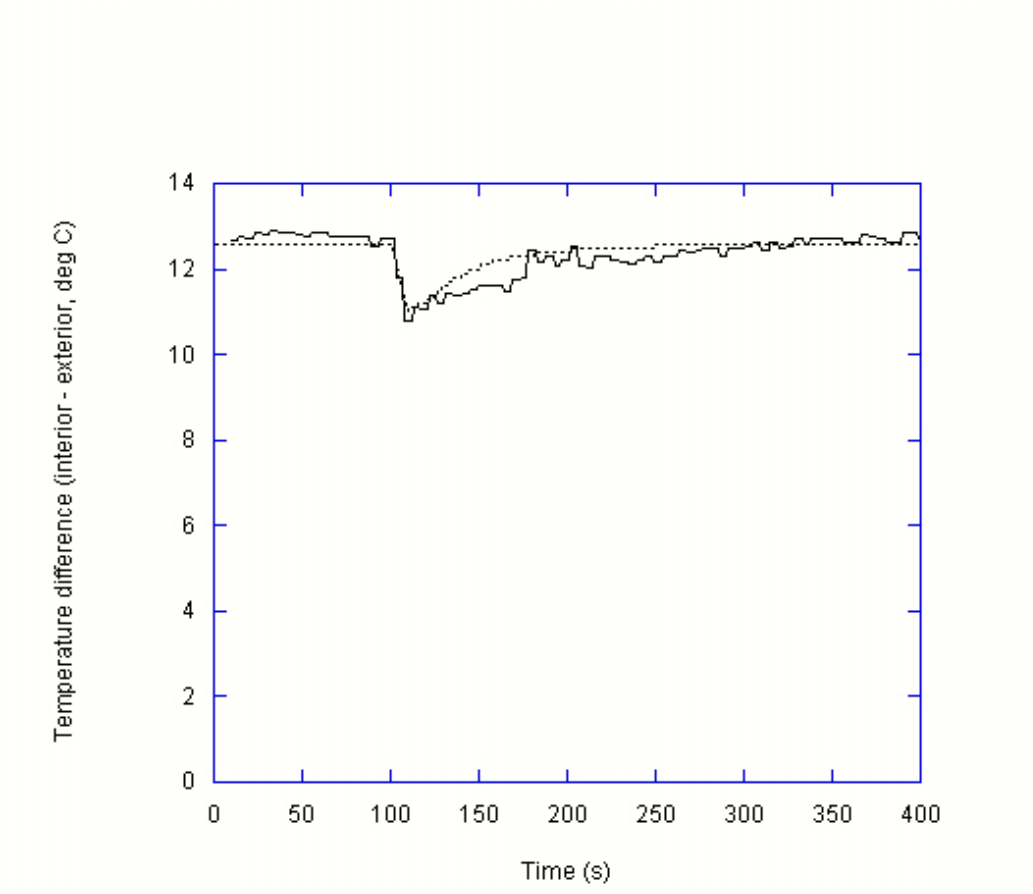


Figure C.5.: *Experimental results showing the effect of wind pulsing on a plot of temperature difference as a function of time. The dotted line shows the theoretically predicted behaviour, while the solid line shows experimental observations. At 100s, the wind pressure is increased from 3.4pa to 10pa. At 110s, the wind returns to 3.4pa.*

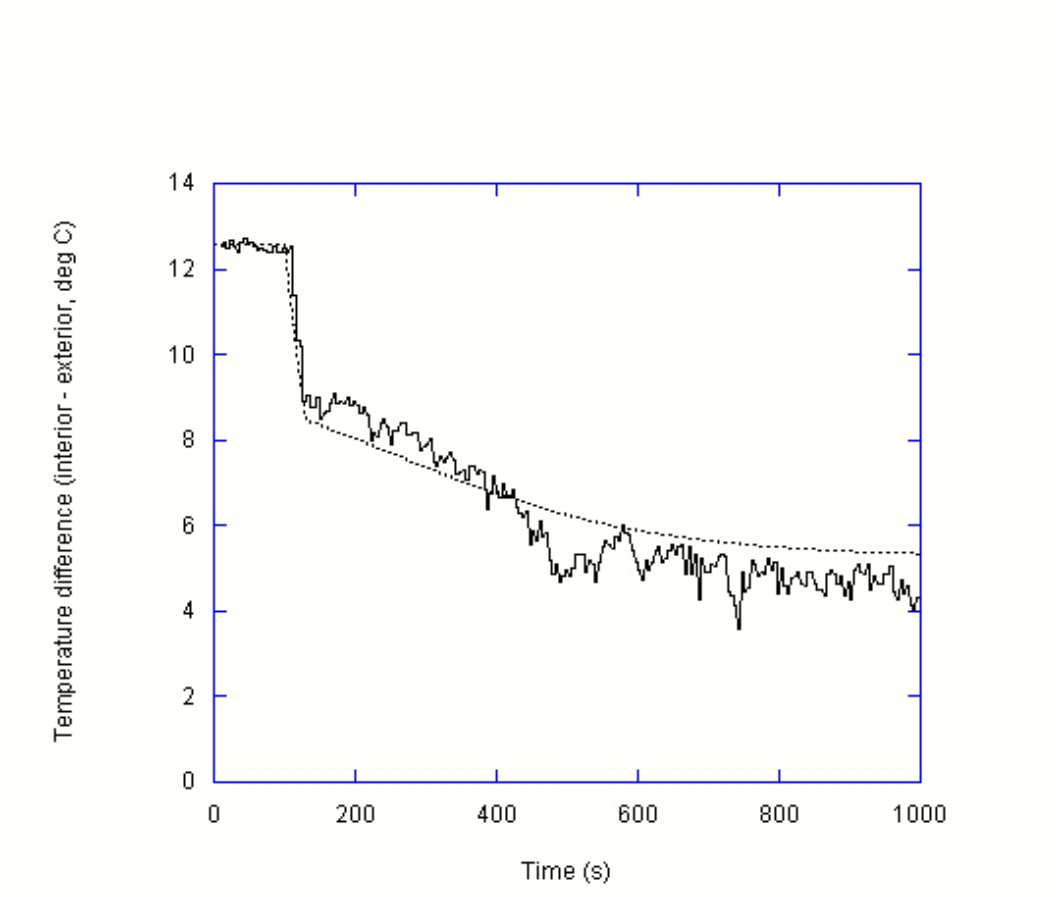


Figure C.6.: *Experimental results showing the effect of wind pulsing on a plot of temperature difference as a function of time. The dotted line shows the theoretically predicted behaviour, while the solid line shows experimental observations. At 100s, the wind pressure is increased from 3.4pa to 10pa. At 130s, the wind returns to 3.4pa.*